

TARGETING THE HEART USING IN VIVO PHAGE DISPLAY

by

Maliha Zahid

M.B., B.S., Aga Khan University, Pakistan, 1993

Submitted to the Graduate Faculty of

Department of Human Genetics

Graduate School of Public Health in partial fulfillment

Of the requirements for the degree of

Doctor of Philosophy

University of Pittsburgh

2009

UNIVERSITY OF PITTSBURGH

Graduate School of Public Health

This dissertation was presented

by

Maliha Zahid

It was defended on

October 14th, 2009

and approved by

Dissertation Advisor:

Paul D. Robbins, PhD

Professor

Department of Microbiology and Molecular Genetics

School of Medicine

University of Pittsburgh

Robert E. Ferrell, PhD

Professor

Department of Human Genetics

Graduate School of Public Health

University of Pittsburgh

Eleanor Feingold, PhD

Associate Professor

Department of Human Genetics

Graduate School of Public Health

University of Pittsburgh

Charles F. McTiernan, PhD

Associate Professor

Department of Medicine

School of Medicine

University of Pittsburgh

Copyright © by Maliha Zahid

2009

TARGETING THE HEART USING IN VIVO PHAGE DISPLAY

Maliha Zahid, PhD

University of Pittsburgh, 2009

Background: Ischemic heart disease remains the number one killer in the developed world. A protein transduction peptide specific for the heart capable of efficiently delivering agents of therapeutic potential at the time of injury, would be of immense public health significance. This work was undertaken to identify peptide(s) able to transduce heart tissue *in vivo* in a tissue-specific manner. Biopanning was performed in cell culture followed by *in vivo* with an M13 phage peptide display library. Using the heart-specific peptide, we delivered nemo-binding domain peptide in a murine infarct model to test if NF- κ B inhibition can reduce infarct size.

Methods and Results: A cardiomyoblast cell line, H9C2, was incubated with M13 twelve amino acid phage peptide display library. Internalized phage was recovered, amplified and subjected to a total of three rounds of *in vivo* biopanning where infectious, internalized phage was isolated from cardiac tissue following intravenous injection. After the third round, 60% of sequenced plaques carried the peptide sequence APWHLSSQYSRT, termed cardiac targeting peptide (CTP). This peptide was synthesized either fluorescently labeled, biotinylated, or in combination with a NEMO-binding peptide (NBD), an inhibitor of the inducible NF-kappa B Kinase (IKK). We demonstrate that CTP was able to transduce cardiomyocytes functionally in culture in a concentration and cell-type dependent manner. Mice injected with CTP showed significant transduction of heart tissue with minimal uptake by lung and kidney capillaries, and no uptake in

liver, skeletal muscle, spleen or brain. The level of heart transduction by CTP also was not observed with a cationic transduction domain. CTP-NBD was able to inhibit NF- κ B activation in cell culture in a dose-dependent fashion. When administered to mice in a murine infarct model, CTP-NBD showed a trend towards smaller infarct size, which did not reach statistical significance.

Conclusions: Biopanning using a peptide phage display library identified a peptide, termed CTP, able to transduce cardiomyoblast cell line *in vitro*, and heart tissue *in vivo*, efficiently and specifically. Administration of CTP-NBD to post-infarct mice showed a trend towards reduction of infarct size. CTP could be used to deliver therapeutic peptides, proteins and nucleic acid specifically to the heart.

TABLE OF CONTENTS

PREFACE	XII
LIST OF ABBREVIATIONS	XIV
1.0 INTRODUCTION.....	1
1.1 SCOPE OF THE PROBLEM.....	1
1.2 PROTEIN TRANSDUCTION DOMAINS	2
1.3 BIOPANNING OR PHAGE DISPLAY	3
1.4 NUCLEAR FACTOR KB.....	10
1.4.1 Classical NF-κB Activation Pathway	12
1.4.2 Alternate NF-κB Activation Pathway	15
1.5 NEMO-BINDING DOMAIN PEPTIDE.....	18
1.6 NF-KB AND THE HEART.....	21
2.0 PHAGE DISPLAY TO TARGET THE HEART.....	25
2.1 PHAGE DISPLAY	25
2.2 <i>IN VITRO</i> TRANSDUCTION EXPERIMENTS: CONFOCAL STUDIES .	33
2.3 <i>IN VITRO</i> TRANSDUCTION: FUNCTIONAL ASSAY	39
2.4 <i>IN VIVO</i> TRANSDUCTION STUDIES.....	45
2.5 HUMAN HEART TISSUE EXPERIMENTS.....	57
2.6 CHAPTER SUMMARY	61

3.0	MURINE INFARCT SIZE STUDIES USING NBD	64
3.1	GENERATION OF THE ANIMAL MODEL OF MYOCARDIAL INFARCTION.....	65
3.2	INFARCT STUDIES USING 8K-NBD.....	67
3.3	INFARCT STUDIES USING CTP-NBD.....	75
4.0	SUMMARY, IMPLICATION OF OUR FINDINGS AND FUTURE DIRECTIONS	83
4.1	SUMMARY OF OUR FINDINGS.....	83
4.2	IMPLICATIONS AND FUTURE DIRECTIONS	85
5.0	METHODS.....	91
5.1	PROTOCOL FOR PEPTIDE PHAGE DISPLAY	91
5.1.1	Materials.....	92
5.1.2	Methods.....	95
5.2	IN VITRO TRANSDUCTION EXPERIMENTS.....	103
5.2.1	Cell transduction experiments with CTP-6CF	103
5.2.2	8% Paraformaldehyde stock solution	104
5.3	METHODOLOGY FOR TRANSFECTION OF CELLS AND INHIBITION OF NF-KB ACTIVATION.....	105
5.3.1	Materials.....	105
5.3.2	Methods.....	106
5.4	MOUSE INFARCT MODEL	107
	BIBLIOGRAPHY	110

LIST OF TABLES

Table 1. Summary of studies utilizing NBD peptide.	19
Table 2. Summary of NF-kappa B studies with cardiac ischemia-reperfusion injury or myocardial infarction.....	23
Table 3. Number of phage injected and recovered from each cycle of phage display.....	29

LIST OF FIGURES

Figure 1. Schema of available display technologies.	4
Figure 2. Structure of M13 bacteriophage.	7
Figure 3. Assembly of phage virion and its release from <i>E. coli</i> cells.	7
Figure 4. Schematic representation of steps in screening a peptide phage display library.	9
Figure 5. Activation of classical NF- κ B signaling by TNF- α	14
Figure 6. Activation of NF- κ B signaling by CD40.	16
Figure 7. Experimental design of the combinatorial <i>in vitro</i> and <i>in vivo</i> phage display.	28
Figure 8. Recovered phage normalized to tissue weight and plotted as a ratio of heart to kidney (a) and output to input ratios (b).	30
Figure 9. Physical properties of Cardiac Targeting Peptide or CTP.	33
Figure 10. Confocal micrographs of H9C2, 3T3, MCA205, HeLa and HK-2 cells incubated with increasing concentrations of CTP-6CF; Nuclei - blue (DRAQ5), CTP-6CF - green, 20x. Scale bars represent 100uM.	36
Figure 11. High magnification confocal micrographs of H9C2 cells incubated with CTP-6CF for 30 (top row) and 60 minutes (bottom row).	37
Figure 12. Live cell imaging of H9C2 cells incubated with RAN-6CF, CTP-6CF or TAT-6CF.	38
Figure 13. Experimental protocol for the <i>in vitro</i> transduction experiments using Luciferase readout.	40

Figure 14. Inhibition of Luciferase activity by CTP-NBD in H9C2 cells.	41
Figure 15. Lack of inhibition of Luciferase activity by CTP-NBD in MCA205 cells.	42
Figure 16. Relative lack of inhibition of Luciferase activity by CTP-NBD in HeLa cells.	43
Figure 17. H9C2 cell viability after transfection, treatment with CTP-NBD and subsequent TNF-alpha treatment.	44
Figure 18. Transduction of mouse heart by intravenously injected CTP-6CF at 15 minutes.	46
Figure 19. Quantification of fluorescence in mouse hearts (n=3 in each group).	47
Figure 20. Transduction of heart tissue after intravenous injection with CTP-biotin-streptavidin-Alexa488 complex.	50
Figure 21. Biodistribution of CTP-biotin-streptavidin-Alexa488 complex after intravenous injection.	50
Figure 22. <i>In vivo</i> , whole mouse imaging after intra-cardiac injection of CTP, RAN or PBS conjugated to fluorescent 40nm beads.	52
Figure 23. Confocal micrographs of hearts injected with PBS+fluospheres, RAN+fluospheres or CTP+fluospheres.	53
Figure 24. Uptake of CTP-6CF preferentially by normal myocardium with exclusion from the infarct area.	55
Figure 25. Comparison of heart tissue transduction between CTP, 8K and RAN peptide.	56
Figure 26. Transduction of human heart tissue ex vivo by CTP-6CF.	58
Figure 27. Results of ex vivo human heart tissue experiment at 30 mins.	60
Figure 28. Inhibition of LPS induced Luciferase signal by 8K-NBD.	69
Figure 29: Post-operative mortality by treatment group in the 8K-NBD study.	70

Figure 30. Heart weight to body weight ratios across the treatment groups in the 8K-NBD study.	71
Figure 31. Infarct size across different treatment groups in the 8K-NBD study.	72
Figure 32. Representative confocal micrographs of TUNEL staining in each treatment group in the 8K-NBD study.	73
Figure 33. Quantification of TUNEL positive data in each treatment group in 8K-NBD study...	74
Figure 34. Post-operative mortality by treatment group in the CTP-NBD study.	76
Figure 35. Infarct size by treatment groups in the CTP-NBD study.	77
Figure 36. Transduction of the mouse heart by the D-CTP-NBD-SA488 complex.	79
Figure 37. Inhibition of NF- κ B activation by the D-isoform of CTP-NBD.	80
Figure 38. Infarct sizes in the two treatment groups.	81
Figure 39. Temperature dependency of CTP's transduction ability.	86
Figure 40. H9C2 cell viability after incubating with increasing concentrations of CTP-NBD.	87
Figure 41. H9C2 cells transfected with different AAV viral vectors expressing EGFP.	90

PREFACE

Lay Summary: Heart disease remains the number one killer in the US as well as the rest of the developed world, and is increasing steadily in the developing world with its industrialization. Heart attacks are the commonest manifestation of it and occur when an atherosclerotic plaque ruptures, exposing a rough surface to the blood leading to blood clotting and the resulting clot completely occluding the said artery. This leads to distal heart muscle tissue being deprived of oxygen and injury, which if it continues unchecked, leads to irreversible muscle death. Current therapies revolve around opening the clogged artery as expeditiously as possible, either with clot busting drugs or catheters. Opening the artery exposes the jeopardized muscle to a surge of oxygen and generation of molecules which are harmful to the muscle as well. Many molecules and therapies have been tested in animal models that have shown efficacy in preventing this, but all suffer from the drawback of lack of an appropriate delivery model. The pathology outlined above occurs within hours of the ruptured plaque and the window of opportunity is measured in hours, with no benefit seen past 12 hours. Therefore a delivery vehicle would have to target the heart efficiently, within hours, to deliver ready-to-go peptides or proteins of therapeutic potential. Also such a mode of delivery should be specific to heart in order to reduce the amount of peptide/protein needed to see a beneficial effect and to potentially decrease side effects. In the work I will be presenting in this thesis, we have done just that. Using the well-established technique of phage display, we have identified a peptide that targets the heart efficiently,

specifically, and very rapidly, within 30 minutes. This peptide can be used as a carrier to deliver peptides or full-length proteins to achieve therapeutic benefit in reducing heart attack sizes and perhaps even for diagnostic purposes.

LIST OF ABBREVIATIONS

6CF	6-carboxyfluorescein
8K	Homopolymer of 8 Lysine Residues
6R	Homopolymer of 6 Arginine Residues
CPP	Cell Penetrating Peptide
CTP	Cardiac Targeting Peptide
Da	Daltons
EBD	Evans Blue Dye
EGFP	Enhanced Green Fluorescent Protein
IKK	I-KappaB Kinase
I κ B α	I-kappa B-alpha
I κ B β	I-kappa B-beta
I κ B γ	I-kappa B-gamma
IL-1	Interleukin 1
IM	Intramuscular
IP	Intraperitoneal
IR	Ischemia-reperfusion
KO	Knock-out
LPS	Lipopolysaccharide
MI	Myocardial Infarction
Mut	Mutant
NBD	Nemo Binding Domain
NEMO	NF-kappa B Essential Modulator

NF- κ B	Nuclear Factor-kappa B
PBS	Phosphate Buffered Saline
PFA	Paraformaldehyde
PTDs	Protein Transduction Domains
RAN	Random Peptide
RT	Room Temperature
SA-488	Streptavidin-Alexa 488
SD	Standard Deviation
SEM	Standard Error of the Mean
TAT	Transactivator of Transcription
TNF α	Tumor Necrosis Factor-alpha

1.0 INTRODUCTION

1.1 SCOPE OF THE PROBLEM

Ischemic heart disease and occlusive coronary artery disease continue to be the number one killer in the developed world. There are an estimated 500,000 acute ST-elevation myocardial infarctions (MI) in the US alone each year [1], and this is becoming an increasingly significant problem in the developing world [2]. Current approaches for management of an acutely occluded coronary artery leading to an MI consist of anti-platelet and anti-thrombotic strategies with intervention aimed at opening the infarct-related artery in a timely fashion. Although this approach is able to protect cardiomyocytes from necrosis, with resulting decrease in morbidity and mortality, it necessitates exposing the heart to post-ischemic reperfusion injury. Limiting this reperfusion injury and decreasing apoptosis would ultimately lead to greater myocardial salvage and prevention of development of heart failure.

Numerous animal studies have identified biological agents able to ameliorate this ischemia-reperfusion injury and reduce the ultimate infarct size [3-5]. The clinical application of these potentially effective biological therapies for cardiac conditions, like myocardial infarction, has been limited by efficiency and specificity of delivery of therapeutic agents. For example, for gene therapy approaches, plasmid delivery to the heart is very inefficient whereas there are significant time delays associated with cardiac gene delivery using viral-based vectors in

addition to issues of pre-existing neutralizing antibodies or exciting an immune responses to certain viral vectors. The well-characterized cell penetrating peptides, like TAT from HIV coat protein, homopolymers of arginine or lysine, are not cell specific and transduce hepatocytes and multiple other organs in addition to the heart. Identifying a peptide with transduction capabilities specific for the heart would allow for new approaches for effective cardiac delivery of therapeutics to be developed.

1.2 PROTEIN TRANSDUCTION DOMAINS

Protein transduction domains (PTD) or cell penetrating peptides (CPP) are small peptides able to transverse plasma membranes and carry peptides, full-length proteins, oligonucleotides, iron nanoparticles and liposomes as “cargoes”. These PTDs can be broadly classified under three classes; cationic or positively charged PTDs, hydrophobic or protein leader sequence-derived domains and peptides identified by phage display that are able to transduce cells in a cell-type specific manner. Interest in these moieties began with the simultaneous reports by Franckel and Pabo [6], and Green and Lowenstein [7], that HIV-1 TAT (transactivator of transcription) protein was able to cross plasma membranes. A few years following these initial reports, the Antennapedia homeodomain of *Drosophila melanogaster* was shown to act in a similar manner [8]. Further investigation revealed that smaller peptides derived from these larger full-length proteins were responsible for their transduction abilities and could carry multiple, different, full-length proteins as cargoes [9-11]. Interest in these unique peptides has been burgeoning leading to identification of multiple naturally occurring [12-14] as well as engineered PTDs [15-16].

Multiple studies have shown the ability of PTDs to deliver peptides of therapeutic potential [17-18], full-length proteins [11, 19], oligonucleotide [20], 40nm iron nanoparticles [21-22], drugs [23], and liposomes [24]. In addition there is intense interest in developing PTDs as vehicles for delivery of small interfering RNA (siRNA) *in vitro* [25-26] and *in vivo* [27-28], with novel strategies aimed at PTD and siRNA complex escaping the endosomal compartment [29-30] or increasing efficacy by avoiding the nuclear compartmentalization [30]. These selected number of publications, involving myriad applications of PTDs, highlight not only the interest but also the potential application of PTDs as delivery tools in a variety of disease models employing many different strategies of therapeutic potential. Although PTDs have shown the ability to deliver biologically active cargo *in vivo*, and even cross the blood-brain barrier [11], the lack of cell or tissue specificity seen with the cationic or hydrophobic PTDs, limits their therapeutic potential and would add to their toxicity limiting use *in vivo*. In light of these considerations, it has become increasingly apparent that for PTDs to be useful, it is necessary to identify peptides that are tissue specific in order to limit toxicity and enhance therapeutic potential. To identify such peptides, biopanning or phage display has emerged as a powerful technique.

1.3 BIOPANNING OR PHAGE DISPLAY

The principal underlying display technologies consist of the ability to physically link phenotypes of polypeptides displayed on a certain platform to their corresponding genotype. Typically the phenotype registered in display experiments is through physical binding and serial selection. Figure 1 shows the schema of available display technologies [31].

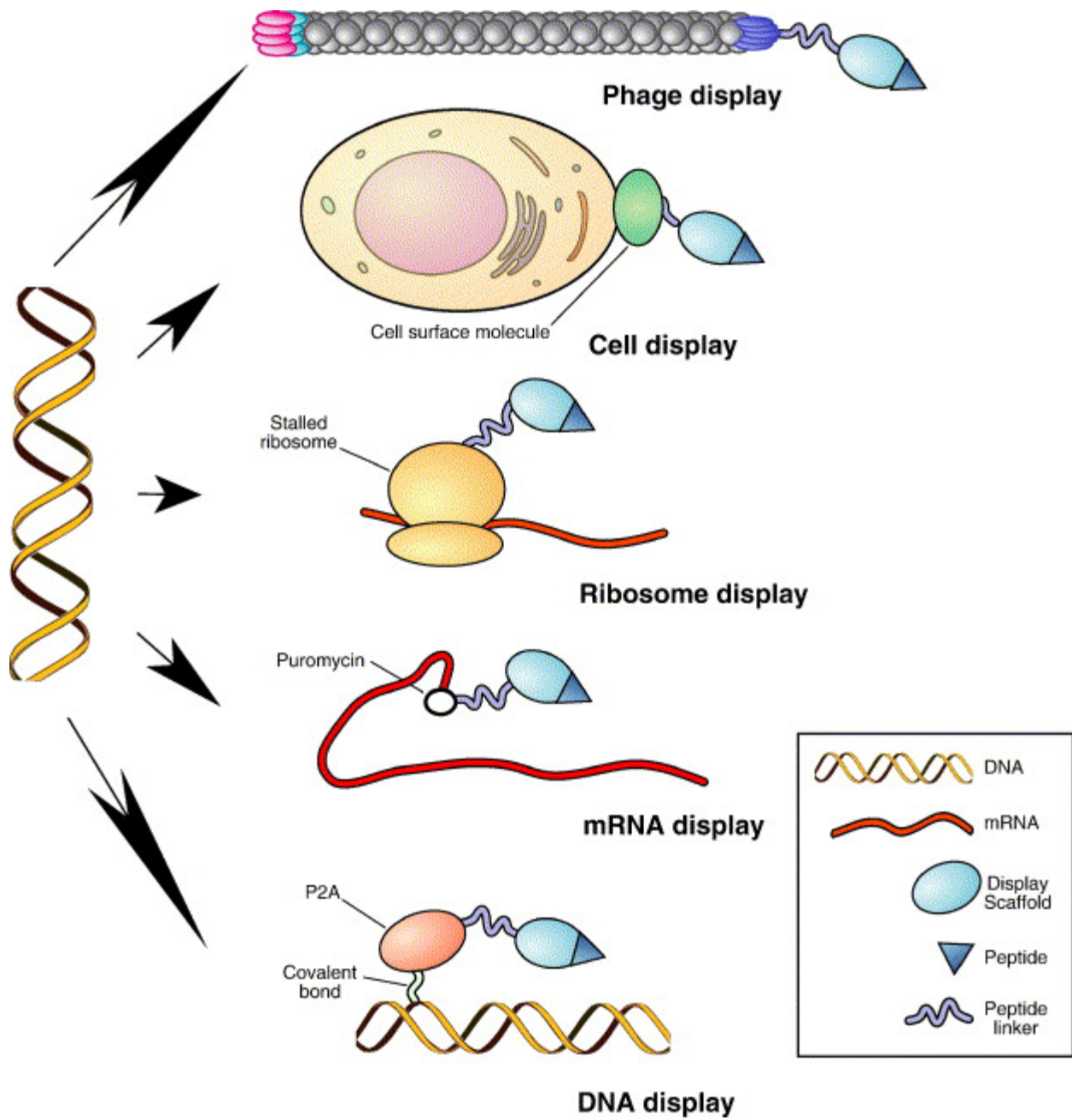


Figure 1. Schema of available display technologies.

All display platforms are based on the ability to physically link the polypeptide produced by a library clone to its corresponding genotype. This allows one to recover the DNA encoding the clone selected based on the desired polypeptide phenotype, such as binding to the target.

The ability to modify filamentous bacteriophage to express polypeptides on the surface as part of the bacteriophage's coat protein was first reported by Smith [32] in 1985. This technique was originally developed to map epitope-binding sites of antibodies by mapping against immobilized immunoglobulins. This seminal work led to phage display being utilized as a powerful method to detect polypeptide binding with a diverse range of biological, as well as technical and medical applications [33].

A brief word on the biology of phage is warranted here. "Phages" or bacteriophage are prokaryotic bacterial viruses, which are the most abundant biological entities in the environment with estimates ranging from 10^{30} to 10^{32} and play a key role in many biological systems. Bacteriophages as a group are extremely diversified. The number of known phage has been expanding for decades at a rate of ~100/year. The Felix d'Herelle Reference Center for Bacterial Viruses is charged with keeping track of these. The first survey was published in 1967 with latest surveys made in 1995 and 2000 [34-35]. Phages are broadly classified as Tailed, Polyhedral, Filamentous or Pleomorphic. According to the latest electron microscopic analysis of over 500 phages [36], the vast majority (~96%) are tailed with polyhedral, filamentous and pleomorphic phage comprising 3.7% of the total number of phage studied. Of these, filamentous phage has been studied widely for the purpose of phage display. Filamentous phage are non-lytic and leave the host by budding through the host plasma membrane without killing their pilli-bearing host bacteria, though markedly slowing it's rate of replication. The filamentous phage best studied

biochemically and genetically is the M13 and its close relative fd bacteriophage. Both are F-specific phages that infect *Escherichia coli* bacteria.

M13 phage is a long, thread shaped particle, 6.5nm in diameter and 900nm in length. Its genome is a single-stranded, circular DNA containing 6,407 nucleotides protected by a long cylindrical protein coat. The most abundant coat protein is the major coat protein pVIII, of which ~2700 molecules are present on the coat. There are only 5 copies of the minor coat protein pIII at one end of the phage particle, which along with 5 molecules of another minor coat protein, pVI, is involved in bacterial cell binding. At the other end of the phage are minor coat proteins pVII and PIX, which are needed for initiation and maintenance of phage assembly inside the host. During the assembly process the resulting fusion coat proteins are transported to the bacterial periplasm or inner cell membrane and incorporated into a new phage particle along with the single stranded DNA genome of the phage carrying the genotypic information for the displayed fusion protein. Figure 2 is a schematic representation of phage structure, followed by a diagrammatic representation of phage assembly and budding from an *E. coli* host cell.

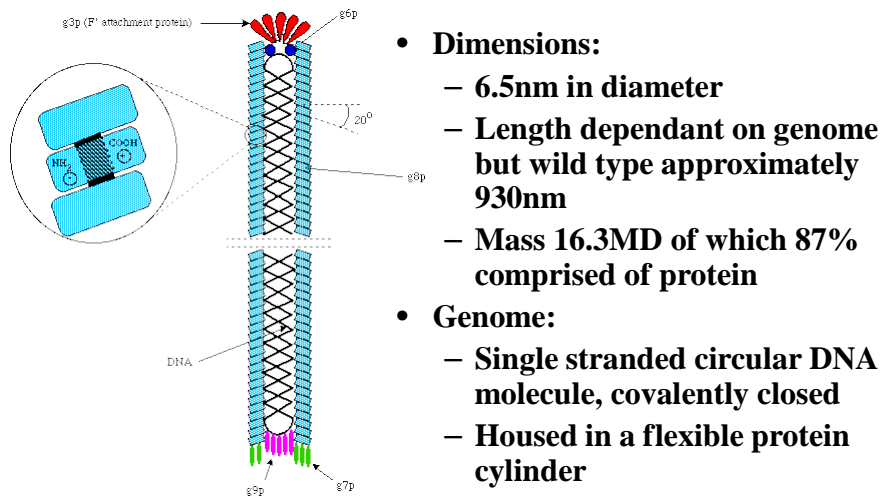


Figure 2. Structure of M13 bacteriophage.

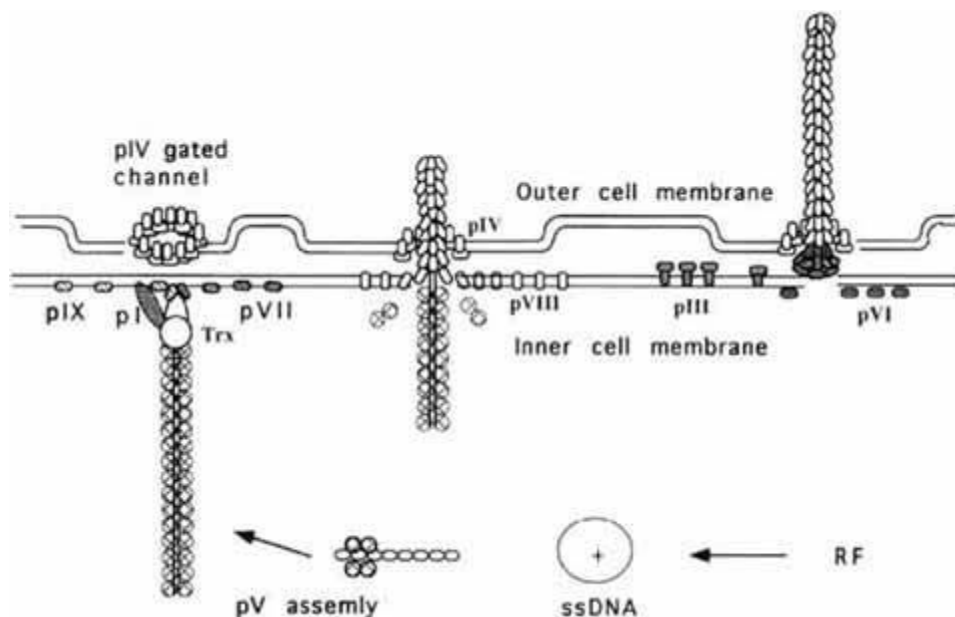


Figure 3. Assembly of phage virion and its release from *E. coli* cells.

Libraries have been constructed utilizing virtually all of the coat proteins of filamentous phage modified for the purpose of phage display. However the commonest filamentous phage libraries consist of phage with modified minor capsid protein pIII, expressing 10^9 peptides, or more, of different permutations. Filamentous phage infect pilus-positive bacteria that are not lysed by the infecting phage and secrete multiple, identical copies of it displaying a particular insert. Phage display constitutes exposing the target of interest to a large, randomized library of phage expressing peptides on a surface coat protein. After binding, the non-relevant phage is washed away, the bound phage eluted, expanded in pilli-positive host bacteria, and re-exposed to the target of interest. Four to six cycles of biopanning lead to adequate enrichment with the relevant clone phage, which can subsequently be sequenced, and the peptide motif carried as a fusion coat protein identified. This technique allows one to identify peptides able to bind immobilized targets, surfaces of different cell types and even target tissues *in vivo* without a priori knowledge of the target ligand, as outlined in the figure below.

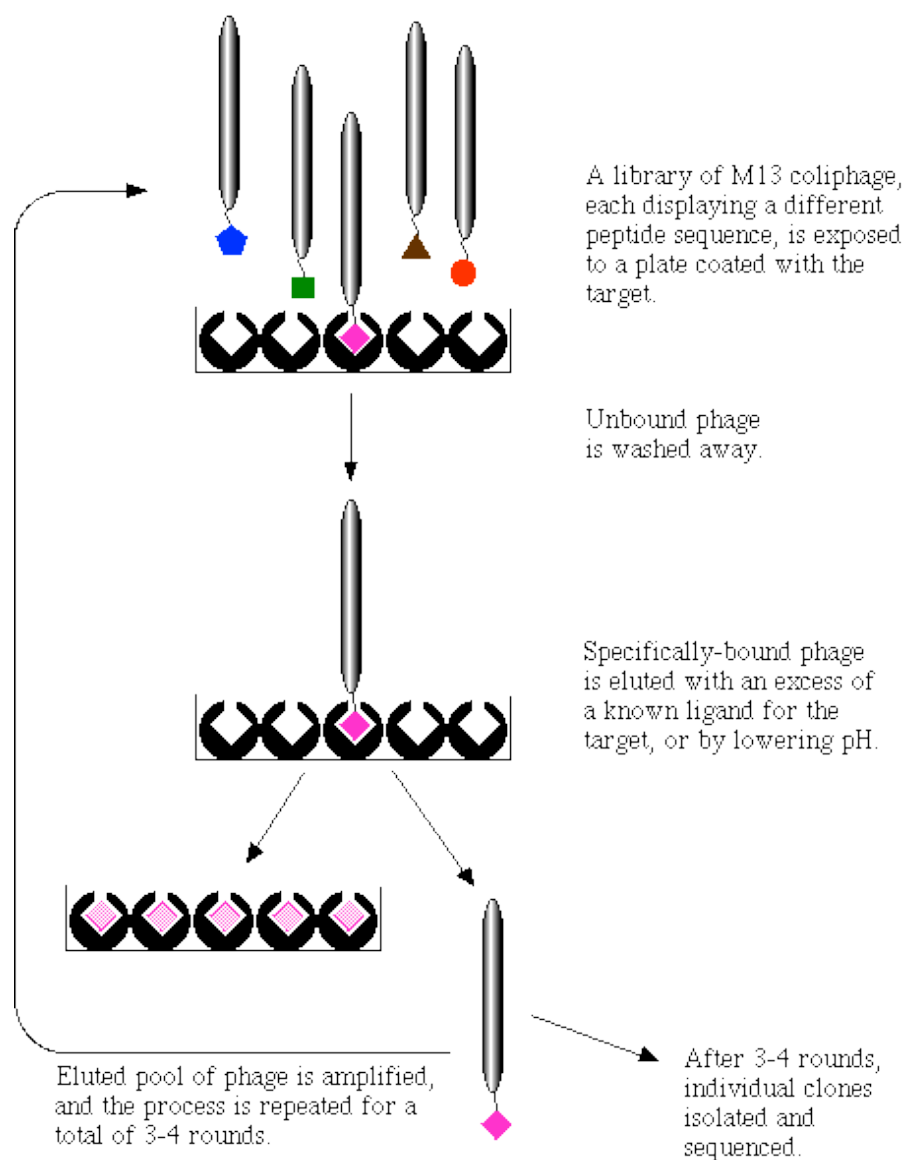


Figure 4. Schematic representation of steps in screening a peptide phage display library.

Initial studies utilizing phage display libraries were limited to *in vitro* work, phage display being carried out against immobilized antigen targets or cell-specific ligands. Arap and colleagues [37] showed the feasibility of *in vivo* phage display leading to identification of peptides homing to tumor vasculature as well as the ability to use these peptides to target anti-

cancer therapy. Further *in vivo* work has clarified that not only tumor vasculature but also normal organs, like adipose tissue [38] and the heart [39], among other organs [40-41], bear ligands that can be targeted by *in vivo* phage display. Work in our lab has identified peptides targeting synoviocytes which are able to deliver therapies to synovial fibroblasts *in vivo* [42] as well as protect islet cells in a mouse model of diabetes [43]. Hence biopanning or phage display has evolved as a powerful technique for identification of peptides targeting not only immobilized antigens, but cell-specific ligands *in vitro*, vasculature of various organs and tissue types *in vivo*.

1.4 NUCLEAR FACTOR KB

NF- κ B was first identified as a transcription factor binding to the intronic enhancer of the Kappa light chain gene in B-cells over 20 years ago [44-45]. It soon became apparent that this transcription factor plays a major role in orchestrating innate and adaptive immune responses that are key to a multicellular organism's ability to respond to environmental, mechanical, chemical and microbial stresses. It also became apparent that deregulation of this transcriptional activity can lead to a myriad of seemingly different autoimmune diseases like rheumatoid arthritis, inflammatory bowel diseases, multiple sclerosis as well as cancer. A Pub Med search today would reveal over 30,000 papers. Therefore the review that follows will, out of necessity, be kept brief, and to the point as it relates to the thesis work done.

NF- κ B transcription factor is a family of five cytosolic proteins; p50, p52, p65 (RelA), c-Rel, RelB, encoded by NFKB1, NFKB2, RELA, REL, and RELB respectively. All of them share an N-terminal Rel-homology domain (RHD) that is responsible for DNA binding and homo- or hetero-dimerization. RelA, c-Rel and RelB also contain C-terminal transcription activation

domains (TAD), whereas p50 and p52 do not and depend on heterodimerization with other subunits to lead to activation of transcription. NF- κ B dimers bind to specific κ B consensus sequences (5' - GGGRNWYYCC - 3'; where N=any base, R=purine, W=adenine or thymine, and Y=pyrimidine) within the promoter-enhancer regions of target genes and regulate transcription through recruitment of co-activators and repressors. These proteins reside in the cytosol in an inactive state either bound to inhibitors called I κ Bs or as the unprocessed or precursor proteins p100 and p105. In response to stimuli, p100 and p105 are processed to form p52 and p50 respectively. Three "classical" proteins, I κ B α , I κ B β and I κ B ϵ , are characterized by the presence of multiple ankyrin repeats that mediate binding of NF- κ B dimers and interfere with the nuclear localizing signal of the latter, thus keeping these proteins cytosolic and hence inactive.

In response to appropriate stimuli, NF- κ B activation occurs, leading to its nuclear accumulation. Activation of NF- κ B by phosphorylation and degradation of inhibitory I κ Bs occurs in the classical or canonical pathway that comes into play in response to TNF- α or IL-1 binding to their receptors. The classical pathway involves phosphorylation of the I κ B proteins at specific serine residues (phosphorylation of I κ B α on serine residues 32 and 36, and phosphorylation of I κ B β on serine residues 19 and 23), marking the protein for ubiquitination and subsequent degradation, with release of the inhibitory influence on the NF- κ B dimers and their subsequent activation. This pathway centers on activation of the trimeric I κ B kinase complex, (IKK), comprising the catalytic subunits IKK α , IKK β and the non-catalytic subunit, IKK γ (also called NEMO for NF- κ B essential modulator). IKK α and IKK β share 50% sequence identity with 65% sequence identity of their catalytic subunits. There are some notable differences with IKK α having a nuclear localizing signal that is unique to it and IKK β having a

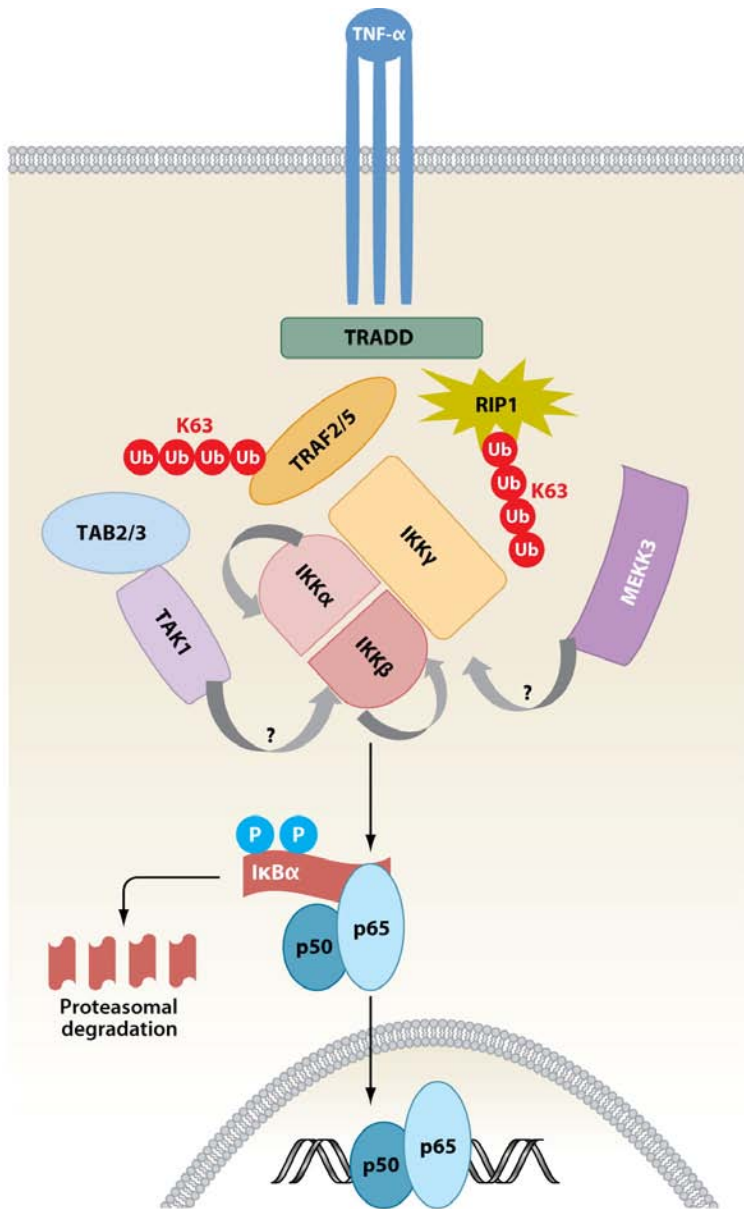
C-terminal NEMO-binding domain that exhibits much greater affinity for IKK γ /NEMO than IKK α . IKK γ or NEMO is obligatory for classical NF- κ B activation as in its absence IKK complex can no longer be formed or activated [46-47]. Of the two catalytic subunits, IKK β is the major I κ B kinase in most cell types with few exceptions, and plays a central role in the canonical activation pathway. In contrast IKK α is essential for activation of the alternate pathway.

1.4.1 Classical NF- κ B Activation Pathway

As mentioned above, NF- κ B activation can occur via the canonical or classical pathway, or the alternate pathway. Activation via the canonical pathway requires activation of the IKK complex. The three major IKK proteins consist of IKK α , IKK β and IKK γ (or NEMO- NF- κ B essential modulator) which dimerize through the leucine zipper domain which is also required for kinase activity. Both IKK α and IKK β bind the third protein component of the IKK complex, NEMO, through the C-terminal hexa-peptide, NEMO-binding domain (NBD; Leu-Asp-Trp-Ser-Trp-Leu). Competition experiments and biophysical analyses using the NBD peptide indicate that IKK β binds to NEMO with higher affinity than IKK α . Activation of the IKK complex requires phosphorylation of at least one of the IKK subunits. Active IKK β is phosphorylated on two serines, Ser177 and Ser181 within the activation loop of the kinase domain. Similarly IKK α is phosphorylated on activation loop serine residues 176 and 180. The exact mechanism of this activation, autophosphorylation or an upstream IKK kinase mediated phosphorylation, remains to be elucidated.

Much of the current understanding of the classical pathway of NF- κ B activation comes from studies of TNF- α signaling. TNF- α binds to two receptors, TNFR1 and TNFR2, of which TNFR1 binding plays a much broader role in NF- κ B activation. Binding of TNF- α to its receptor

TNFR1 leads to recruitment of TNFR1-associated death domain protein (TRADD). Receptor engagement also results in a biphasic ubiquitination of RIP1, a member of related protein kinases. However studies of RIP1 deficient cells show that it is likely needed for a docking action for IKK through its interaction with IKK γ [48]. How this leads to IKK activation is unclear but one mechanism proposed is recruitment of MEKK3, a kinase to the TNFR1 signaling complex, leading to phosphorylation of the IKK α and IKK β activation loops [49]. However MEKK3 is not unequivocally an essential IKK kinase and there are likely many others, like TAK1, and the relative importance/role of an IKK kinase is likely to be cell-dependent. TAK1 might be recruited to the TNFR1 signaling complex via TRAF-2 dependent polyubiquitination of RIP1 or by more direct recruitment of TAK1 via TRAF2 or TRAF6. Although the exact nature and events leading to IKK activation differ depending on the stimulus (TNF- α , IL-1, antigen binding etc), the ultimate common path is activation of the IKK α and/or IKK β by phosphorylation of serine residues in the activation loop. This activation of the IKK complex leads to phosphorylation of I κ B α , leading to its proteasomal degradation and release of its inhibition of p50/p65 heterodimers, their nuclear translocation and initiation of transcriptional activity. This is schematically represented in the figure below (Figure 5) for TNF- α mediated NF- κ B activation [50].



AR Vallabhapurapu S, Karin M. 2009.
 Annu. Rev. Immunol. 27:693–733

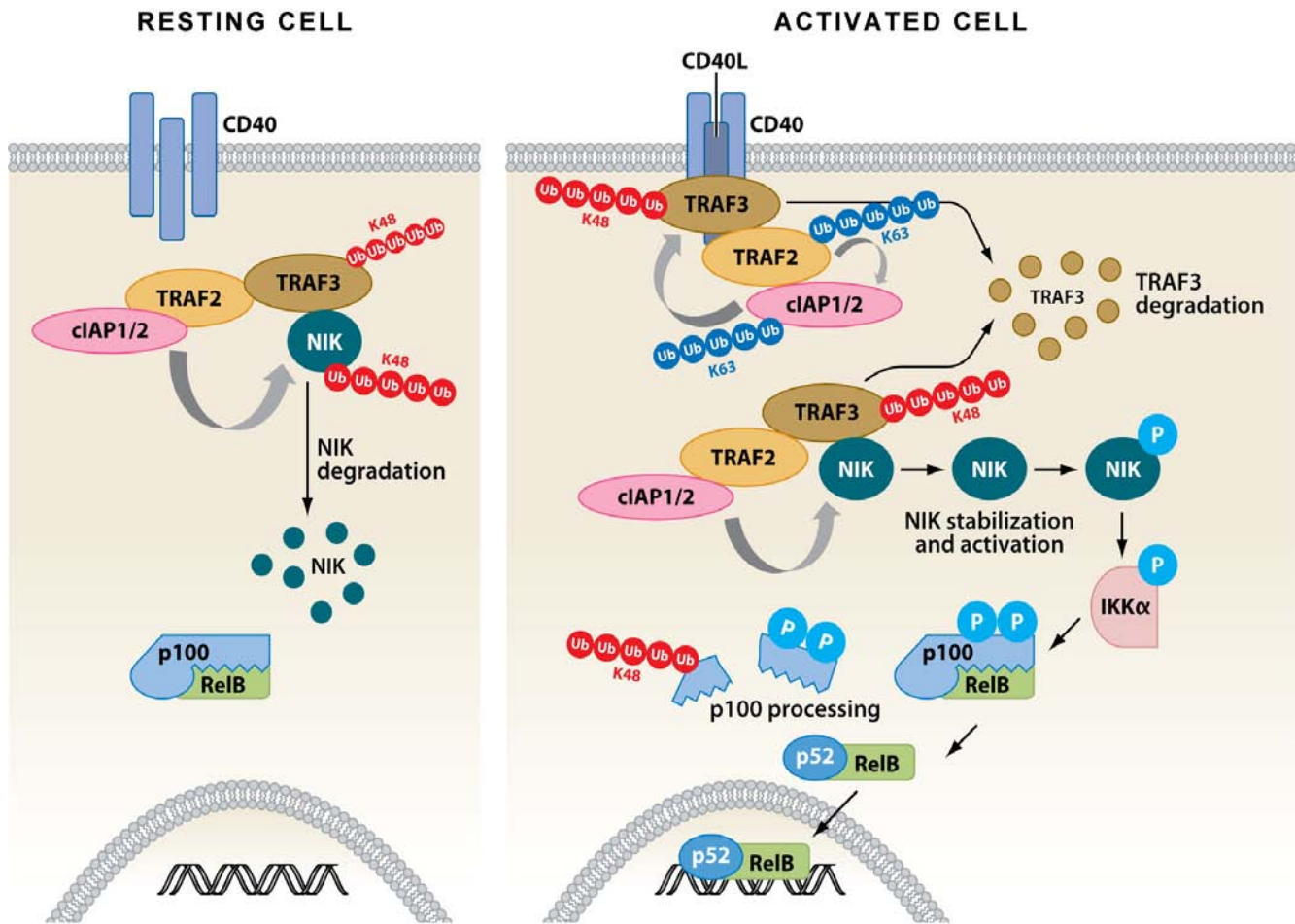
Figure 5. Activation of classical NF-κB signaling by TNF-α.

Ligation of TNFR1 results in TRADD-dependent TRAF2/TRAF5 and RIP1 recruitment. TRAF2 causes K63-linked ubiquitination of RIP1 and also recruits IKK to the receptor complex, where binding of IKK γ to ubiquitinated RIP1 stabilizes IKK interaction with the receptor complex. This may also lead to a conformational change of the IKK complex. TAB2 and TAB3 interact with TRAF2 and TAK1, leading to TAK1 activation that may then phosphorylate IKK β . Alternatively, MEKK3, which is brought near the receptor complex presumably by RIP1 may also phosphorylate and activate IKK. On the other hand, IKK may also be activated by autophosphorylation. Activated IKK phosphorylates I κ B α at specific serine residues, leading to the proteasome-mediated degradation of the latter. Degradation of I κ B α releases the NF- κ B heterodimers, which then migrate to the nucleus and regulate gene expression.

1.4.2 Alternate NF- κ B Activation Pathway

NIK is an unstable protein, subject to rapid turnover in non-stimulated cells, first identified as a protein kinase, whose over-expression results in NF- κ B activation [51]. Stimulation of B cells with certain TNF family members, such as CD40L, results in stabilization of NIK trans-autophosphorylation, its subsequent accumulation leading to activation of IKK α . In the resting state, NIK is associated with TRAF2, TRAF3 and cIAP1/2. TRAF3 appears to function as an adapter linking NIK to the ubiquitin ligase complex consisting of TRAF2/cIAP1/1. This complex causes ubiquitination of NIK and consequent degradation. Upon cell stimulation with appropriate receptor-ligand binding, a protein ubiquitination cascade ensues with TRAF2 ubiquitinates cIAP1/2 through a K63-linkage leading to the activation of their K48-specific ubiquitin ligase activity towards TRAF3. This cascade leads to NIK stabilization, accumulation, and activation of IKK α through phosphorylation, leading to processing of p100 to its p52 residue and release of

RelB/p52 heterodimers allowing for nuclear translocation, as demonstrated in Figure 6 below [50].



 Vallabhapurapu S, Karin M. 2009. Annu. Rev. Immunol. 27:693–733

Figure 6. Activation of NF-κB signaling by CD40.

In resting cells (*left*), p100, via its C-terminal ankyrin repeats, binds and keeps RelB in the cytosol. NIK, which is an essential kinase involved in the phosphorylation and proteasome-

mediated C-terminal processing of p100, is maintained at very low levels owing to rapid proteasome-dependent degradation. TRAF3 links NIK to an E3 complex containing TRAF2 and cIAP1/2, thereby promoting cIAP1/2-mediated K48-linked NIK polyubiquitination and proteasomal degradation. TRAF3 also undergoes a low level of K48-linked polyubiquitination under resting conditions. Activation of CD40 by CD40L (*right*) leads to recruitment of the cIAP1/2:TRAF2:TRAF3 complex to the receptor, where cIAP1/2 undergoes TRAF2-dependent K63-linked polyubiquitination. TRAF2 also undergoes K63-linked self-ubiquitination. K63-linked ubiquitination of cIAP1/2 enhances their K48-specific E3 ubiquitin ligase activity toward TRAF3, leading to proteasomal degradation of the latter. As a result, TRAF3 levels in the cell drop below a critical threshold, and NIK can no longer be recruited to the cIAP1/2:TRAF2 complex. This leads to stabilization and accumulation of newly synthesized NIK and its activation presumably via autophosphorylation, resulting in activation of IKK α . Activated IKK α phosphorylates p100, leading to proteasome-mediated processing of p100 to p52. C-terminal truncation of p100 releases the p52:RelB heterodimer, which migrates to the nucleus and regulates transcription of its target genes.

Once activated, the termination of active NF- κ B heterodimers is poorly understood. Studies have focused on upstream targets and shown that among the myriad of genes activated by NF- κ B, I κ B protein synthesis is up regulated, thus serving as a negative feedback loop. However terminating the activity of DNA-promoter bound NF- κ B remains poorly understood and is a subject of active ongoing research.

1.5 NEMO-BINDING DOMAIN PEPTIDE

As detailed above, activation of NF- κ B, via the canonical pathway, requires activation of the I κ B-Kinase, or IKK complex. This complex consists of three major proteins, IKK α , IKK β and IKK γ , the latter also known as NEMO (NF- κ B essential modulator). An elegant study by May et. Al. [52] revealed that this interaction occurs not only between IKK β and NEMO, but also IKK α and NEMO, albeit with lesser affinity. This study also mapped the region interacting with NEMO to the NH₂-terminal α -helical region of both IKK α and IKK β , consisting of 6 amino acids, Leu-Asp-Trp-Ser-Trp-Leu, and was termed the nemo-binding domain (NBD). In the study a cell permeable peptide was created consisting of the Antennapedia homeodomain, a PTD, fused to the 11 amino acids from T735 to E745 of IKK β . This peptide was termed NBD peptide. A mutant NBD peptide was also generated with W739 and W741 replaced with alanines. The NBD peptide inhibited *in vitro* interaction of IKK β with NEMO and disrupted formation of endogenous IKK complexes in HeLa cells. Pre-treating HeLa cells with this NBD peptide inhibited TNF- α induced NF- κ B activation. Interestingly, the basal NF- κ B activity was enhanced approximately two-fold by the NBD peptide, suggesting that removal of NEMO slightly increases the basal activity of the IKK complex. The differential binding abilities of IKK α and IKK β with NEMO were further characterized by mutational analysis showing that for IKK β nemo-binding domain to interact with NEMO, the aspartate residues at 738 and two tryptophan residues at 739 and 741 were critical [53]. The requirement for binding to IKK α was not equally stringent, with the first tryptophan residue at position 740 being most important.

Since the description of the NEMO-binding domain and generation of a small peptide able to inhibit IKK complex activation, this peptide has been studied in numerous animal models of inflammatory diseases. The original report detailed efficacy of this peptide in reducing

phorbol 12-myristate 13-acetate induced ear edema, repressing E-selectin expression by HUVEC cells in response to TNF- α , as well as decreasing peritonitis in mice injected with intraperitoneal zymosan [52]. Following these initial reports, the NBD peptide in association with various protein transduction domains (PTD-5, TAT or Antennapedia homeodomain), has been shown to protect pancreatic islet cells from detrimental effects of IL-1 β [43], block osteoclastogenesis, synovial inflammation and bone erosion in inflammatory arthritis [54-55], and be beneficial in two different models of murine colitis [18, 56]. In addition to murine models of inflammatory bowel disease, NBD peptide was able to decreased bowel injury and decrease mortality in a neonatal rat model of necrotizing enterocolitis [57]. The table below summarizes the studies that have been undertaken to date utilizing NBD peptide.

Table 1. Summary of studies utilizing NBD peptide.

Authors	Journal/Year	Model	Result
Long, YM et. Al. [58]	W J Gastro/2009	Rat/Pancreatitis	↓ Inflammation
Ianaro, A et. Al. [59]	Canc Lett/2009	Melanoma cell line	↓ Proliferation
Dave, SH et. Al. [18]	J Immun/2007	Mice/Colitis	↓ Inflammation/colitis
Tapia, MA et. Al. [60]	Cell Cycle/2007	Breast cancer cell line	↑Doxorubicin sensitivity
Shibata, W et. Al. [56]	J Immun/2007	Mice/Colitis	↓ Inflammation/colitis
De Plaen, IG et.	Pediat Res/2007	Rat/Necrotizing colitis	↓ Bowel Injury

Table 1 - continued

Al. [57]			
Tas, SW et. Al. [61]	Arthir Res Ther/2006	Rat/Arthritis	↓ Arthritis Severity
van den Tweel, ER et. Al. [62]	Pediat Res/2006	Rat/Cerebral ischemia	↑ Neuronal Damage
Di Meglio, P et. Al. [55]	Arthrit rheum/2005	Mice/Carrageenan-induced paw edema	↓ Paw Edema
Dai, S et. Al. [54]	JBC/2004	Mice/Inflammatory arthritis	↓Inflammation ↓erosions
Biswas, DK et. Al. [63]	PNAS/2004	Breast cancer cell line	↑Apoptosis/↓cell proliferation
Ashikawa, K et. Al. [64]	Bioch Pharma/2004	Lymphoid/myeloid cell line	↓Doxorubicin sensitivity
Rehaman, KK et. Al. [43]	JBC/2003	Mouse islet cell line	↑Viability ↑islet cell function
Thomas, RP et. Al. [65]	Surgery/2002	Pancreatic cancer cell line	↑Apoptosis/↓cell viability

From the foregoing studies, it would appear that the NBD peptide, with an appropriate protein transduction domain acting as a delivery vehicle, could be of use as a beneficial, anti-inflammatory agent.

1.6 NF- κ B AND THE HEART

Many of the key elements of the canonical NF- κ B pathway have been identified in cardiac myocytes. Exposing cardiac cells to stimuli like LPS, cytokines or reactive oxygen species as well as ischemia-reperfusion leads to phosphorylation and subsequent degradation of I κ B α . The cytoplasmic to nuclear shuttling of p65/p50 heterodimers has also been confirmed in cardiac myocytes, using electrophoretic mobility shift assays that employed κ B sequence-containing probes that confirmed the identity of the proteins within these complexes [66-68]. Of the 5 NF- κ B family proteins, only p65, p50, p52 and RelB have been identified in cardiac myocytes thus far. These family members can form heterodimers and act as transcription factors, or p50 can homodimerize to act as a repressor of transcription. Although detailed studies of the dimeric species present in the heart have not been performed, it would appear that NF- κ B-dependent transcription activation or repression is regulated primarily by p65/p50 or p50/p50 dimers respectively [69-72]. As detailed earlier, NF- κ B dimers reside in the cytoplasmic compartment and are kept inactive by their association with inhibitor I κ B proteins. Of the 8 I κ B family members, only I κ B α , I κ B β , I κ B ϵ , Bcl-3, p100 and p105 have been identified in the heart.

Studies have revealed a role for NF- κ B stimulation in macrophages in atherosclerotic plaques [73-75] as well as inhibition of endothelial NF- κ B protecting mice from atherosclerosis [76]. In addition several studies have high-lighted the importance of NF- κ B in generation of cardiac hypertrophy in response to mechanical stretch [77-78], transverse aortic banding [79], in response to Angiotensin II [80] with blockade of NF- κ B in transgenic I κ B α dominant-negative mice or RNA interference leading to prevention of cardiac hypertrophy and heart failure [81-84]. The role of NF- κ B appears to be quite complex in murine models of infarction or ischemia/reperfusion. *In vivo* molecular imaging utilizing transgenic mice expressing Luciferase

under an NF- κ B promoter site revealed that post infarction NF- κ B is up regulated with a peak occurring at day 3. After that, the activity level decreases but remains elevated for up to 8 weeks post-infarct (the maximum length these mice were followed) [85]. On one hand, NF- κ B activation is necessary to generate the cardioprotective response associated with ischemic preconditioning, as several groups have demonstrated that this beneficial effect is lost with inhibition of NF- κ B signaling [72, 86-88]. On the other hand inhibiting NF- κ B activation by using p50 knockout mice [89], over-expressing A20 (an inhibitor of NF- κ B protein) [90], adenoviral delivery of I κ B [91-92], or adenoviral delivery of MyD88 [93] led to decrease in infarct size in rodent models of ischemia-reperfusion or infarction. Double-stranded oligodeoxynucleotides with specific affinity for NF- κ B used as decoys in rat hearts led to more rapid recovery of heart function after heart transplantation [94] and reduced infarct size in a murine model of ischemia-reperfusion [95]. In an isolated report, transgenic mice harboring a mutated form of I κ B α had increased susceptibility to tissue injury after acute left anterior descending occlusion [96]. In addition small molecular inhibitors of NF- κ B have shown beneficial effects in reducing infarct size in murine models [97-101]. Interestingly one group of researchers showed curcumin as having effective NF- κ B inhibitory actions and ability to attenuate plasma inflammatory cytokine surge and cardiomyocyte apoptosis following cardiac ischemia-reperfusion [102-103]. These studies and the models they used are summarized below in Table 2.

Table 2. Summary of NF-kappa B studies with cardiac ischemia-reperfusion injury or myocardial infarction.

Authors	Journal/Year	Model	Infarct Size
Timmers, L et. Al. [104]	Circ Res/2009	p50 KO/MI/mouse	↔/Adverse Remodeling
Kawano, S et. Al. [3]	AJPHCP/2006	p50 KO/MI/mouse	↔/Improved Remodeling
Wakatsuki, S et. Al. [105]	Expert Opin Ther/2008	IMD-0560/MI/rat	↔/Improved Remodeling
Frantz, S et. Al. [106]	FASEB J/2006	p50 KO/MI/mice	↔/Improved Remodeling
Misra, A et. Al. [96]	Circ/2003	mut IκBα/MI/mice	↑ Infarct Size
Meili-Butz, S et. Al. [97]	Eur j Pharm/2008	Dimethyl fumarate/rat/IR	↓ Infarct Size
Moss, NC et. Al. [98]	AJPHCP/2007	Bay65-1942/mice/IR	↓ Infarct Size
Frantz, S et. Al. [89]	Am J Pathol/2007	p50 KO/mice/IR	↓ Infarct Size
Trescher, K et. Al. [91]	Cardiovasc Res/2006	↑IκB expression/rat/MI	Improved Remodeling
Hua, F et. Al. [93]	Bioch Biop Res /2005	Ad5-dnMyD88/mice/IR	↓ Infarct Size
Yeh, CH et. Al. [102]	J Surg Res/2005	Curcumin/rabbit/IR	↓ Infarct Size
Trescher, K et. Al.	Eur J Cardioth Surg/2004	Ad-IκBα	↔/Improved

Table 2 - continued

[92]			Remodeling
Onai, Y et. Al. [99]	Cardiovasc Res/2004	IMD-0354/rat/IR	↓/Improved Remodeling
Squadrito, F et. Al. [107]	Lab Invest/2003	rAAV/I κ B α /mice/IR	↓ Infarct Size
Pye, J et. Al. [100]	AJPHCP/2003	20S proteasome inh/pig/IR	↓ Infarct Size
Kupatt, C et. Al. [108]	Gene Ther/2002	NF- κ B decoy/pig/IR	↓/Improved Remodeling
Morishita, R et. Al. [95]	Nat Med/1997	NF- κ B decoy/pig/IR	↓ Infarct Size

None of these studies were designed to differentiate between inhibition of basal NF- κ B activity versus inhibition of surge in activity associated with ischemic damage and cytokine release. With this background in mind, we hypothesized that blockade of cytokine mediated surge in NF- κ B occurring via the canonical or classical pathway with the NBD peptide, in association with a PTD, would reduce infarct size in a mouse model of myocardial infarction.

2.0 PHAGE DISPLAY TO TARGET THE HEART

It is clear from the preceding chapter that protein transduction technology is rapidly evolving and expanding in its applications, even though the exact mechanism of transduction remains incompletely elucidated, and is unlikely to be the same for the different PTDs. The one limitation these general PTDs have is their non-tissue specificity and ability to transduce a wide-range of cell types limiting therapeutic efficacy and potentially increasing toxicity. Biopanning or phage display would then be one useful technique to identify new PTD(s) which are tissue selective. We therefore undertook phage display to screen a large peptide-display M13 phage library with the goal of identifying peptide(s) able to transduce heart tissue selectively *in vivo*.

2.1 PHAGE DISPLAY

We screened a 12-mer M13 phage peptide display library (NEB, E8110S) for possible cardio-selective peptide(s). We utilized a combinatorial *in vitro* single cycle followed by 3 *in vivo* biopanning cycles. The M13 phage display peptide library is based on a library of randomized dodecapeptides fused to a minor coat protein (pIII) of M13 phage. The displayed peptide (12-mer) is expressed at the N-terminus of pIII, i.e., the first residue of the mature protein is the first randomized position. The peptide is followed by a short spacer (Gly-Gly-Gly-Ser) and then the wild-type pIII sequence. The library consists of approximately 2.7×10^9 electroporated

sequences amplified once to yield approximately 100 copies of each sequence in 10 μ l of the supplied phage. Hence in the library there will be few phage that are relevant with a far excess of irrelevant phage clones. To maximize selection of the relevant phage and minimize the large pool of non-specific phage, the first cycle was carried out *in vitro* on H9C2 cells, a rat cardiomyoblast cell line. These H9C2 cells have been characterized biochemically, morphologically as well as electrophysiologically [109]. Although these cells showed similar sugar residues on the surface coat as isolated rat cardiomyocytes, heart-specific morphological structures were not detected. These cells did show outwardly rectifying, transient K⁺ current as well as inward current through Ca²⁺ channels. Nevertheless, despite these differences, these cells have been widely utilized to study molecular pathways involved in ischemia-related apoptosis, hypertrophy as well as doxorubicin-mediated cardiac toxicity [110-114].

Rat cardiomyoblast cell line, H9C2 cells, (ATCC, CRL-1446), were passaged at least for 4 cycles. These cells were trypsinized and re-plated once they were ~70-80% confluent. After 4 cycles they were grown again to ~70% confluence in a 6-well plate and incubated with 10ul, or ~10¹¹ pfu phage, for 6 hours, at 37°C/5% CO₂. At the end of the incubation period, the cells were washed 6 times with pre-warmed PBS, trypsinized with 0.25% Trypsin EDTA (GIBCO/BRL) for 5 minutes, and the cells pelleted by centrifugation for 5 minutes at a speed of 500rpms. The cells were lysed by a single freeze-thaw cycle, and the internalized phage tittered by infecting and growing in the provided *E. coli* bacteria. The recovered phage was amplified and re-tittered before use in mice for *in vivo* biopanning.

For *in vivo* phage display, Balb/c, female, 10-12 week old mice were pre-treated with intra-peritoneal chloroquine at a dose of 20mg/Kg the day before and the day of phage injection. This is in contrast to prior reports of *in vivo* phage display, where short circulation times

(typically 10-60 minutes) were used, since the purpose was to target the vascular endothelium of various organs and tumors of interest. We utilized a prolonged incubation time as our aim was to go beyond the endothelium and target cardiomyocytes. Molenaar et. Al. had reported that the *in vivo* half-life of the M13 phage was 4.5 hours [115]. Since we aimed to recover actual, internalized phage and reduce contamination from the pool of circulating phage, we employed a much longer circulation time of 24 hours, equivalent to 5.5 half lives. In order to reduce intracellular breakdown of internalized phage, we pre-treated mice with Chloroquine the day before and day of phage injection (10mg/Kg, intraperitoneally), an agent shown to increase intralysosomal pH in an attempt to increase chances of recovering internalized phage [116]. Phage were injected intravenously (retro-orbitally), mice euthanized 24 hours later, heart and kidneys dissected out, weighed and put through a collagenase digestion step. The isolated cells were lysed with a single freeze-thaw cycle, recovered phage tittered, amplified, re-tittered and injected again for a total of three *in vivo* phage display cycles. This experiment is represented schematically in the figure (Figure 7) below. The reagents utilized for these experiments, as well as the exact protocol details are presented in a step by step manner in Chapter 5, section 5.1: Protocol for Peptide Phage Display.

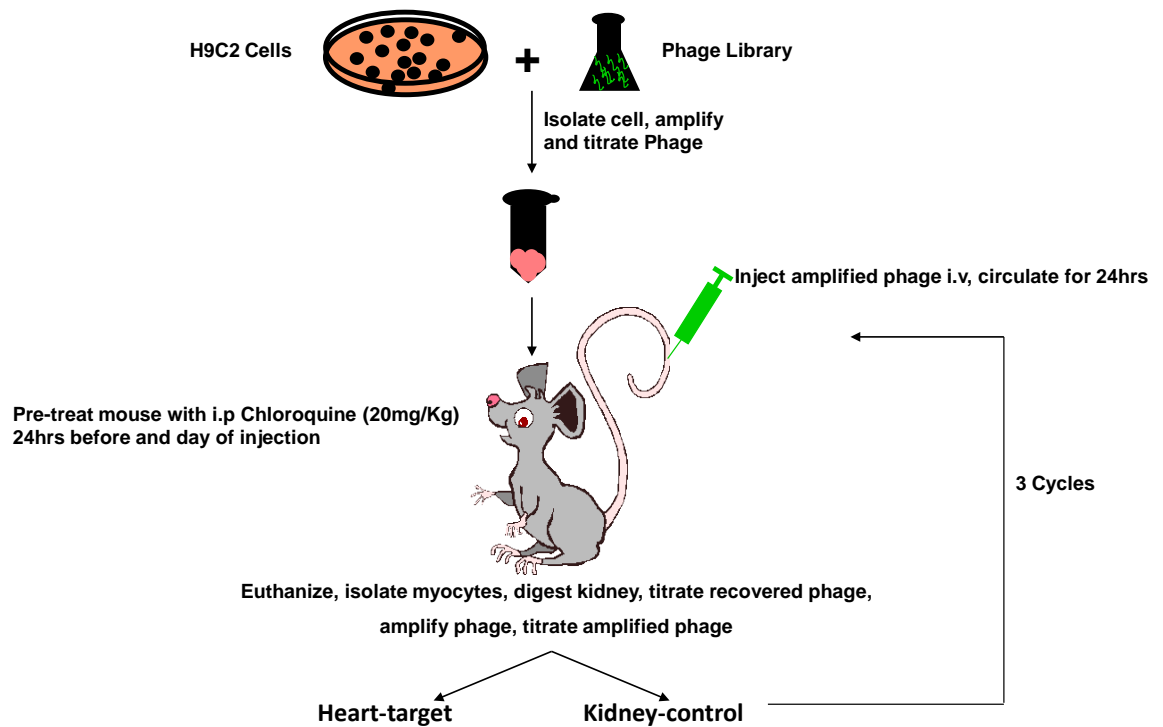


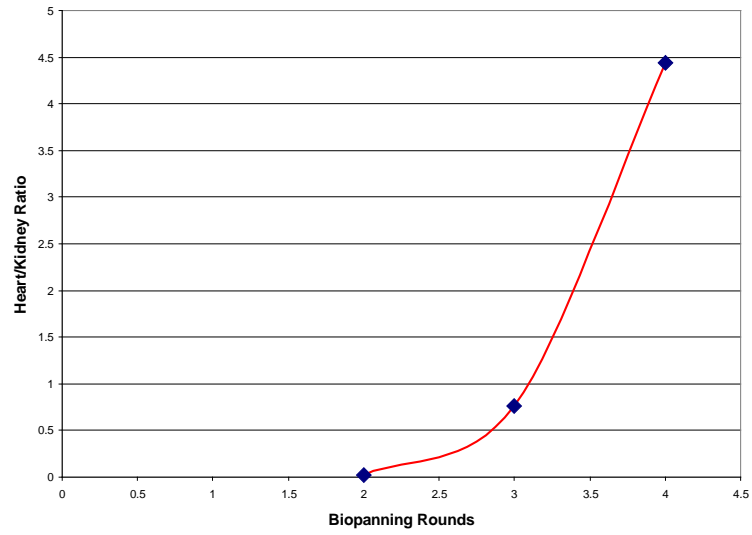
Figure 7. Experimental design of the combinatorial *in vitro* and *in vivo* phage display.

The recovered phage was normalized by gram of tissue digested and expressed as a ratio of heart to kidney and as an output to input ratio. The number of phage injected and recovered with each cycle is presented in Table 3 below.

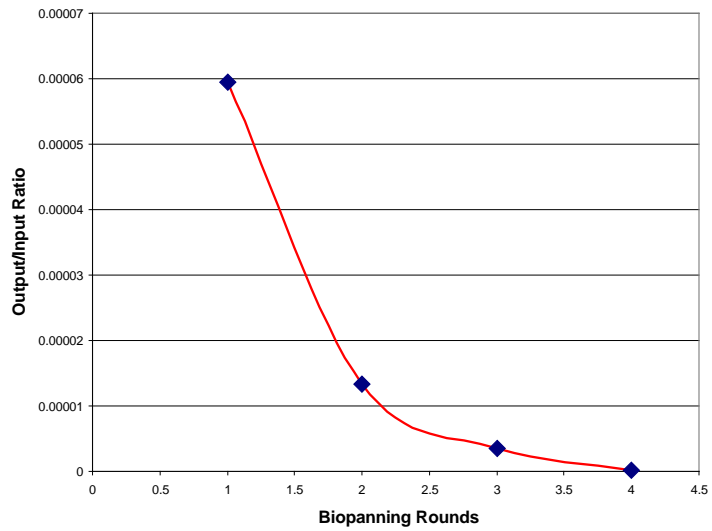
Table 3. Number of phage injected and recovered from each cycle of phage display

Round	Input Phage	Output-Heart	Output-Kidney	Output/Input Ratio	Heart/Kidney Ratio
1	1.00E+11	5.95E+06		0.0000595	
2	3.48E+10	4.63E+05	2.04E+07	0.0000133	0.023
3	3.42E+08	1.19E+03	1.55E+03	0.0000035	0.767
4	9.98E+08	2.46E+02	5.55E+01	0.0000002	4.436

These results are represented graphically in the figure below (Figure 8) showing heart to kidney ratios (a.) and output to input ratios (b.).



a). Heart to kidney ratio



b). Output to input ratio

Figure 8. Recovered phage normalized to tissue weight and plotted as a ratio of heart to kidney (a) and output to input ratios (b).

Although the recovered number of phage and the output-to-input ratio decreased over subsequent biopanning rounds, the ratio of heart-to-kidney phage increased with an exponential increase from 3rd to the 4th cycle. The number of recovered phage decreasing over time is not surprising as the viability is likely to decrease with repeat freeze-thaw cycles and storage over time.

After the 4th round of biopanning, 10 plaques were picked and the inserted sequences elucidated using the primers provided by New England Biolabs. Of these 10 plaques, 6 (60%) were identical and carried the sequence *gcccgtggcatctttcgtcgcagtattctcgtact*. This translates into the following peptide sequence: Ala-Pro-Trp-His-Leu-Ser-Ser-Gln-Tyr-Ser-Arg-Thr (APWHLSSQYSRT). This peptide was termed *Cardiac Targeting Peptide* or CTP and synthesized by the peptide synthesis facility either conjugated to 6-carboxyfluorescein, biotinylated at the N-terminus, or as a combination peptide carrying the nemo-binding domain peptide (NBD; sequence TALDWSWLQTE), which has been shown to inhibit activation of the inducible NF-kappa B Kinase (IKK) by binding to the regulatory subunit (Nemo) of IKK.

Peptides were synthesized by Fmoc (*N*-(9-fluorenyl)methoxycarbonyl) solid phase synthesis, N-terminally biotinylated or labeled with 6-carboxyfluorescein, purified by reversed-phase high performance liquid chromatography to >90% purity on an acetonitrile/H₂O-trifluoroacetic acid gradient, and confirmed by electrospray ionization mass spectrometry (Peptide Synthesis Facility, University of Pittsburgh). Lyophilized peptides were reconstituted in PBS to a 1 mM stock solution concentration. In some peptide preparations, due to variability in the salt concentration, the peptide would not go completely into solution in PBS. In those instances, a 40mM stock solution was made in DMSO, with subsequent dilution to 1mM working solution by addition of PBS. Care was taken to use peptides suspended only in PBS or

dH₂O for use in cell culture, and minimal DMSO used to re-suspend peptides for use in animal injections. All peptides were stored at -20°C as a lyophilized powder, and re-constituted on the day of use.

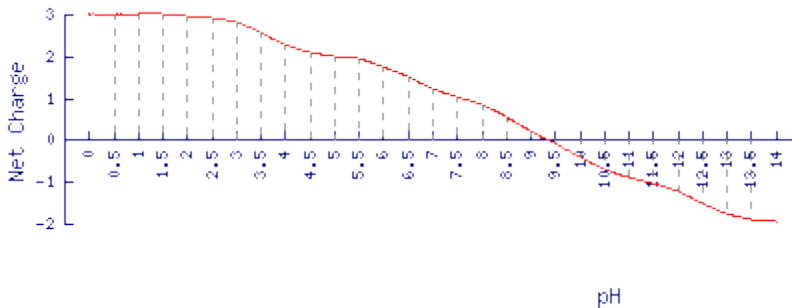
Calculating the physical properties of this peptide sequence CTP, using online tools, reveals a molecular weight of 1432.6, a net charge of 1.1 at pH of 7.0, an isoelectric point occurring at a pH of 9.35, with an average hydrophilicity index of -0.4 (https://www.genscript.com/ssl-bin/site2/peptide_calculation.cgi).

MW:

1432.55

PI:

9.35



Hydrophilicity Analysis:

Peptide	Charge	Attribute
APWHLSSQYSRT	2	Basic

Note:

- **Red:** acidic residues, like D E and C-terminal -COOH
- **Blue:** basic residues, like R K H and N-terminal -NH₂
- **Green:** hydrophobic uncharged residues, like F I L M V W and Y
- **Black:** other residues, like G A S T C N Q and P

- **Z**: Unrecognized codes are replaced of 'Z'.

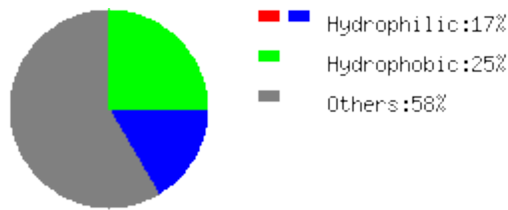


Figure 9. Physical properties of Cardiac Targeting Peptide or CTP.

In contrast to the earlier reported PTDs, like TAT or 16 amino acids from the third helix of *Drosophila Antennapedia* homeodomain (penetratin), which are rich in cationic, basic amino acids like arginine and lysine, this peptide sequence has only one arginine residue and is near-neutral at physiological pH.

2.2 *In vitro* Transduction Experiments: Confocal Studies

In order to determine the ability of CTP to transduce cells *in vitro*, multiple different cell types, along with H9C2 cells were incubated with varying concentrations of 6-carboxyfluorescein labeled CTP (CTP-6CF). A cardiomyoblast cell line (H9C2), a fibroblast cell line (NIH/3T3), a murine fibrosarcoma cell line (MCA205), a cervical cancer cell line (HeLa) and a human tubular cell line (HK-2), were passaged for a minimum of 3 cycles. After three cycles, cells were split and plated onto collagen-coated cover-slips (H9C2, HK-2 cells) or regular cover-slips (NIH/3T3, MCA205, HeLa cells) at a cell density of 2×10^5 /well in a 6-well cell-culture plate. 24-hours after plating, the media was aspirated, cells washed with 1ml of pre-warmed (to 37°C) Optimem once and left in 1ml of Optimem. Cells were then incubated at 37C/5%CO₂, with increasing

concentrations (50uM, 100uM and 200uM) of CTP-6CF (1mM working solution in PBS) for 30 minutes, at the end of which cells were washed 6 times with pre-warmed PBS, fixed with 2% paraformaldehyde (see Chapter 5, Methods, Section 5.2.1 for “cell transduction experiments with CTP-6CF, and section 5.2.2 for details on making 8% paraformaldehyde stock solution) for 30 minutes to which 1ul of a 1000X DRAQ5 (Molecular Probes, F1303), a nuclear stain, was added. After 30 minutes, PFA was aspirated, cells washed with pre-warmed PBS once, and the cover-slips mounted onto glass slides using gelvitol. After setting overnight, at 4°C, light-protected, cells were examined by confocal fluorescent microscopy. Below are confocal micrographs of various cell types showing preferential transduction of H9C2 cells over other cell types (Figure 10).

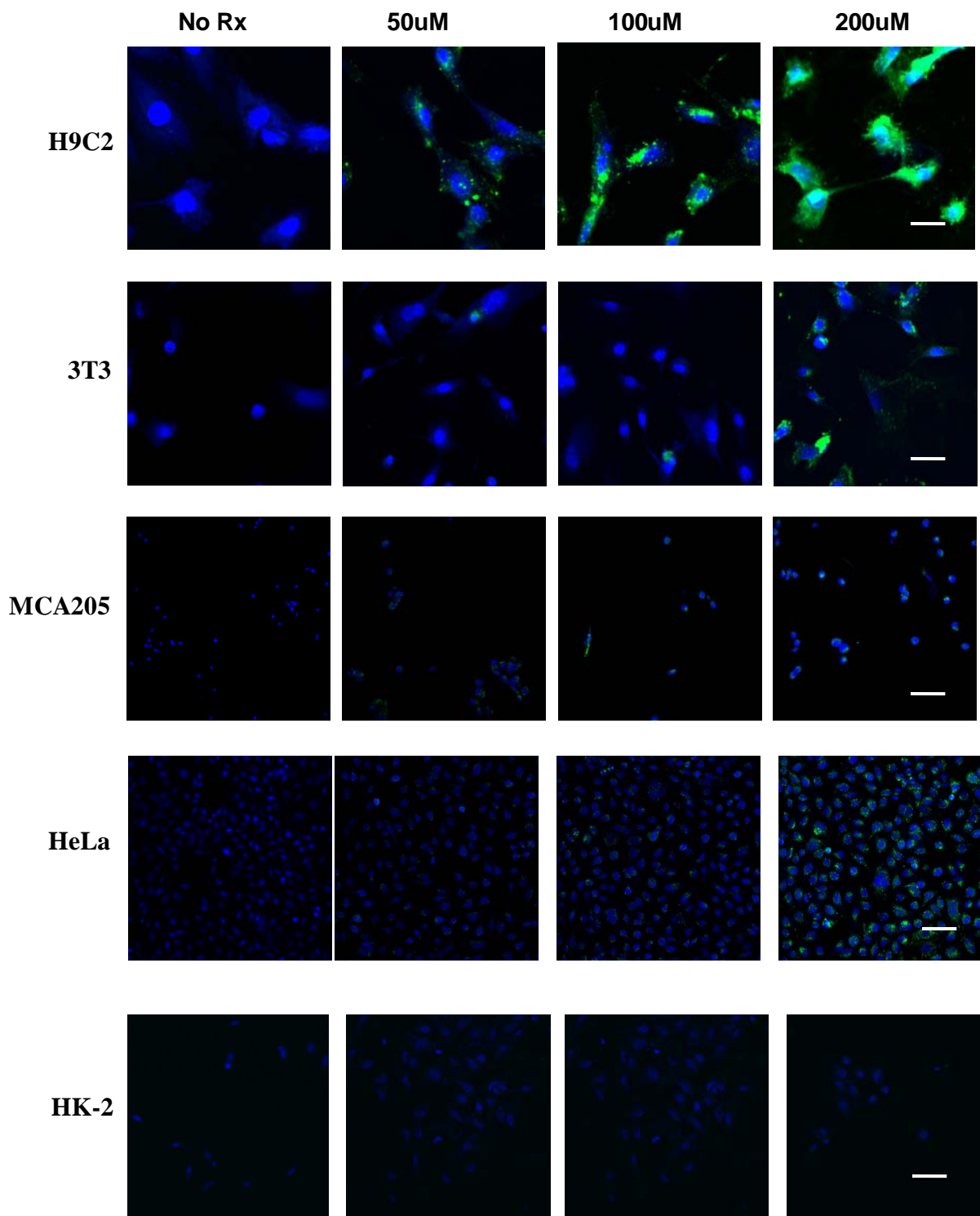
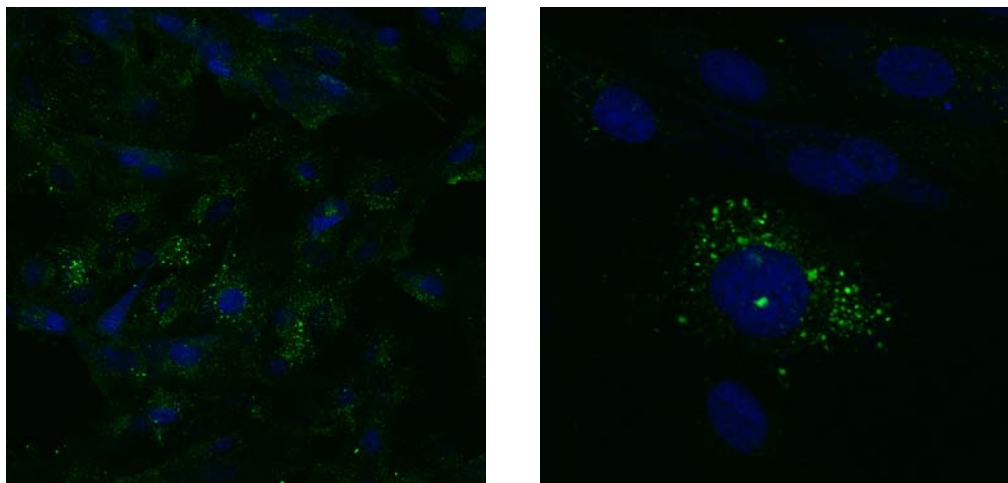


Figure 10. Confocal micrographs of H9C2, 3T3, MCA205, HeLa and HK-2 cells incubated with increasing concentrations of CTP-6CF; Nuclei - blue (DRAQ5), CTP-6CF - green, 20x. Scale bars represent 100uM.

These micrographs show uptake of CTP-6CF by H9C2 cells in a dose-dependent fashion with increasing uptake at higher concentrations. Uptake by 3T3, MCA205 and HeLa cells occurs to a much lesser extent and only at the highest end of the dose used (200uM, last panel). No uptake at all was seen at any of the tested doses by HK-2 cells, a human renal tubular cell line.

Transduction experiments with H9C2 cell line were repeated with 200uM of CTP-6CF, incubated for 30 and 60 minutes and higher magnification confocal micrographs obtained. As shown in the figure below (Figure 11), CTP-6CF is intracellular with a punctuate distribution, similar to what has been reported for TAT, suggesting perhaps an endosomal localization of the peptide after internalization.

H9C2 cells incubated with CTP-6CF for 30 mins: 40x and 60x



H9C2 cells incubated with CTP-6CF for 60 mins: 40x and 60x

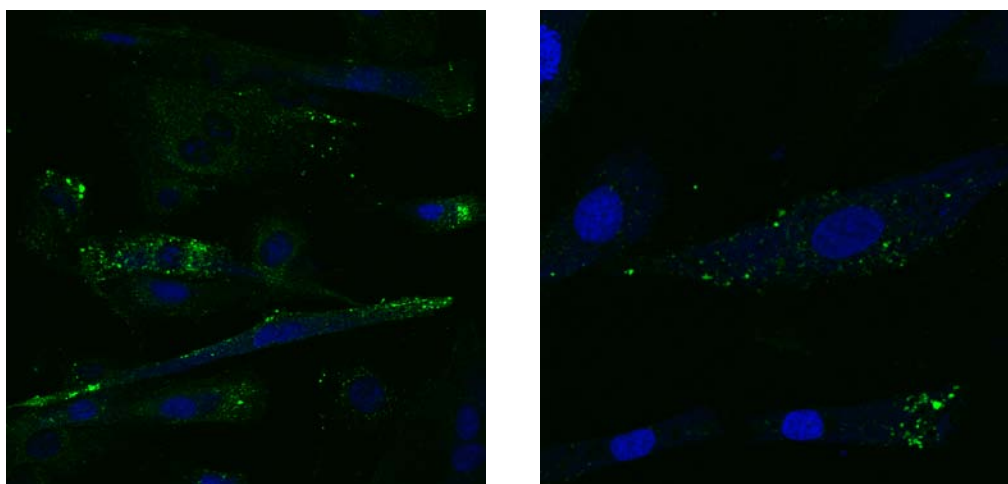


Figure 11. High magnification confocal micrographs of H9C2 cells incubated with CTP-6CF for 30 (top row) and 60 minutes (bottom row).

There has been concern voiced in literature following the reports on cationic cell penetrating peptides (CPP) that transduction with nuclear localization might be a result of a fixation artifacts [117-118]. TAT, a cationic, basic PTD, because of large number of arginine and lysine residues, has been shown to bind strongly to surface glycoproteins especially heparan

sulfate. This binding has been shown to be followed by endocytosis leading to internalization [119]. Thus the concern has been that transduction may simply be binding of positively charged peptides to heparan sulfate followed by endocytosis and any cytosolic or nuclear localization is a fixation artifact. To confirm that the above findings are actual transduction and not simply a fixation artifact, we followed H9C2 cells incubated with a random peptide sequence labeled with 6CF (RAN-6CF), CTP-6CF or TAT-6CF with live imaging without any fixation protocols. The random peptide (ARPLEHGSDKAT) was the sequence of a phage picked from the original library that had not undergone any selection pressures of phage display. The figure below (Figure 12) presents the results after 60 minutes of incubation in which a DIC image is over-laid on the fluorescent image to give cell structural detail.

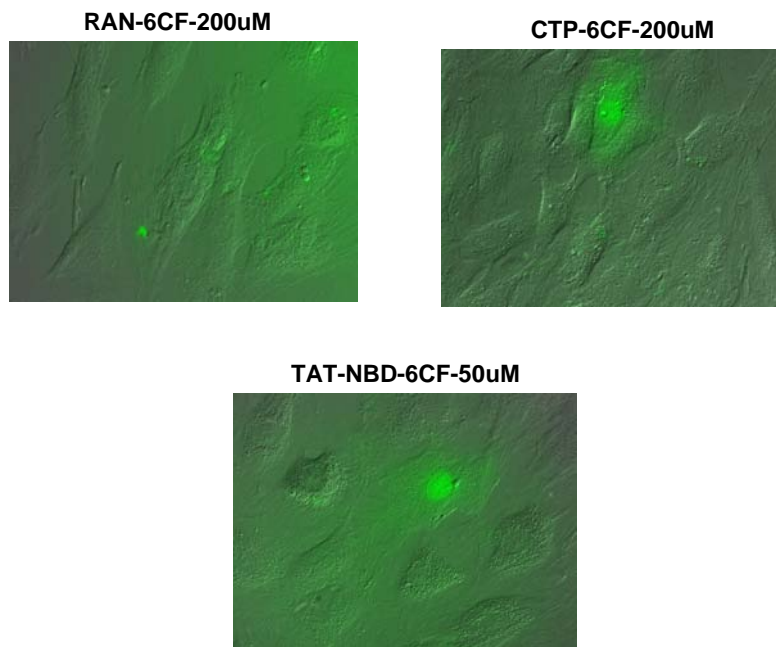


Figure 12. Live cell imaging of H9C2 cells incubated with RAN-6CF, CTP-6CF or TAT-6CF.

These micrographs show intracellular and intranuclear fluorescence with both TAT-6CF and CTP-6CF, with no fluorescence uptake with RAN-6CF. To assess transduction without fixing cells or using fluorescent microscopy, we also did a functional assay to prove transduction, as detailed below.

2.3 *IN VITRO* TRANSDUCTION: FUNCTIONAL ASSAY

In order to assess transduction of H9C2 cells with CTP peptide, we used a reporter-Luciferase based cell assay, as described by Madge and May [120]. H9C2 cells were plated onto 96-well plates at a cell density of 2×10^4 cells/well. Next day cells were transfected with a reporter plasmid expressing Luciferase under an NF- κ B binding promoter site and a control Renilla expressing plasmid, using Lipofectamine. Twenty-four hours post-transfection, cells were pre-treated with increasing concentrations of the CTP-NBD (nemo-binding domain) peptide. NBD binds to the nemo binding site of IKK β and to a lesser extent IKK α , preventing its association with NEMO or IKK γ , thus preventing activation of the IKK complex. This prevents phosphorylation of I κ B and its subsequent degradation and release of NF- κ B, which is not activated and remains cytosolic. Cells pre-treated with CTP-NBD were then challenged with TNF α , an NF- κ B activator, and Luciferase activity measured in cell lysate. The methodological details of these set of experiments are provided in Chapter 5, Methods, section 5.3: Methodology for transfection of cells and inhibition of NF- κ B activation. Figure 13 gives a schematic presentation of the experimental protocol.

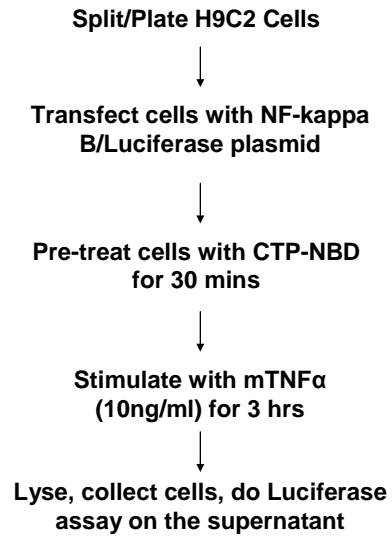


Figure 13. Experimental protocol for the *in vitro* transduction experiments using Luciferase readout.

All work was done in quadruplicate. The Luciferase readings were corrected for transfection efficiency differences using the Renilla readout. Differences across groups were compared using a two-tailed Student's t-test. A p-value of <0.05 was considered statistically significant. Below are the results of experiments carried on H92 cells.

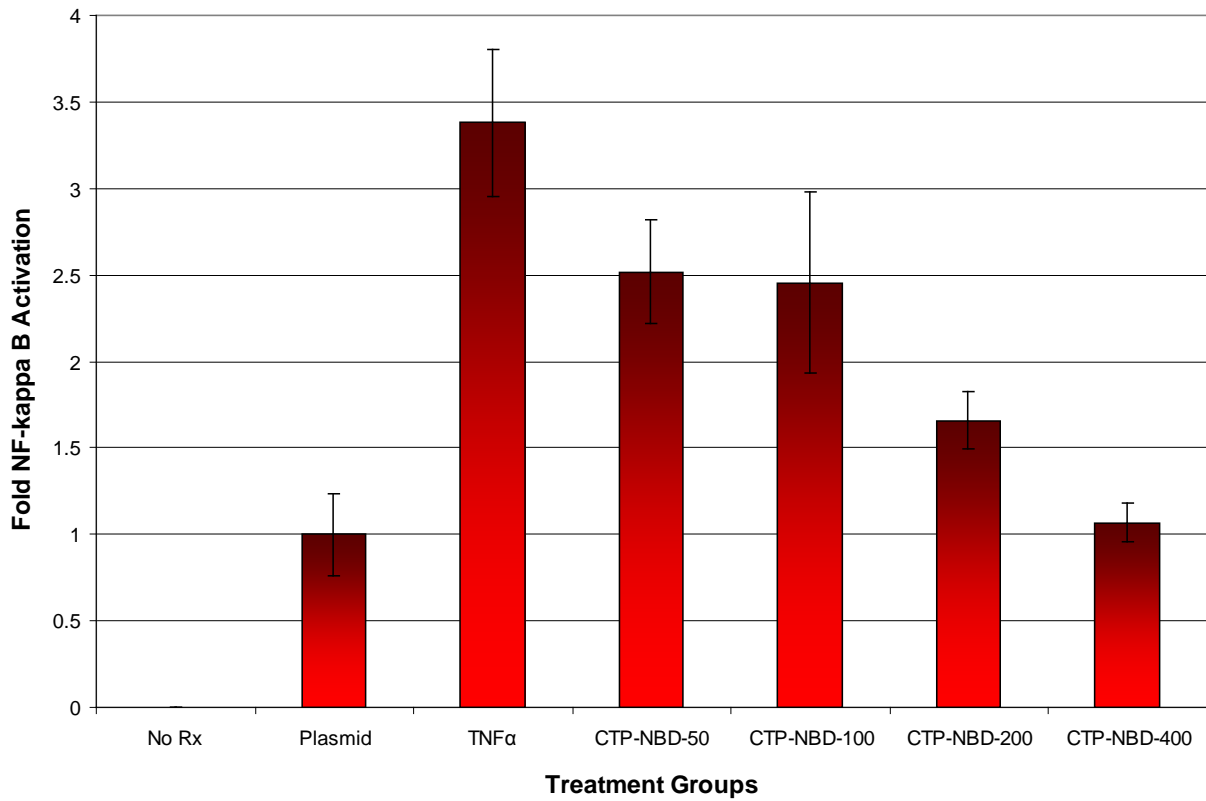


Figure 14. Inhibition of Luciferase activity by CTP-NBD in H9C2 cells.

The exact same experiment with identical conditions was repeated in MCA205 cell line (Figure 15) as well as in HeLa cells (Figure 16).

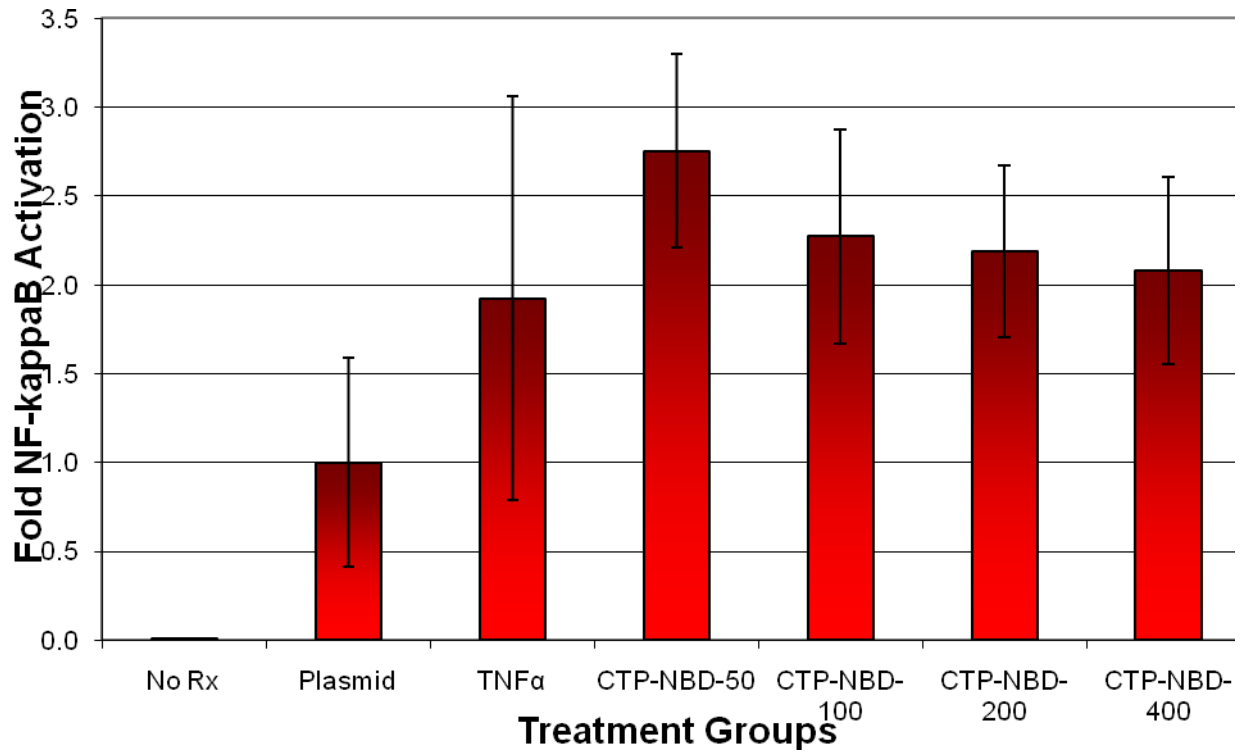


Figure 15. Lack of inhibition of Luciferase activity by CTP-NBD in MCA205 cells.

CTP-NBD was not able to inhibit TNF α mediated activation of NF- κ B in MCA205 cells even at the highest tested dose of 400uM.

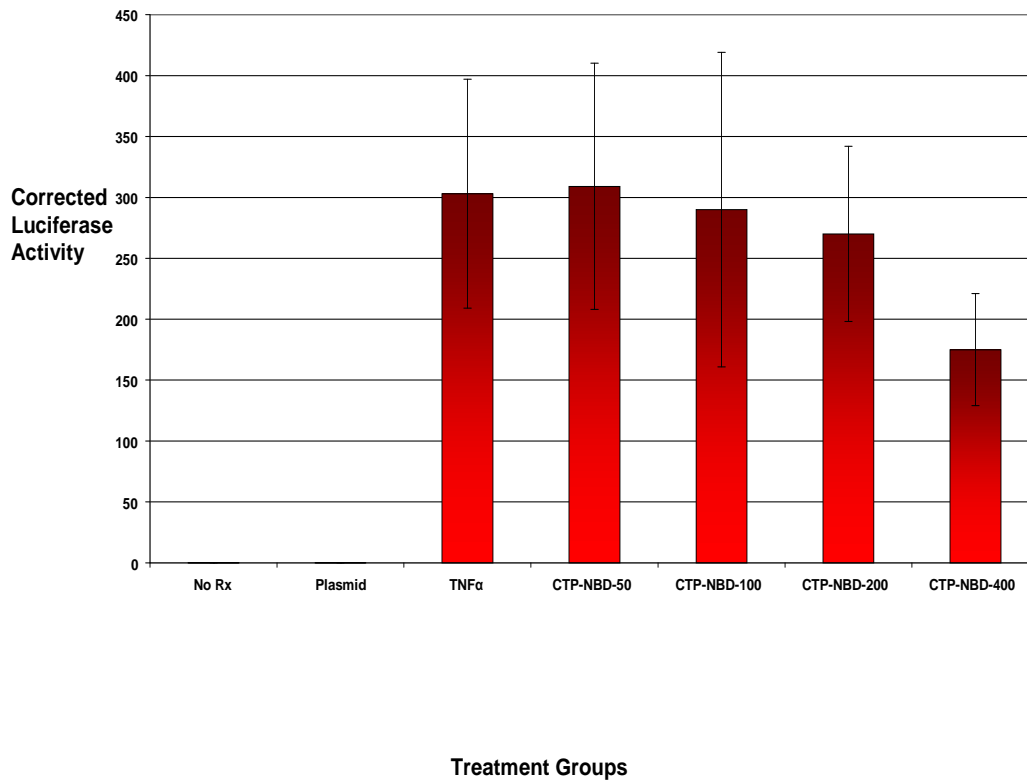


Figure 16. Relative lack of inhibition of Luciferase activity by CTP-NBD in HeLa cells.

CTP-NBD failed to inhibit TNF α mediated NF- κ B activation, except at the very highest dose used (400uM). This is consistent with the confocal micrograph data where transduction of HeLa cells by CTP-6CF occurred marginally at the highest dose used of 200uM (Figure 10).

Following these inhibition of NF- κ B activation studies, we performed cell viability studies to assess changes related to peptide treatment. The experiment was repeated with H9C2 cells being doubly-transfected and pre-treated with CTP-NBD in increasing concentrations, followed by TNF α (10ng/ml) challenge for 3 hours. After this time period, the media was aspirated and replaced with MTT assay media to assess for cell viability. As shown below, inhibition of NF- κ B with CTP-NBD led to decrease in cell viability in a CTP-NBD dose-

dependent fashion. All treatment groups were done in quadruplicate. Error bars represent 1 standard deviation (SD).

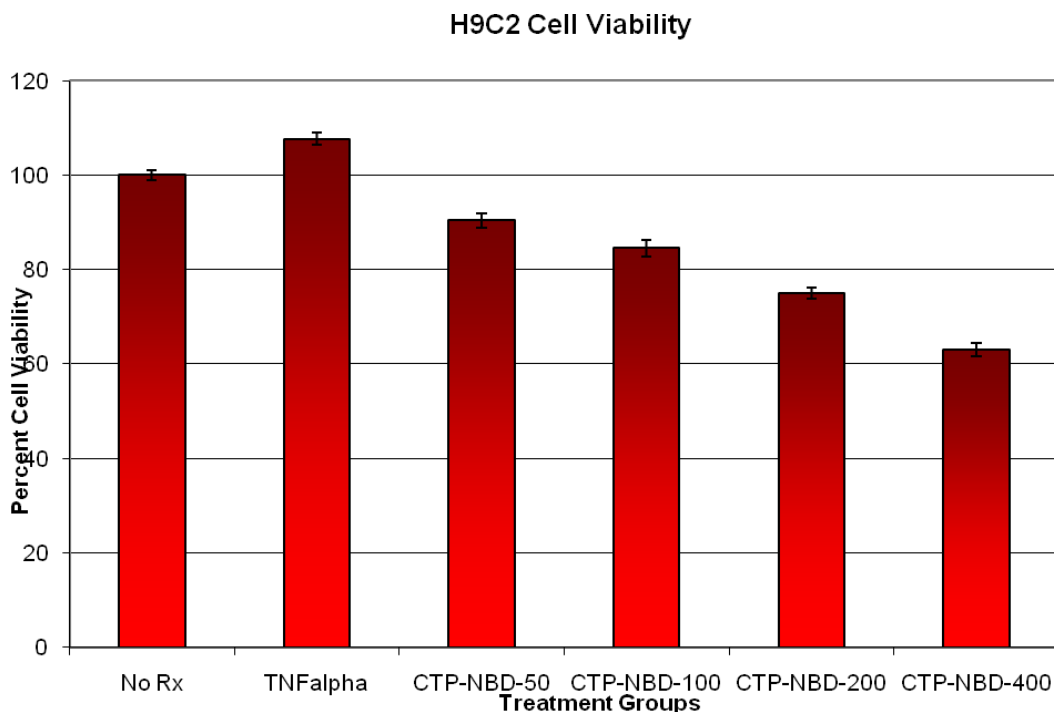


Figure 17. H9C2 cell viability after transfection, treatment with CTP-NBD and subsequent TNF-alpha treatment.

This finding is consistent with reports in the literature that NF- κ B inhibition increases apoptosis in H9C2 cells challenged with TNF α [121]. These results clearly demonstrate a biological effect of the NBD peptide that can only occur if the peptide was internalized by the PTD action of CTP. This decrease in cell viability did not occur with TNF α treatment or CTP-NBD treatment alone as shown in Chapter 4, Figure 40.

In summary, in this section we have shown transduction occurring preferentially of H9C2 cells, a rat cardiomyoblast cell line, over a fibroblast, a fibrosarcoma, a cervical epithelial cancer cell line and human tubular kidney cell line using confocal fluorescent microscopy. We have also

demonstrated preferential transduction of H9C2 cell line over MCA205 cells or HeLa cells using a reporter plasmid carrying Luciferase expression under the control of an NF- κ B binding promoter site. Next we will show transduction of heart tissue occurring *in vivo* with fluorescently labeled CTP.

2.4 *IN VIVO* TRANSDUCTION STUDIES

Our *in vitro* data showed preferential targeting of H9C2 cells over other, tested cell lines as assessed by confocal imaging, as well as a functional assay using Luciferase as a readout. This naturally led to the next question of whether preferential targeting of heart tissue will occur *in vivo* as well. The initial *in vivo* targeting studies were performed using CTP-6CF. Female Balb/C mice were anesthetized using 2.5% Avertin, 12-15ul/gm of body weight, injected intraperitoneally. After adequate anesthetic levels were achieved, as assessed by lack of limb withdrawal to toe pinch or lack of a corneal reflex, mice were injected retro-orbitally with CTP-6CF (25 mg/Kg) and euthanized 15 minutes later. The heart was dissected out, washed in PBS, placed in 2% paraformaldehyde (PFA) for 4 hours at room temperature (RT), followed by 30% sucrose, 4°C, over night. Next day hearts were flash frozen in liquid nitrogen-chilled Isopentane and placed in -80°C for later cryosectioning. After embedding in OCT, hearts were cryosectioned in the short-axis as 6uM thick sections and stained with DRAQ5, a nuclear stain. The sections were also stained for actin using phalloidin Alexa- 647 (Molecular Probes, A22287) and stained for laminin using a rabbit anti-laminin antibody followed by a goat anti-rabbit Cy3 (Jackson ImmunoResearch, [111-167-003](#)) secondary antibody. Confocal microscopy was performed on these heart sections. The figure below (Figure 18) illustrates a section showing intracellular

localization of CTP-6CF, co-localizing with Actin. Laminin, which is present only on the surface of cells and hence has a ring-like appearance around myocytes, does not co-localize with CTP-6CF, which has a distinctly different distribution pattern.

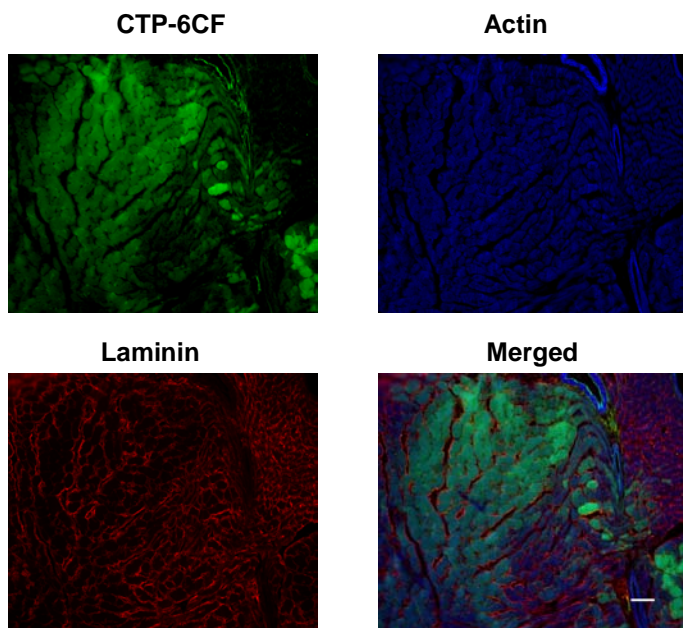


Figure 18. Transduction of mouse heart by intravenously injected CTP-6CF at 15 minutes.

Female, Balb/C mice were injected retro-orbitally with PBS or CTP-6CF at a dose of 25mg/Kg, euthanized at 15 minutes, hearts dissected and treated as outlined above. Five non-overlapping, contiguous sections were taken from each heart for quantification of green fluorescence (CTP-6CF) expressed as a percentage of total area (blue; stained for actin). There were 3 mice in each group, and 5 sections quantified from each heart and averaged.

The figure below (Figure 19) shows the mean amount of fluorescence in all sections. The error bars represent one standard error of the mean.

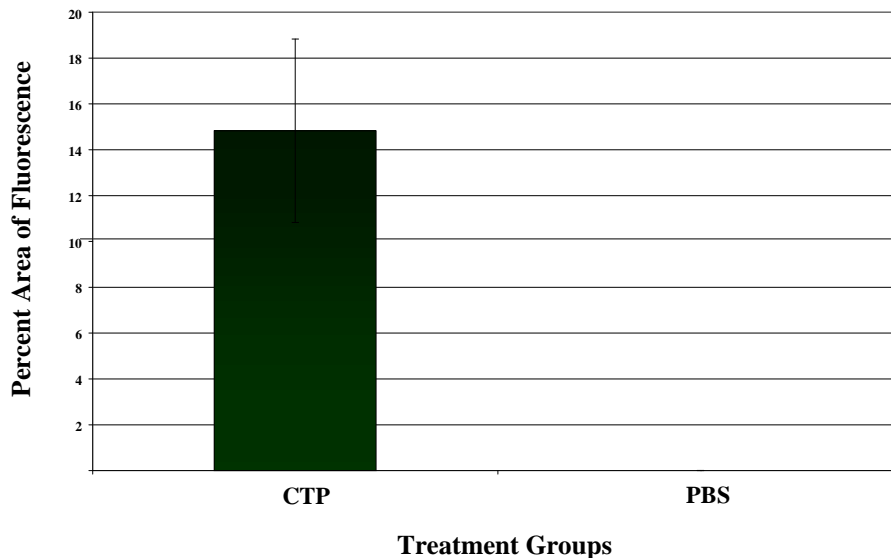


Figure 19. Quantification of fluorescence in mouse hearts (n=3 in each group).

Next the biotinylated form of CTP (200uM) or PBS was incubated with Streptavidin-Alexa488 conjugate (10ul of a 2mg/ml solution), at RT, light-protected, for 60 minutes, prior to injection intravenously (retro-orbitally) into Balb/C, female mice. An equivalent volume of PBS+streptavidin-alexa488 was injected as a negative control. Mice were euthanized at 30 minutes, heart, liver, kidney, lung, skeletal muscle (hind-limb quadriceps), brain and spleen dissected out and treated as outlined above. The sections were stained with DRAQ5, cover-slipped and confocal microscopy performed. For confocal microscopy, laser intensities/gains were set using negative control (PBS injected) heart tissue to minimize background fluorescence. Once laser intensity for the negative control hearts was set, it was kept constant across all subsequent imaging. Also serial scanning was performed to prevent “bleed-through” from one laser wavelength to another. Figure 20 below illustrates robust uptake of the peptide, as judged

by tissue fluorescence, with very little uptake by lung and kidney glomerular capillaries and none by skeletal muscle, brain, liver or spleen (data for spleen not shown).

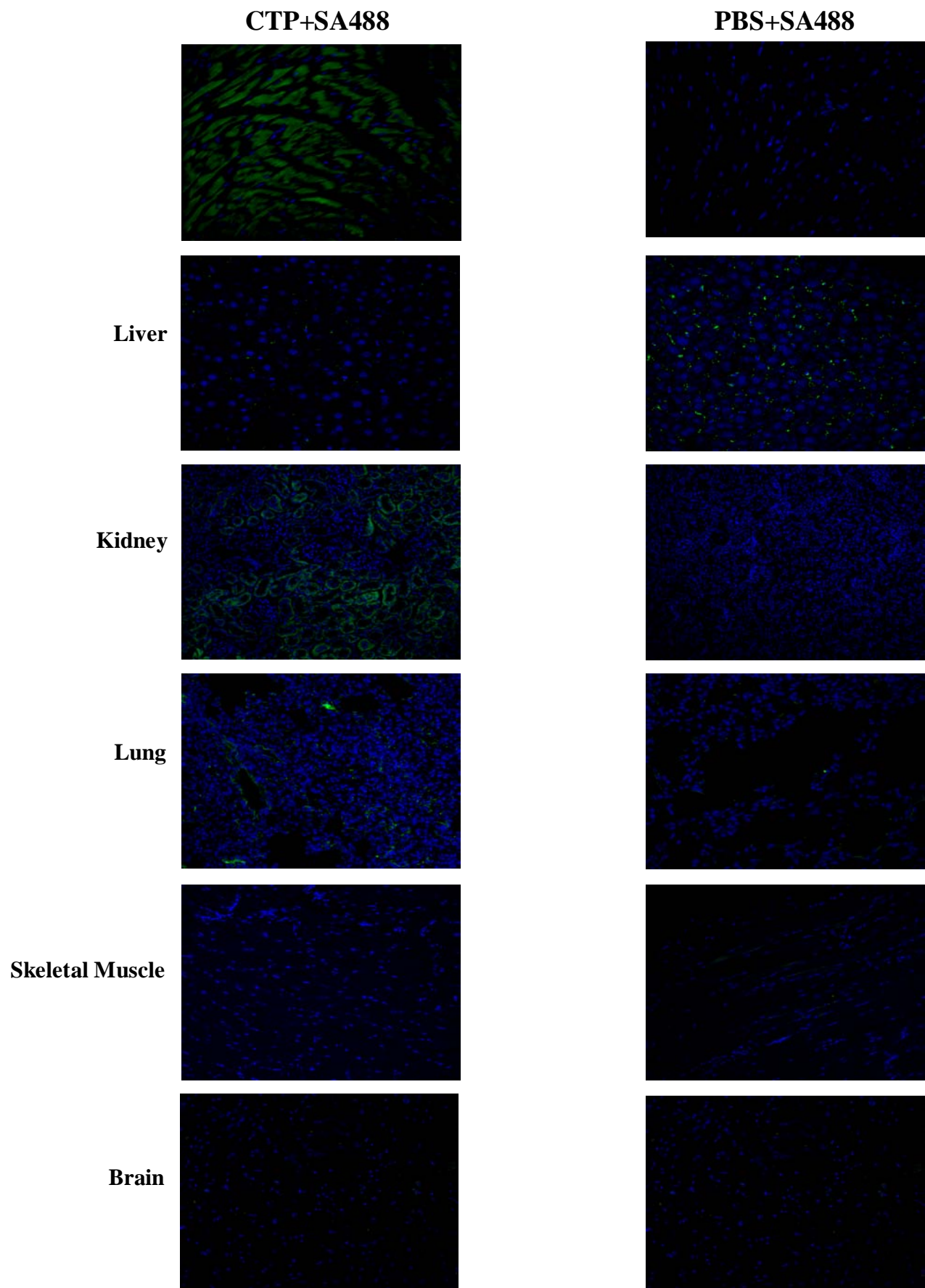


Figure 20. Transduction of heart tissue after intravenous injection with CTP-biotin-streptavidin-Alexa488 complex.

Balb/C, female mice were also injected with the CTP-biotin-streptavidin-Alexa488 conjugates and euthanized at different time points to study the biodistribution of this complex. The figure below, (Figure 21), shows transduction beginning at 15 minutes, localized to the sub-epicardial region, with more diffuse uptake at 30 minutes and almost complete absence of fluorescence at 120 minutes.

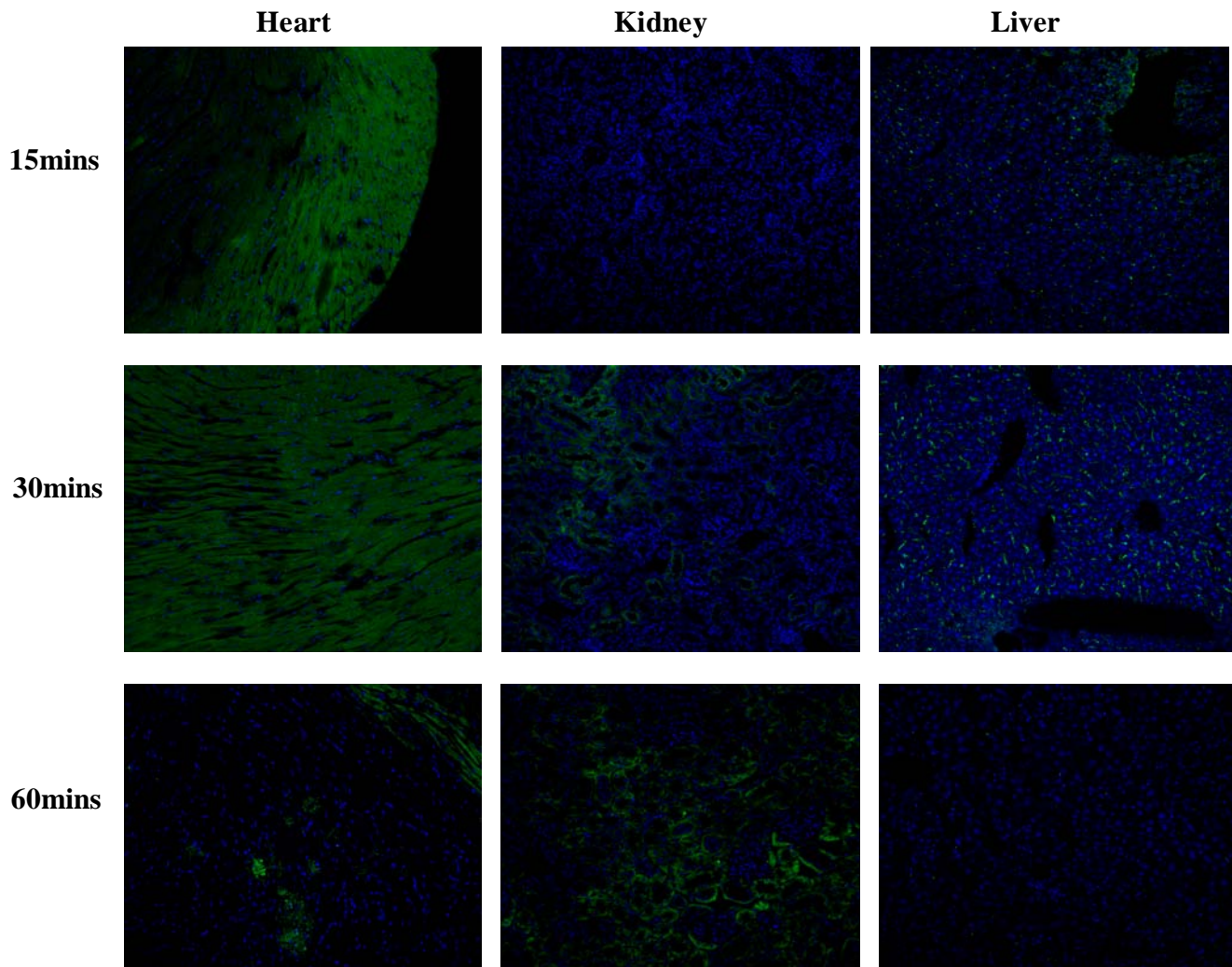


Figure 21. Biodistribution of CTP-biotin-streptavidin-Alexa488 complex after intravenous injection

A random peptide (RAN; ARPLEHGSDKAT), picked from the original, unselected M13 phage library, was synthesized in a biotinylated form. Biotinylated RAN or CTP peptides were labeled with neutravidin-conjugated fluospheres (Molecular Probes, F8770) with an overnight incubation at 4°C. These fluospheres are 40nm in diameter and fluoresce at an excitation wavelength of 605 nm, allowing for *in vivo* bead tracking. Female Balb/C mice received intracardiac injections of fluospheres-labeled RAN peptide, CTP peptide or control PBS incubated with fluospheres alone. Mice were anesthetized with isoflurane delivered by the XGI-8 Gas Anesthesia System (Xenogen). Initial isoflurane concentration was set to 2.5% and was reduced to 1.5% once the animal was anesthetized. Mice were then imaged at 30, 60, 120, and 180 minutes post-injection with the IVIS Lumina (Caliper Life Sciences Inc.). The figure below (Figure 22) shows localization of fluorescence to the heart in mice injected with CTP+fluospheres, with rapid dissipation of fluorescence after injection with RAN+fluospheres or PBS+fluospheres. After three hours of imaging, these mice were euthanized, hearts dissected, processed as detailed above, cryosectioned, cross-stained with DRAQ5 and confocal microscopy performed.

The confocal micrographs below (Figure 23) show a few myocytes with uptake of the fluospheres, actually much less than the whole mouse, *in vivo* imaging would suggest. Confocal microscopy did show fluorescent beads sticking to the endocardial region suggesting that these beads might only be able to stick to the surface and not be internalized as readily as CTP-6CF or CTP-biotin-streptavidin-alexa488 complexes. These beads are 40nm in size and the association with CTP-biotin may not necessarily be a one-to-one association leading to larger complex formations. This is indirectly supported by the observation that the solution injected was a highly viscous one and required a large-bore, 18G needle, precluding a peripheral tail-vein or retro-orbital injection.

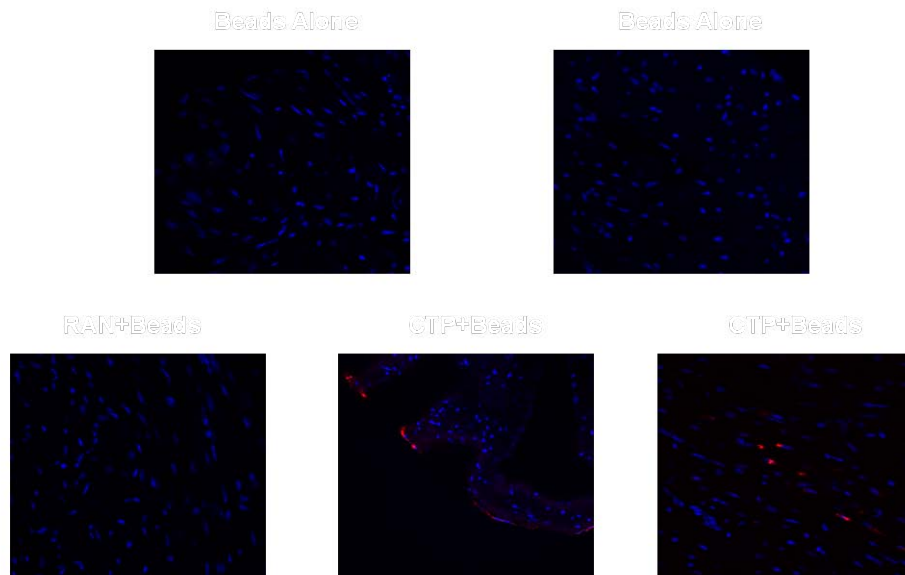


Figure 23. Confocal micrographs of hearts injected with PBS+fluospheres, RAN+fluospheres or CTP+fluospheres.

To demonstrate cell specificity of the CTP peptide *in vivo*, we undertook a second set of experiments. Balb/C, female mice were anesthetized with intra-peritoneal Avertin (2.5%, 10-

15ul/gm of body weight), intubated with a 22G cannula using direct laryngoscopy and visualization of the vocal chords, and placed on a rodent ventilator (Harvard apparatus). The chest cavity was entered using a left, lateral thorotomy approach, and an anterior infarct produced by placing a suture through the anterior wall, 2mm inferior to the lowest dip of the left atrial appendage to blindly ligate the left anterior artery. Infarct was confirmed by the resulting pallor of the anterior wall and apex as well as wall motion abnormality produced in the region. The chest wall was closed in two layers, and the animal placed on a heating pad until awake. One week post-infarct, mice were re-anesthetized and injected intravenously with CTP-biotin-Streptavidin-Alexa488 (SA488) complex or an equivalent volume of PBS with SA488 (10mg/Kg body weight). After 30 minutes of circulation time, mice were euthanized, hearts dissected out, washed, fixed, cryosectioned, cross-stained with DRAQ5, and confocal microscopy performed. Contiguous sections were also H&E stained to show the infarct area. Figure 24 below shows uptake of the fluorescently labeled CTP by normal heart tissue with exclusion of uptake from the infarcted, scarred myocardium (arrows). No uptake of PBS+SA488 alone was seen in any area of the heart. This experiment demonstrates *in vivo* cell specificity of our peptide, CTP, as it is taken up by normal myocardium and excluded from the scarred, infarcted heart. The infarct is demonstrated in the H&E section by the lighter pink, thinned out area.

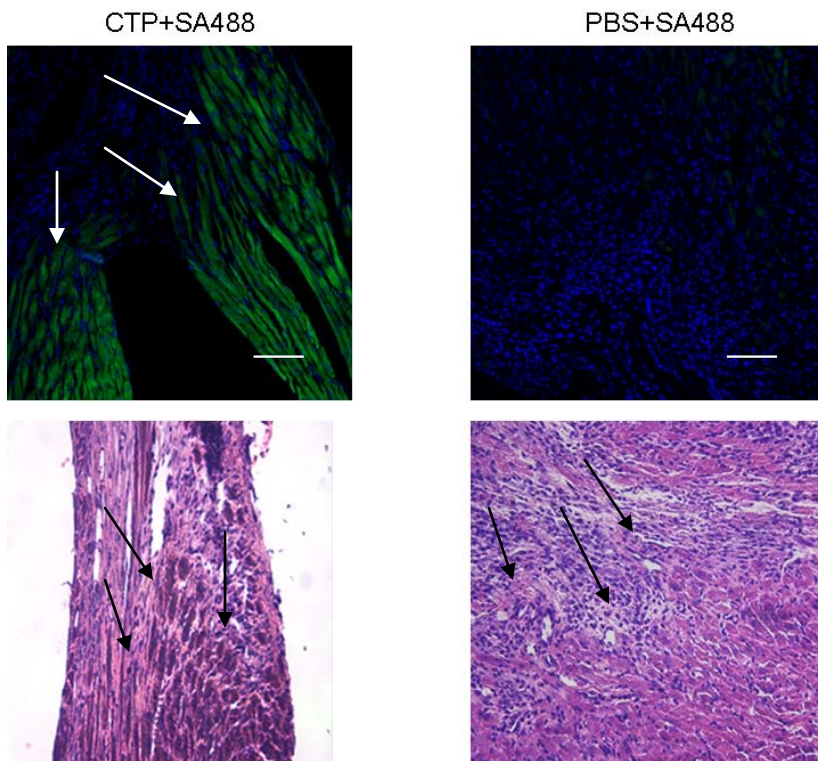


Figure 24. Uptake of CTP-6CF preferentially by normal myocardium with exclusion from the infarct area.

Our lab has shown that a homopolymer of lysine, 8K, is able to transduce multiple cell types effectively and consistently exceeding those of TAT and arginine homopolymers [16]. In order to compare transduction of heart tissue by CTP versus 8K, biotinylated form of these two peptides as well as a random peptide (RAN; mentioned above) were incubated with Streptavidin-Alexa488 (SA488) for 60 minutes. Balb/C, female mice were anesthetized with intra-peritoneal Avertin and injected intravenously with CTP-SA488, 8K-SA488, or RAN-SA488 at a dose of 10mg/Kg. At the end of a 30 minute circulation time, mice were euthanized, hearts and other organs dissected and processed as detailed above for cryosectioning and subsequent confocal microscopy. The figure below (Figure 25) shows transduction of heart tissue by CTP-SA488 in a

generalized manner at 30 minutes, with little uptake by kidney capillaries and none by the liver. In contrast 8K demonstrates robust transduction of kidney glomeruli and liver tissue, with little uptake by the heart. In contrast RAN-SA488 is not taken up by any of the tissues tested.

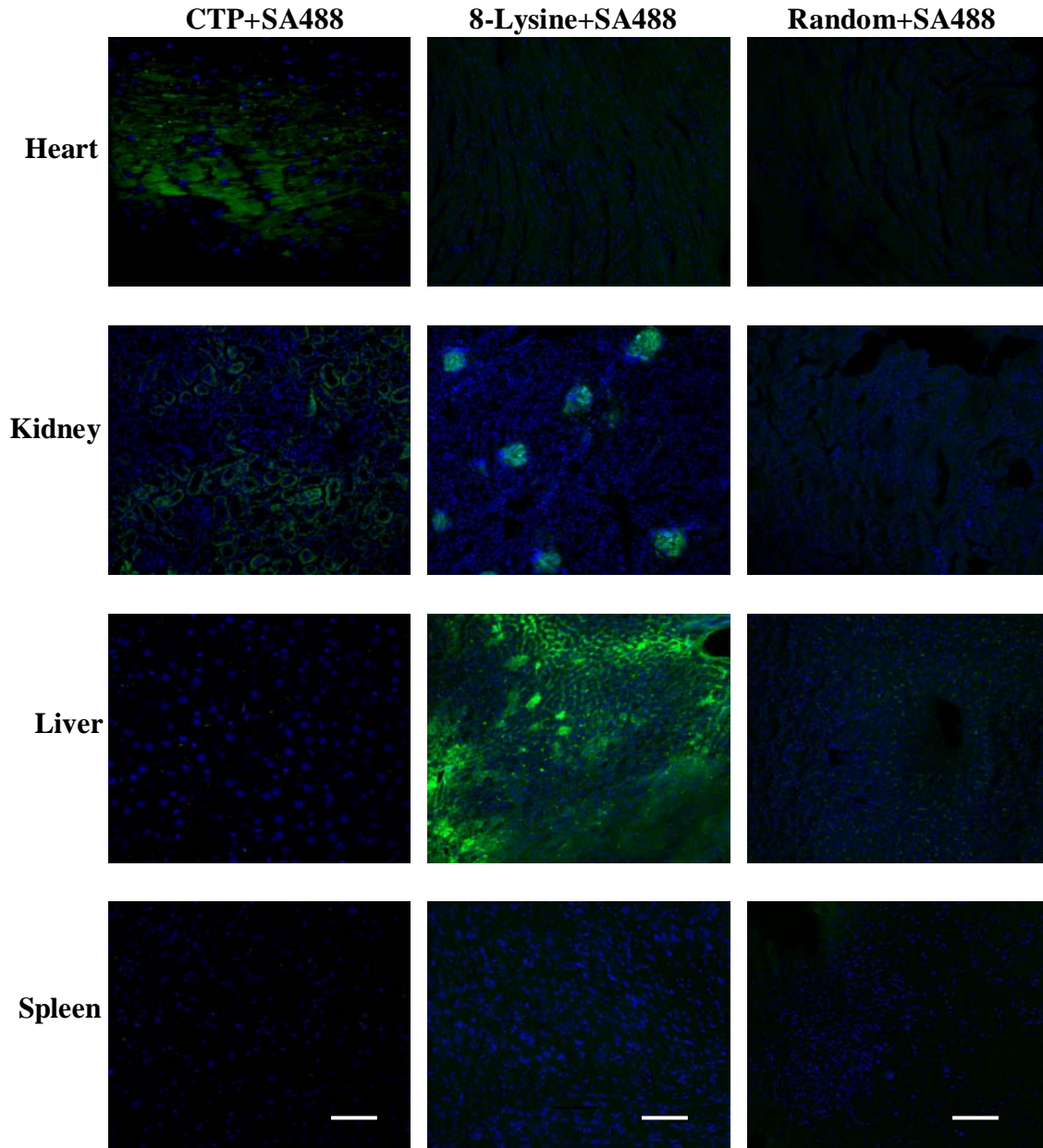


Figure 25. Comparison of heart tissue transduction between CTP, 8K and RAN peptide.

2.5 HUMAN HEART TISSUE EXPERIMENTS

Our work above has shown that *in vivo* phage display can be used to screen large phage display libraries for peptide(s) able to transduce cardiomyoblasts cell lines and heart tissue preferentially *in vivo* after a systemic, peripheral intravenous injection. The identification of such a peptide, CTP, raises many interesting and relevant questions. One key one would be whether this cardiac targeting is species specific or not. If such was the case, the utility of this peptide would be limited. In order to test whether CTP is able to transducer human heart tissue, we performed experiments *ex vivo* on explanted heart tissue.

Heart transplantation is a destination, life-saving therapy for end-stage congestive heart failure. At the University of Pittsburgh Medical Center (UPMC) anywhere from 30 to 50 heart transplants are performed in a year. The Institutional Review Board has approved a protocol whereby patients awaiting heart transplant can consent to the use of explanted, diseased hearts for scientific experimentation with appropriate measures taken to protect patient identification and privacy. An extension of this protocol was sought where I could share tissue obtained at the time of heart transplant, in a blinded fashion, to run *ex vivo* incubation experiments with various fluorescently labeled peptides, including CTP.

Human explanted hearts were obtained from the operating rooms of UPMC at the time of ongoing heart transplants. Heart tissue was dissected from the proximal part or the base of the heart to avoid the more scarred, infarcted, distal tissue. Small 1-2mm thick slices of heart tissue were taken and incubated with CTP-6CF (500ul of a 1mM solution) or PBS, for 30 and 60mins, at 37°C / 5% CO₂. At the end of the incubation period, the heart slices were washed in PBS 6 times, fixed in 2% paraformaldehyde for 4 hrs at room temperature, followed by 30% sucrose overnight at 4°C. Next day the tissue was frozen in liquid nitrogen-chilled isopentane and stored

at -80°C, for later cryosectioning, cross-staining with DRAQ5 and confocal microscopy. Confocal micrographs were obtained avoiding the edges because of the necessary damage associated with dissecting the heart tissue pieces. Confocal micrographs were taken 3-4 cell layers away from any edges. The figure below (Figure 26) demonstrates internalization of the peptide into heart myocytes.

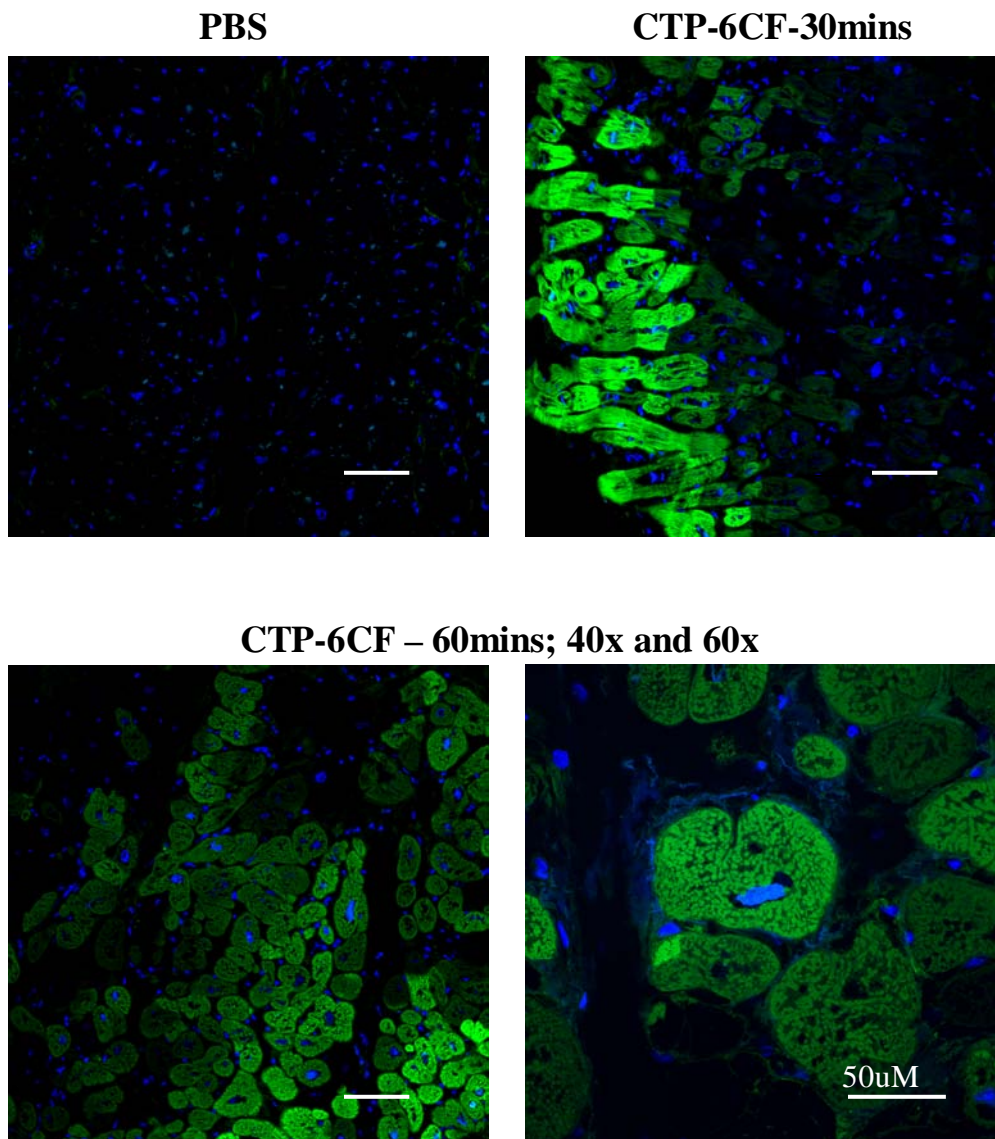


Figure 26. Transduction of human heart tissue ex vivo by CTP-6CF.

To investigate if this transduction was indeed peptide specific, and not secondary to increased membrane leakiness resulting from tissue being ischemic, we incubated thin, 1-2mm thick, heart slices, from a separate explanted heart, in only 6CF in PBS, CTP-6CF, RAN-6CF as well as 6CF labeled 6-Arginine, a known PTD. We also incubated heart slices with Evans blue dye (EBD) to assess for membrane leakiness. Evans blue dye fluoresces with an excitation wavelength of 620nm and emission wavelength of 680nm [122-123], making it possible to be imaged with fluorescent microscopy using the appropriate lasers for excitation. Heart tissue was incubated in 500ul of 1mM solution of all the peptides in PBS, for 30mins at 37C/5%CO₂. At the end of the incubation period, heart slices were rinsed thoroughly 6 times in 1ml of PBS and fixed in 2% paraformaldehyde for 4 hours, at room temperature, light-protected, followed by 30% sucrose, overnight at 4C. Next day tissue was frozen in liquid nitrogen chilled Isopentane, embedded in OCT, cryosectioned, cross-stained with DRAQ5, mounted and confocal microscopy performed as detailed above. Confocal microscopy showed robust and diffuse uptake of both 6R-6CF and CTP-6CF, with occasional cells showing fluorescence in RAN-treated or 6CF-treated hearts. Confocal microscopy of the EBD treated hearts did not show any fluorescence indicative of uptake which would have occurred had the membranes been significantly damaged by length of ischemia. The figure below (Figure 27) shows confocal micrographs of heart tissue treated with different peptides or controls.

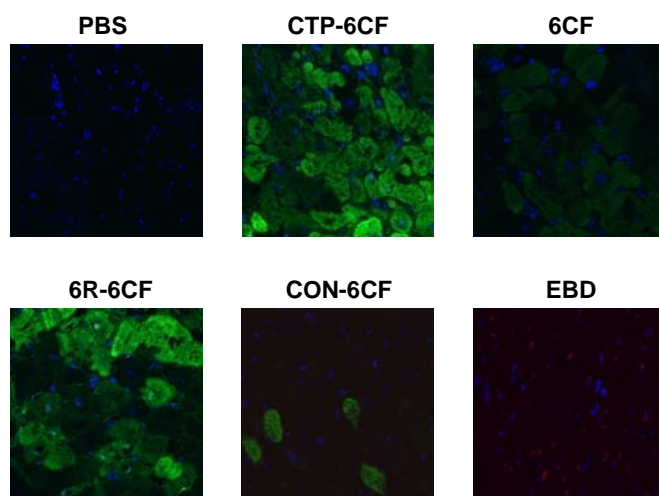


Figure 27. Results of *ex vivo* human heart tissue experiment at 30 mins.

The result of these *ex vivo* experiments demonstrates that CTP-6CF is indeed internalized by human myocytes as demonstrated by confocal microscopy and is not simply sticking to the outer surface. Moreover, this internalization is not seen with simply 6CF, the fluorescent chemical used to label all our synthesized peptides, and is not seen also with a random peptide. In contrast, 6R-6CF (homopolymer of 6 arginine amino acid residues), a known PTD, is indeed able to transduce these human myocytes *ex vivo*. Lastly, this internalization is not simply a result of increased membrane leakiness due to ischemia, as evidenced by lack of Evans blue dye uptake by the myocytes.

2.6 CHAPTER SUMMARY

In this chapter we have presented data demonstrating that a combinatorial approach of cell culture and *in vivo* biopanning or phage display can be utilized to identify a peptide, *Cardiac Targeting Peptide* (CTP), of transduction potential. This peptide is able to transduce a rat cardiomyoblast cell line, H9C2 cells, *in vitro*. This transduction is cell-specific and does not occur at all, or occurs at very low levels, in mouse fibroblast cell line, a fibrosarcoma cell line, human epithelial cancer cell line or human tubular endothelial cell line. We demonstrate that this peptide is not simply sticking to the surface and being internalized as a result of a fixation artifact with our functional Luciferase assay. In our assay Luciferase is expressed under the control of an NF- κ B promoter that requires NF- κ B activation to lead to expression of the protein. NF- κ B is a cytoplasmic protein that acts as a transcription regulator and enters the nucleus after activation and joining of its sub-units, the commonest being hetero- or homo-dimers of p50 and p65 subunits. Our peptide is able to carry and internalize an 11-amino acid peptide, NBD (nemo-binding domain), that inhibits this activation. In order to inhibit Luciferase expression, CTP must be internalized and escape the endosomal compartment and deliver NBD to the cytoplasm where NF- κ B resides and prevent its subsequent activation.

We have gone on to demonstrate that this transduction is indeed occurring *in vivo* as well, and is specific for the heart in mice. After a peripheral intravenous injection, CTP-6CF is seen to transduce mouse hearts robustly with little uptake by liver or spleen, with only a few lung and kidney capillaries showing fluorescence. This transduction peaks at 15mins for the smaller CTP-6CF, a 1790 Da molecule, but occurs at 30mins for the larger CTP-biotin-Streptavidin-Alexa488 (CTP-SA488), an ~55kDa in size complex. The biodistribution studies revealed that transduction begins to occur as early as 15mins, peaks at 30mins and is almost gone

by 120mins. At the same time, the fluorescence seems to increase in kidney glomerular capillary cells, suggesting that this might be a route of excretion for the peptide or at least the fluorescent marker, 6CF, after peptide breakdown.

Labeling the biotinylated form of our peptide CTP with red fluorescent streptavidin conjugated fluospheres made it possible to track this peptide *in vivo* using whole mouse imaging. CTP complexed with these 40nm fluospheres was injected intracardiac and mice followed by whole mouse imaging over multiple time points. The fluorescence was seen localized to the heart over 3 hours, as opposed to unconjugated beads or random peptide (RAN) conjugated to these beads. To further demonstrate the *in vivo* specificity of this peptide for normal heart tissue, mice underwent infarcts and a week post-infarct were injected with CTP-SA488 or PBS+SA488 complex. Confocal microscopy revealed fluorescence in normal heart tissue with complete exclusion of fluorescence from the thinned-out, infarcted, scarred heart tissue, thus demonstrating cell specificity *in vivo*.

In order to compare transduction efficiencies relating to the heart, mice were injected with fluorescently labeled CTP, 8K or RAN. Confocal microscopy showed transduction of the heart with CTP, with no significant heart transduction noted with 8K or RAN peptide, at similar doses and identical time-points studied.

A peptide able to transduce heart tissue *in vivo* in mice alone would have limited applicability in terms of developing therapeutics or new imaging agents of ultimate clinical use. Therefore we sought to determine if CTP is able to transduce human cardiac myocytes *ex vivo*. As per a pre-existing IRB protocol, explanted heart tissue was collected from consenting patients undergoing heart transplants for end-stage congestive heart failure. A modification of this protocol allowed us to have access to this tissue in a blinded fashion. Thin, 1-2mm, slices of

freshly explanted human heart tissue were incubated with varying concentrations of CTP-6CF for 30 mins. Tissue was washed thoroughly in PBS and fixed and cryosectioned for later confocal microscopy. This revealed robust transduction of heart tissue, with minimal uptake of just 6CF, RAN, and no uptake of Evans blue dye (a marker used to assess membrane permeability). 6R, a known PTD used as a positive control in our experiments, was taken up by cardiomyocytes robustly as well.

In conclusion, using a combinatorial approach of cell culture and *in vivo* phage display we have identified a peptide able to transduce rat cardiomyoblasts in a cell-specific manner *in vitro*, mouse heart tissue selectively *in vivo* and human heart tissue *ex vivo*.

3.0 MURINE INFARCT SIZE STUDIES USING NBD

NF- κ B was first identified as a transcription factor binding to the intronic enhancer of the Kappa light chain gene in B-cells over 20 years ago [44-45]. Since that initial description interest and research regarding this factor has been occurring at a blistering pace. As detailed in Section 1.6, NF- κ B is unregulated in response to ischemia-induced surge in cytokines, primarily TNF- α and IL-6. Interestingly neutrophil depletion reduced this increase in TNF- α and IL-6, and reduced nuclear translocation of NF- κ B [124]. In section 1.4, we detailed the role of IKK γ or NEMO and its interaction with the catalytic proteins IKK α and IKK β . The specific domain responsible for the interaction of NEMO with NBD has been worked out and termed the NEMO-binding domain [52]. The same report also detailed out how a peptide, NBD peptide, complexed with Anntenapedia homeodomain, a PTD, was able to reduce TNF- α mediated NF- κ B activation without diminishing the basal levels of NF- κ B activity. In fact the basal NF- κ B levels were somewhat increased in HeLa cells treated with the peptide (two-fold) as compared with untreated, control cells (40). Furthermore, NBD in association with varying PTDs (TAT or Anntenapedia) has been demonstrated to decrease inflammation associated pathologies (rheumatoid arthritis, inflammatory bowel disease) in animal models (see section 1.5 for more details). We therefore hypothesized that inhibiting NF- κ B activation in a murine model of infarction by delivering NBD in association with a PTD at the time of ischemia would reduce infarct size.

3.1 GENERATION OF THE ANIMAL MODEL OF MYOCARDIAL INFARCTION

In order to test the above hypothesis, an animal model of myocardial infarction was necessary. The following protocol was used and kept consistent from one set of experiments to another and between groups. Female, Balb/c, 10-20 week old mice were used for these set of studies. Female mice were chosen because of the ability to house 5/cage, as opposed to male mice (4/cage) and more importantly because female mice are able to tolerate cardiac insults better with lower post-operative mortality [125]. Mice were anesthetized with intraperitoneal (i.p.) injection of 2.5% Avertin (a mixture of 15.5 ml tert-amyl alcohol to 25 grams of 2-2-2 Tribromoethanol - stock solution diluted to 2.5% concentration with PBS) at a dose of 15ul/gm of body weight. Adequate anesthetic level was assessed by lack of response to toe-pinch and lack of a gag reflex. Mice were intubated, using direct visualization of the vocal chords, with a 22G cannula and placed on a Harvard rodent ventilator apparatus. Tube placement was confirmed by symmetric expansion of the thoracic cavity. Mice were ventilated with ~0.1cc/breath tidal volume at a rate of 110 breaths/minute.

Following successful intubation/ventilation, the chest cavity was opened using a left lateral thorotomy approach. Care was taken not to extend the surgical incision cephalad to the level of the sternal head, as a large venous confluence is present in that region and cutting through them can lead to major, exsanguinating bleed. A self-retaining mouse retractor was placed inside the incision and the teeth opened to reveal the anterior surface of the heart. The pericardium was gently removed with blunt forceps. A suture, 6-0 prolene, blue, monofilament (Owens & Minor: #8714H) was placed along the lateral wall of the left ventricle (LV), ~2mm below the lowest dip of the left atrium and ligated with exactly 5 squarely-placed knots. Ischemia was confirmed by the resulting pallor of the myocardium and development of wall motion

abnormality. The muscle layer and skin were closed in two layers with running sutures with 8-0 black, monofilament nylon suture (Owens& Minor: #2808G). The mice were extubated once spontaneous breathing was confirmed, and recovered on a heating pad. Post-operative pain was managed with subcutaneous injection of Ketoprofen, 5mg/Kg, on post-op day 0, 1 and 2 or with subcutaneous Buprenorphine, at a dose of 0.1mg/Kg body weight given once on the day of surgery and twice daily on post-op day 1 and 2. Mice also got one injection of subcutaneous Ampicillin, 100mg/Kg, after surgery for prophylaxis against post-surgical infection. Right after ligation and suture placement on the anterior surface of the heart to produce myocardial infarction, and before closing the chest wall, mice received i.p. peptides in different doses. The surgeon (myself) was always blinded to the treatment. Also surgeries were carried out in a rotational fashion so that any variation due to surgical technique was distributed equally over the treatment groups.

Mice were euthanized on post-operative day 7. On day of euthanasia, mice were anesthetized, chest cavity opened, and 1cc of 1M KCl injected via the right ventricle (RV) in order to arrest the heart in diastole to prevent contraction band necrosis. This was followed by injecting, through the right ventricle, 5cc of Glyo-fixx (formalin-substitute), heart dissected out and placed in 15ml of Glyo-fixx, until tissue embedded for sectioning. After paraffin embedding, cross-sections of the heart were taken starting at the apex. The first section was taken once the LV cavity appeared, with second and third sections taken 10 microns apart and cephalad of the first section. The three sections were H&E stained, light microscopy photographs taken, and area of infarct in each section mapped out using computer software Metamorph and expressed as a percent of the whole heart. The infarct area from the three sections was averaged to give the final

infarct size for each mouse. All mouse protocols were approved by the University of Pittsburgh Institutional Animal Care and Use Committee (IACUC).

3.2 INFARCT STUDIES USING 8K-NBD

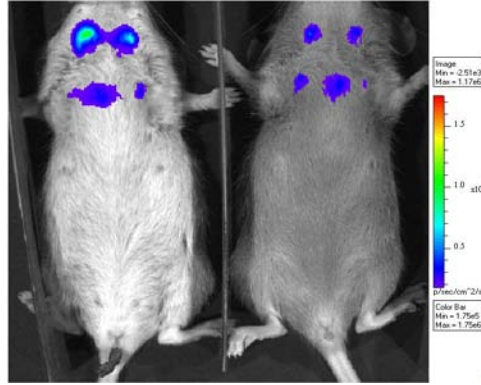
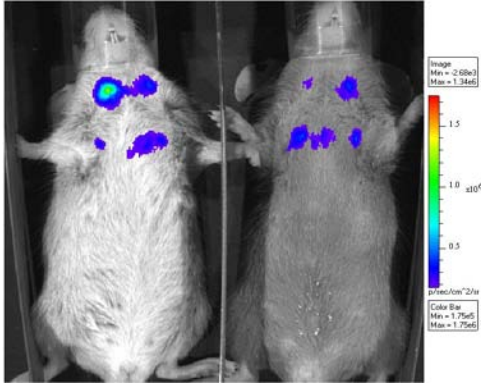
In view of the above background and after establishing the murine infarct model, we set out to test the following hypothesis. We hypothesized that suppression of NF- κ B activation using the NBD peptide, with 8K as a delivery PTD, would reduce infarct size in a mouse model of myocardial infarction. Prior to the actual infarct study, we undertook whole mouse *in vivo* imaging to show that 8K-NBD is able to suppress NF- κ B activation in response to LPS stimulation, a known activator of NF- κ B.

To demonstrate that 8K-NBD is indeed able to suppress NF- κ B stimulation, we used Luciferase expressing transgenic mice with Luciferase expression controlled by an NF- κ B promoter site. Mice were injected intraperitoneally (i.p.) with 8K-NBD (10mg/Kg) at time 0 and 2 hrs with LPS injected immediately after the first 8K-NBD injection. Whole mouse *in vivo* imaging for Luciferase activity was performed at 30mins, 2hrs, 4hrs and 6hrs. As illustrated in the figure below, initial Luciferase signal was similar between the two groups of mice but at 4 and 6hrs the signal increased in the LPS injected mice and remained stable/suppressed in the 8K-NBD treated mice.

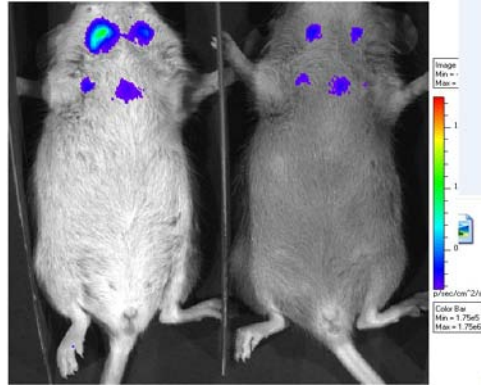
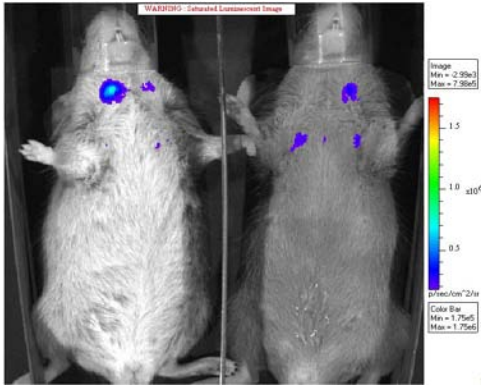
LPS

8K-NBD+LPS

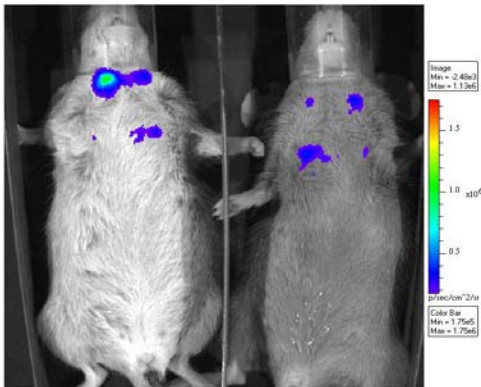
Baseline



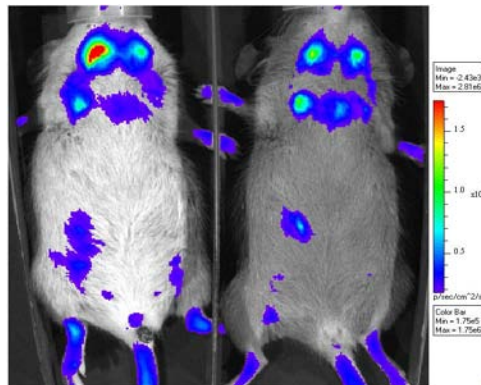
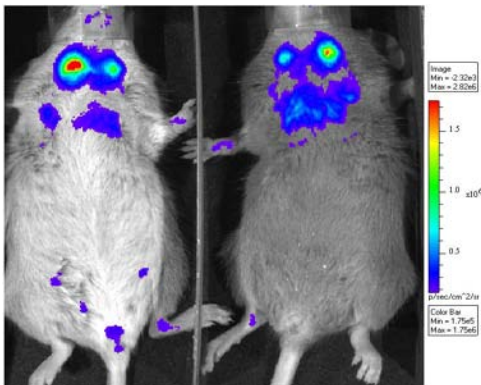
30 mins



2 hrs



4 hrs



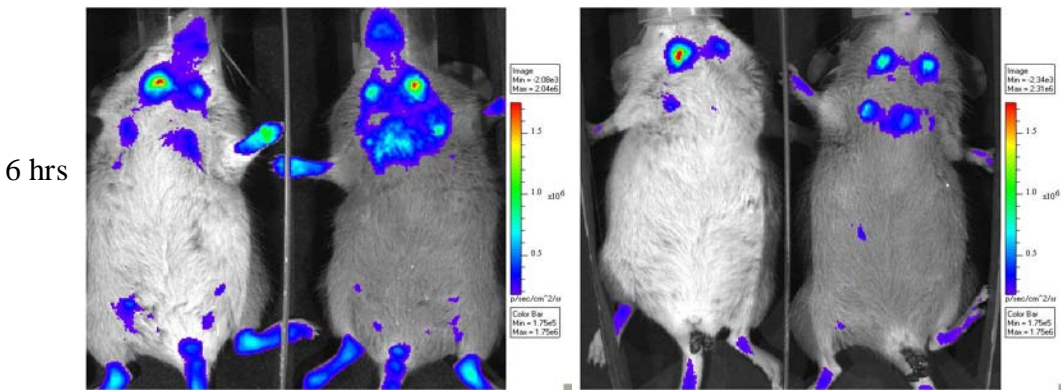


Figure 28. Inhibition of LPS induced Luciferase signal by 8K-NBD

After these initial imaging experiments, we proceeded to the infarct studies. Mice underwent left artery ligation, as detailed above, and were treated with i.p. PBS, 8K-NBD or 8K-mutant NBD (8K-mutNBD; KKKKKKKK-TTLDASALQME), at a dose of 5mg/Kg/injection, on post-op day 0 (immediately post-ligation) and post-op day 1 and day 2. Treatments were color-coded and administered in a rotational fashion. The surgeon was blinded to the treatment groups. Mice were euthanized on post-op day 7, heart dissected out and infarct size calculated, as detailed above in Section 3.1. A record of post-op mortality was kept. Also body weight and heart weight were recorded on day of euthanasia. There was an n=6 in each group. Figure 29 below shows the post-op mortality in each of the three groups.

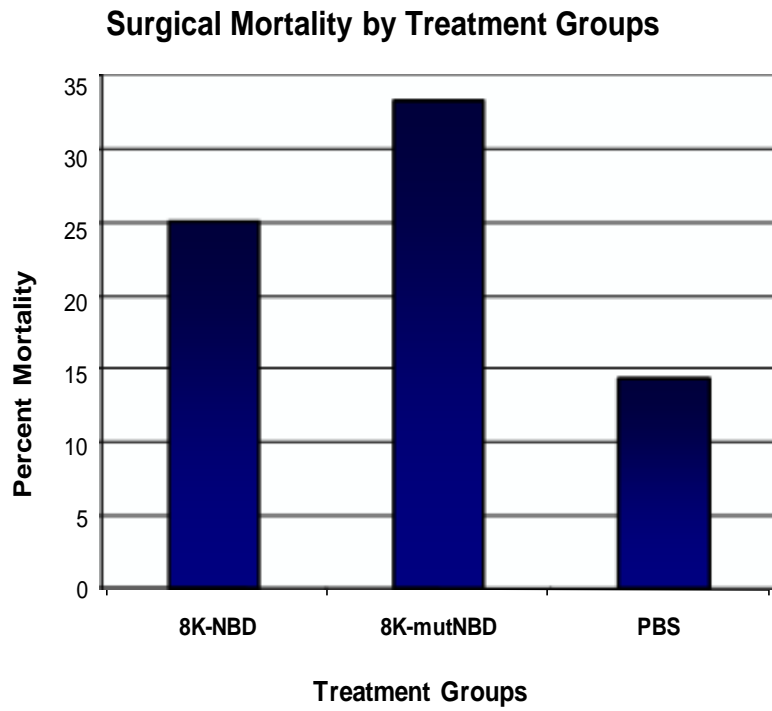


Figure 29: Post-operative mortality by treatment group in the 8K-NBD study.

However the heart-weight to body-weight ratios did not differ across the three groups as illustrated in Figure 30 below.

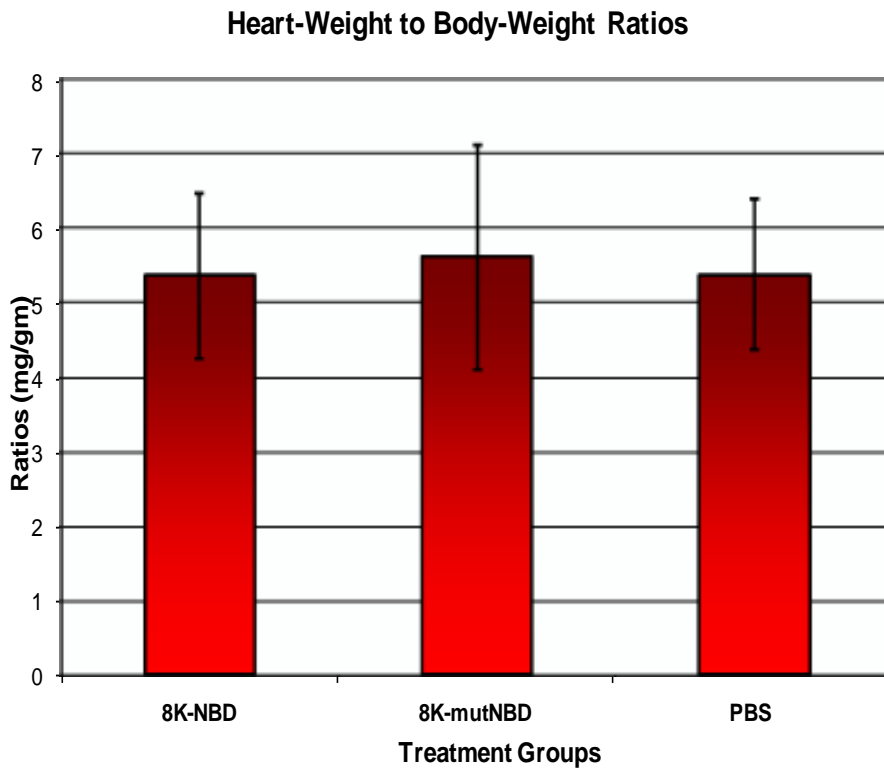


Figure 30. Heart weight to body weight ratios across the treatment groups in the 8K-NBD study.

In contrast, and contrary to our expectations, the infarct size were significantly different across groups and worse in mice treated with 8K-mutNBD (Figure 31). Mice treated with 8K-NBD had larger infarct sizes than PBS treated mice, though the difference showed a trend without reaching statistical significance.

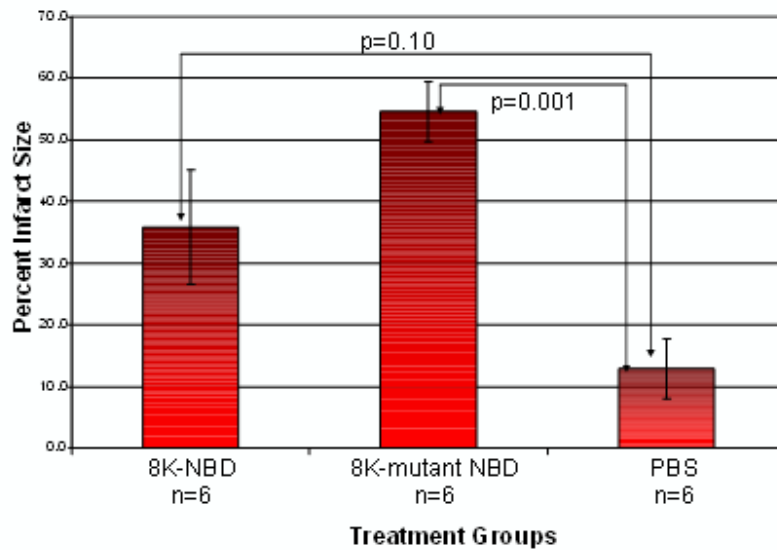


Figure 31. Infarct size across different treatment groups in the 8K-NBD study.

A cross-section from each heart was taken and apoptosis assessed by TUNEL staining. The nuclei were stained with Dapi, and the number of TUNEL positive nuclei expressed as a percentage of total nuclei in each field. The whole heart cross-section was taken into consideration by taking 5-6 contiguous, non-overlapping sections from each heart. The figure below demonstrates that the highest number of apoptotic nuclei occurred in 8K-NBD treated hearts, followed by 8K-mutNBD hearts with least number seen in the PBS treated heart sections.

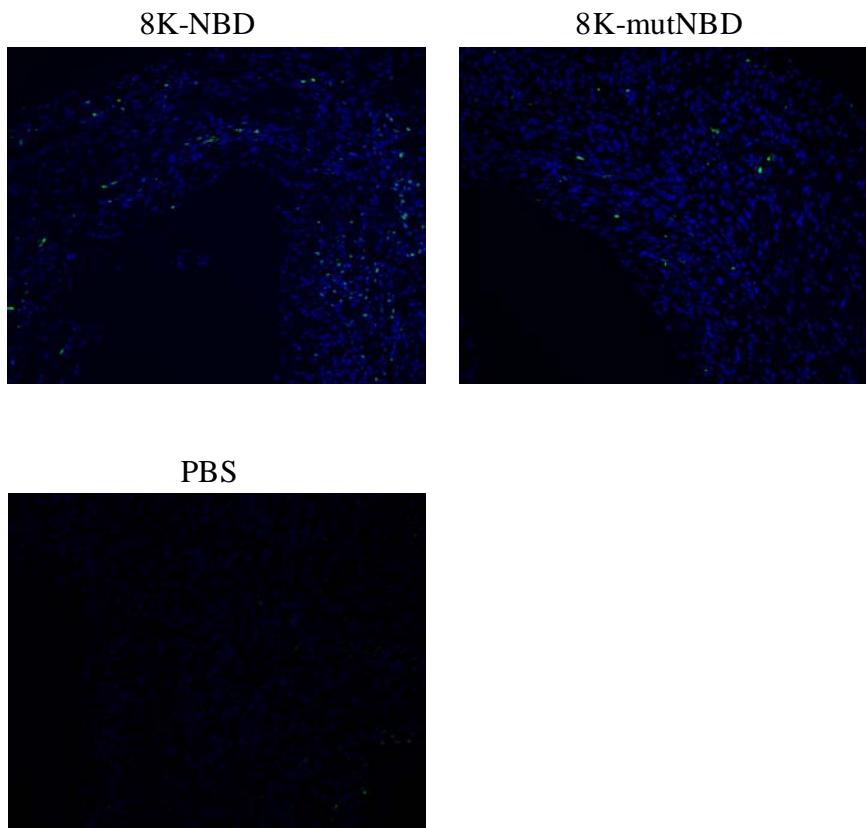


Figure 32. Representative confocal micrographs of TUNEL staining in each treatment group in the 8K-NBD study.

The figure below (Figure 33) illustrates the TUNEL staining data in a quantitative manner.

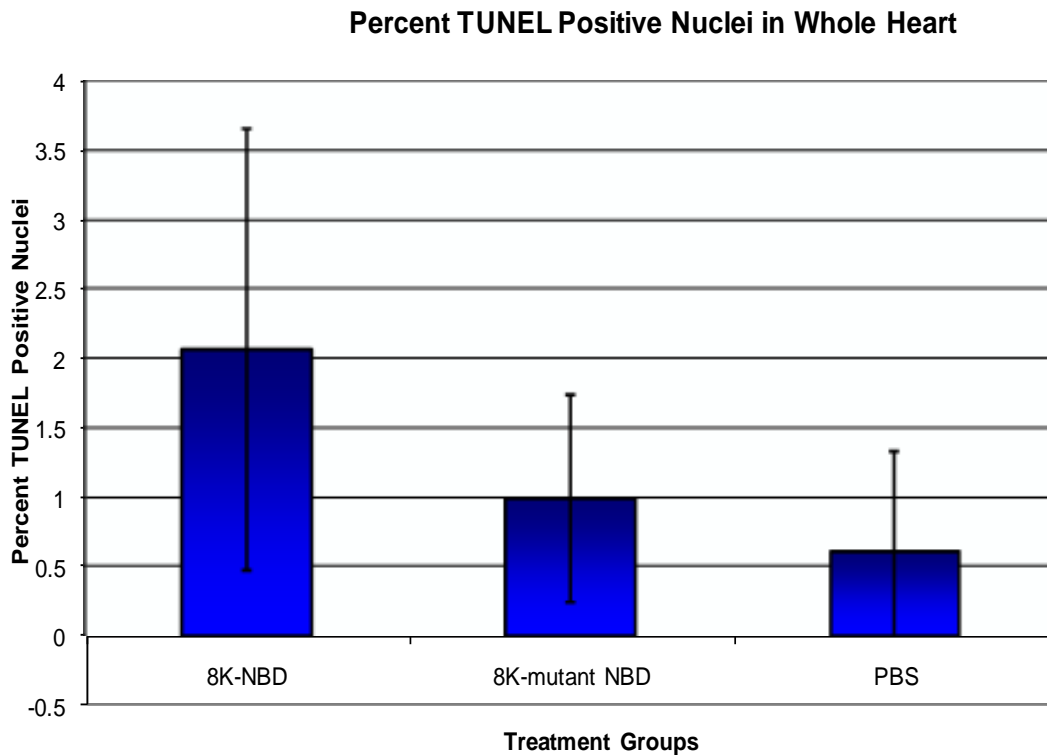


Figure 33. Quantification of TUNEL positive data in each treatment group in 8K-NBD study.

From these set of experiments we conclude that although 8K-NBD is able to inhibit NF- κ B activation in response to LPS stimulation, this inhibition in a mouse infarct model appears to be detrimental and results in increased apoptosis occurring, as assessed by TUNEL staining, and a larger infarct size. Although 8K-mutNBD had lesser number of apoptotic nuclei, the infarct size was actually larger. This difference from the PBS treated group reached statistical significance. It is possible that although 8K-mutNBD has much reduced NF- κ B inhibitory activity, it still has some level of inhibition which in an acute infarct model is detrimental. The apoptosis being less with a larger infarct size is difficult to explain and possibly within the realm

of biological variability as the infarct size in 8K-NBD treated and 8K-mutNBD treated mice was not statistically significant.

3.3 INFARCT STUDIES USING CTP-NBD

From the above section we conclude that although 8K-NBD is able to inhibit LPS-induced NF- κ B activity, such inhibition led to increased apoptosis and increase in infarct size. However the nature of these apoptotic nuclei, white blood cells/infiltrating cells versus cardiomyocytes was not clear. Data from this lab in a mouse model of inflammatory bowel disease in which treatment with 8K-NBD peptide was efficacious [18]. From our phage display experiments, we also noted that the transduction of heart tissue by 8K is quite inferior compared to CTP. We therefore hypothesized that the superior transduction ability of CTP would lead to better delivery of the NBD peptide to the heart tissue under ischemic stress and by inhibiting NF- κ B activation above its basal level would be cardioprotective and reduce infarct size.

Female, Balb/c mice underwent left artery ligation as detailed in Section 3.1 above. Mice were treated either with PBS, CTP-NBD or 8K-NBD (both at a dose of 10mg/Kg body weight) on day of surgery, delivered i.p., right after ischemia was confirmed. Peptides were suspended in PBS. The surgeon was blinded to the treatment allocation and treatment was given in a rotational fashion. Post-operative pain control was achieved with I/M Ketoprofen (5mg/Kg) on day 0, 1 and 2. Mice were euthanized on post-op day 7, heart dissected and processed for infarct size determination as detailed in Section 3.1 above. The post-operative mortality in each group is shown in the figure below (Figure 34).

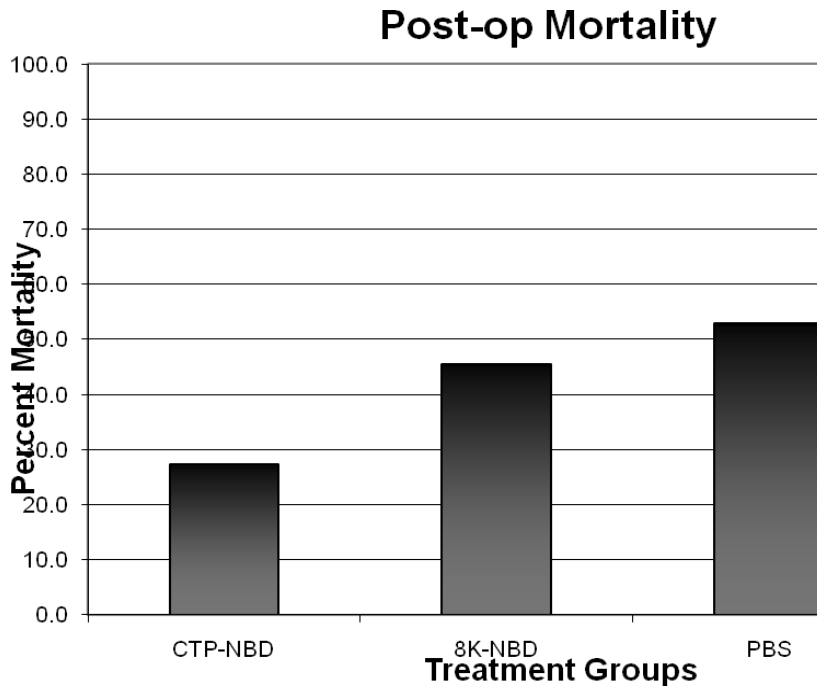


Figure 34. Post-operative mortality by treatment group in the CTP-NBD study.

The infarct size is shown in the figure below (Figure 35). As before, the infarct size was slightly more in the 8K-NBD treated group compared to the PBS treated group. However the CTP-NBD treated group showed a trend towards smaller infarct sizes.

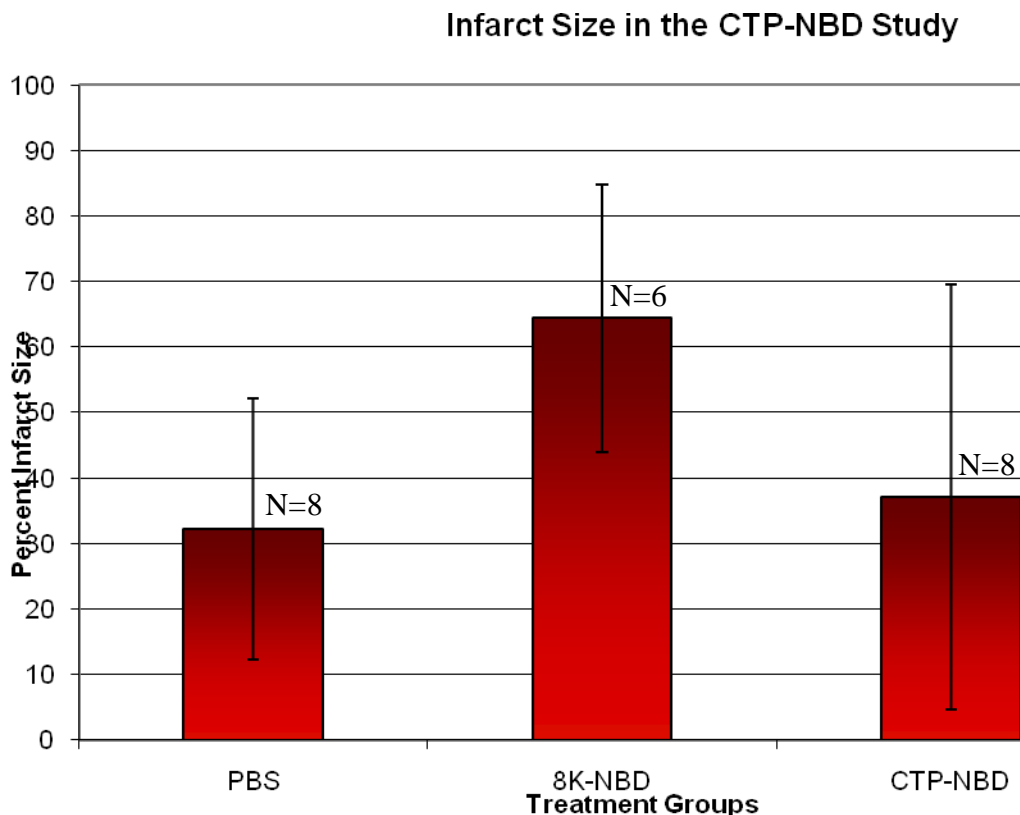


Figure 35. Infarct size by treatment groups in the CTP-NBD study.

Although this data was encouraging, the effect size was small and statistical analysis using this data showed that a prohibitively large sample size in each group would be needed to show significance. We decided to take an alternative approach. We hypothesized that the D-isomer of CTP-NBD would be resistant to degradation, have a longer half-life and be able to inhibit NF- κ B activation above its basal level much more effectively. To test this hypothesis, the D-isomer of CTP-NBD was synthesized in the University of Pittsburgh Peptide Synthesis Facility, with a fraction biotinylated at the C-terminus for conjugation with Streptavidin-Alexa488 (SA488) for tracking studies.

Using the D-isoform of CTP-NBD (D-CTP-NBD) to reduce infarct studies raised a few questions. Since the mechanism of transduction with CTP is not known, would switching the L-isoform with the D-isoform affect the transduction abilities adversely? Also would the D-isoform of NBD not be able to bind the IKK complex and therefore not inhibit NF- κ B activation? To answer these questions the following studies were undertaken prior to repeating the mouse infarct studies with D-CTP-NBD.

Two hundred microliters of a 1mM solution of D-CTP-NBD, biotinylated form, was incubated with 20ul of SA488 (2mg/ml stock solution) at room temperature (RT), light-protected for 60 minutes. 1ml of PBS was also incubated with 20ul of SA488 under identical incubation conditions. Female, Balb/c mice were anesthetized with i.p. Avertin and injected retro-orbitally with the D-CTP-NBD-SA488 complex at a dose of 10mg/Kg or PBS+SA488. Mice were then euthanized at 30 minutes (time to peak transduction with L-isoform CTP) or 120 minutes, hearts taken, fixed in 2% paraformaldehyde at RT for 4 hrs, overnight 30% Sucrose at 4°C, frozen in liquid N₂ chilled Isopentane and cryosectioned. PBS injected mice were euthanized at only 30 minutes. After cross-staining with DRAQ5, a nuclear stain, confocal microscopy was performed to look for fluorescence. Confocal microscopy showed robust uptake of D-CTP-NBD-SA488 complex albeit at a slower rate than L-isoform CTP. There was beginning of transduction noted at the edges with deeper tissue showing transduction at 120 minutes, as shown in figure below (Figure 36).

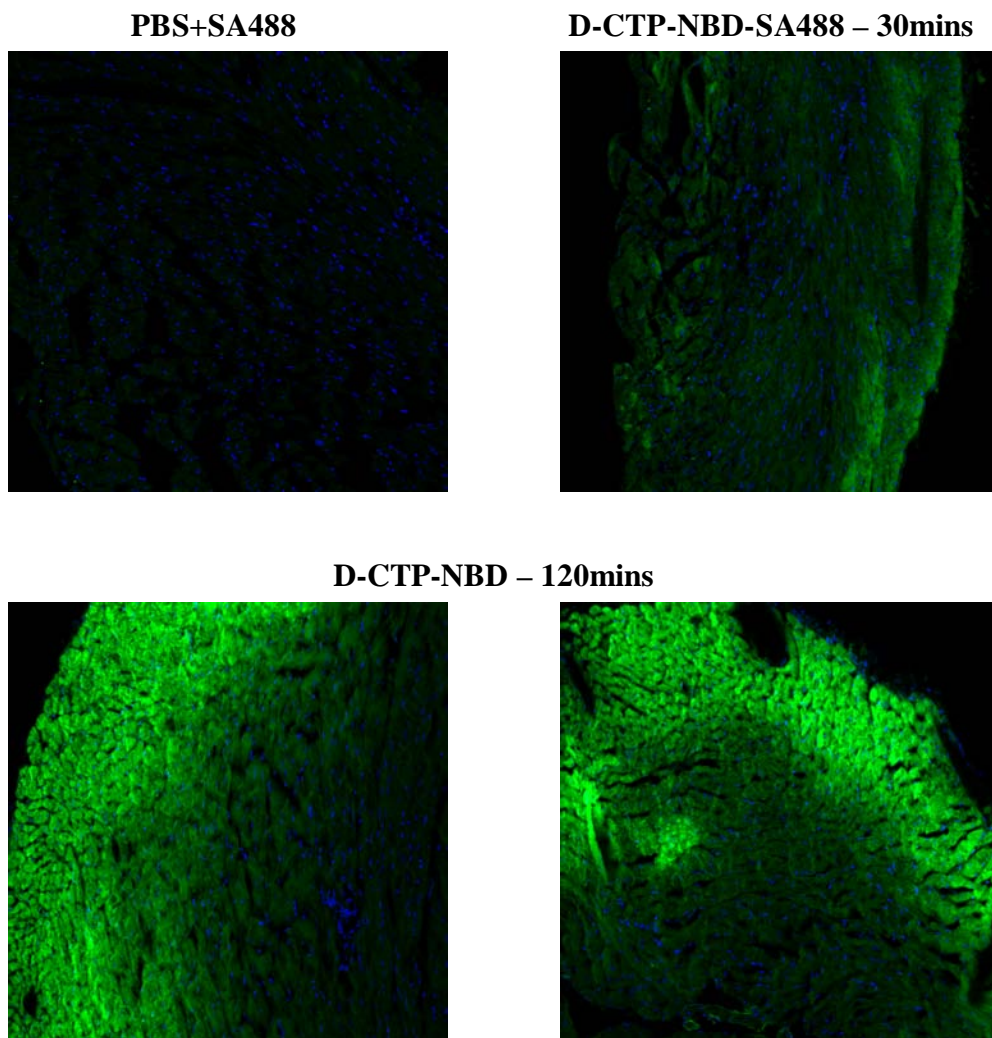


Figure 36. Transduction of the mouse heart by the D-CTP-NBD-SA488 complex.

To investigate if D-CTP-NBD retains its ability to inhibit NF- κ B activation in response to TNF α stimulation, the cell culture Luciferase studies were repeated. H9C2 cells were plated onto 96-well plates and double transfected with a plasmid carrying Luciferase under an NF- κ B promoter site as well as a Renilla expressing control plasmid. 24 hours post transfection, cells were pre-treated with increasing concentrations of the D-CTP-NBD peptide and 30 minutes later challenged with TNF α for 3 hours. After three hours, cells were washed, trypsinized, lysed and Luciferase and Renilla activity quantified in a luminometer. All work was done in quadruplicate.

The figure below (Figure 37) shows that D-CTP-NBD is a less potent inhibitor of NF- κ B activation with any appreciable inhibition occurring only at the highest tested dose (400uM).

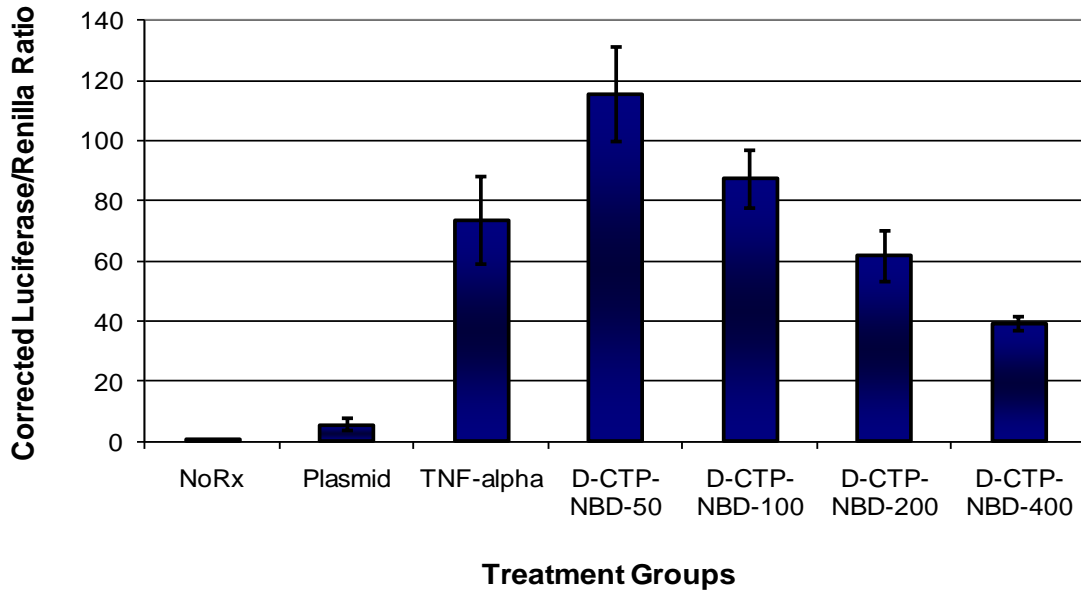


Figure 37. Inhibition of NF- κ B activation by the D-isoform of CTP-NBD.

Although inhibition of NF- κ B did occur, it was seen only at the highest tested dose. Given that the transduction process was slowed down as seen in the *in vivo* imaging mouse study (Figure 36), we hypothesized that perhaps 30 mins of incubation/lead time was not adequate with D-CTP-NBD. However pre-incubating with 60 mins or 120 mins produced identical results with ~40% inhibition seen, only with the highest dose (400uM), as compared with the TNF α -stimulated cells (results not shown). In spite of these findings, we choose to test the peptide in a mouse infarct model, hypothesizing that although inhibition occurs only at the highest tested dose, this dose might be achievable given the robust transduction seen at 120 mins as well as

probable accumulation of D-CTP-NBD inside cardiomyocytes to a high enough concentration given it's resistance to intracellular degradation.

Mice underwent left artery ligation, as detailed above. Only one dose of D-CTP-NBD or PBS was administered at time of surgery (5mg/Kg, i.p.), and mice were euthanized on post-op day 7. The surgeon was blinded to the treatment allocation and post-op pain control was achieved with s.q. Buprenorphine (0.1mg/Kg body weight). As shown in the figure below, infarct size did not differ between the two groups.

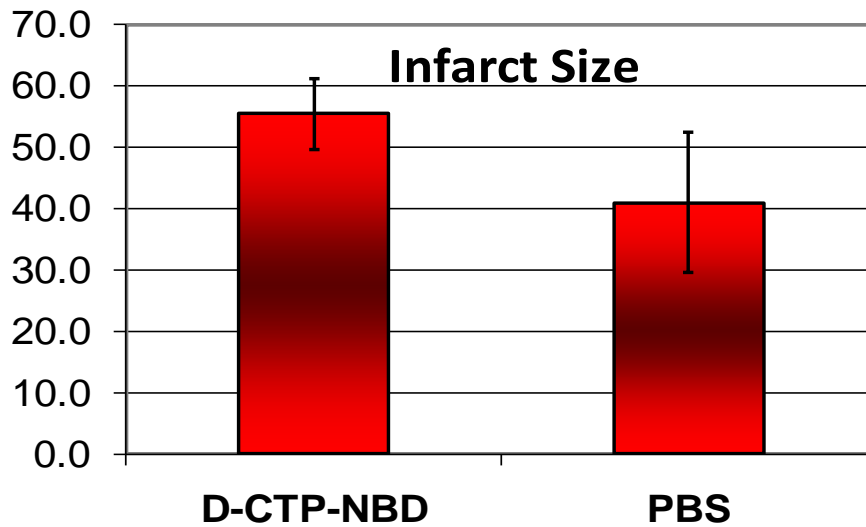


Figure 38. Infarct sizes in the two treatment groups.

In addition, if infarct sizes of less than 10% were excluded, the mean infarct size in the two groups was nearly identical leading us to conclude that treatment with D-CTP-NBD did not have any significant effect on infarct size. Probably the most likely explanation for this lack of

an effect, despite promising earlier data, is the lack of adequate inhibition of NF- κ B activation by the D-isoform of NBD. Although inhibition in cell culture studies, utilizing H9C2 cells, did occur, it was apparent only at the highest dose tested (400 μ M). This level might not have been achievable at the dose of 10mg/Kg body weight *in vivo* to produce a biological effect. In addition, later studies of NF- κ B inhibition [3, 105, and 106] have shown that infarct sizes are similar in control and NF- κ B inhibited mice, but remodeling is favorably affected in the latter group. In our studies, mice were euthanized at post-op day 7, which would be too early to see differences in post-infarct modeling or differences in left ventricular function.

In summary, these set of experiments demonstrated lack of a significant biologically favorable effect of inhibiting NF- κ B, utilizing 8K-NBD. In fact a trend towards worsening of infarct size was apparent in multiple studies suggesting that the initial surge of NF- κ B activation that follows ischemic myocardium may have a protective role. Also 8K, as a protein transduction domain, may be targeting cell types different than the actual myocytes and may be targeting more of the inflammatory infiltrating cells. Inhibiting NF- κ B in neutrophils, utilizing NBD, has been shown to increase apoptosis of these cells in response to LPS stimulation [17]. Increasing neutrophil apoptosis, at the earliest stage of the inflammatory response to myocardial ischemia, may well be detrimental. Lack of a response of any kind to D-CTP-NBD in the subsequent studies was likely not a failure of transduction with the D-CTP isoform but rather a lack of adequate NF- κ B inhibition by the D-isoform of NBD.

4.0 SUMMARY, IMPLICATION OF OUR FINDINGS AND FUTURE DIRECTIONS

4.1 SUMMARY OF OUR FINDINGS

In this body of work we have utilized a combinatorial cell culture and *in vivo* phage display to identify a peptide that targets rat cardiomyoblast cells (H9C2 cells) *in vitro* and mouse cardiac tissue *in vivo*. This peptide, which we termed cardiac targeting peptide, or CTP, is able to deliver a cargo peptide, NBD or nemo-binding domain to H9C2 cells in culture, and deliver Streptavidin-Alexa488 complex to mouse cardiac tissue *in vivo*. The method of phage display was first demonstrated by Smith [32], and *in vivo* phage display by Pasquallini and colleagues [37]. Since the initial description of *in vivo* phage display, studies have been carried out to target vasculature ligands of different organs demonstrating that the endothelial lining of various organs is far from being homogenous. Such heterogeneity of vasculature ligands has been demonstrated for different normal organs as well as diverse disease states like tumor vasculature [37] and atherosclerotic plaques [126]. Most of these studies have focused on targeting vascular ligands. In contrast, our work was meant to target more the cardiomyocytes *in vivo*, going beyond the vasculature. We aimed to identify a peptide that would be able to traverse the endothelial barrier of the heart, traverse the interstitium, bind and be internalized by cardiomyocytes *in vivo*. Such a unique peptide would have to be teased out of a large library, with high background of contaminating, non-specific phage, especially as the heart is an

extremely vascular organ and would be rich in the circulating blood pool of phage. We optimized our chances by pre-enriching the phage pool with a single cell culture cycle on H9C2 cells before undertaking the *in vivo* cycles of phage display. The problem of contaminating phage in the blood pool was minimized with prolonged circulation times to allow for clearance of phage from the circulation and maximize the chances that phage recovered from the heart would be the relevant, internalized one. Further, to maximize our chances of recovering phage, mice were pre-treated with chloroquine to minimize degradation of internalized phage by preventing acidification of the intracellular lysosomal compartment. Using these methodological changes, we were able to identify CTP and show that it is not simply associated with vascular or cardiomyocytes surface, but able to be internalized.

As a separate, though related, piece of work we went on to establish a mouse model of myocardial infarction and test nemo-binding domain (NBD) peptide's ability to reduce infarct size in association with 8K, a known PTD from this lab. Later as the identity and transduction ability of CTP was established, we utilized CTP-NBD to assess if this peptide was able to reduce infarct size *in vivo*. As detailed in Chapter 3, though 8K-NBD was able to inhibit surge of NF- κ B activation in response to LPS, it actually increased infarct size in our model. Although CTP-NBD was able to somewhat reduce infarct size in earlier studies, the effect size was modest and would require large sample sizes to reach statistical significance. To prolong the action duration of CTP-NBD, we utilized the D-isoform of all the amino acids constituting the peptide. Although transduction ability of CTP was retained, it slowed down considerably and NBD was not able to inhibit NF- κ B activation, except at the highest concentration tested, and likely non-physiological doses (400uM), *in vitro*. Such high concentrations were likely not achieved, *in vivo*, and may explain the lack of effect noted with D-CTP-NBD.

4.2 IMPLICATIONS AND FUTURE DIRECTIONS

A protein transduction domain able to transduce heart tissue specifically *in vivo* would open up avenues for better imaging, as well as a delivery agent for potential therapeutics. We believe that this is what we have achieved with identification of CTP. However this work has opened many interesting questions. Foremost is the mode of transduction pathway that this peptide utilizes. From the above discussion (Section 4.1), it is clear that this mode of delivery is likely to be complex and has to overcome many barriers to actual transduction of the cardiomyocytes *in vivo*. There has been immense interest in the mode of transduction utilized by PTDs in general with greatest body of work gathered on TAT. This work has revealed that TAT, being a highly cationic peptide, binds to heparan sulfate groups on cell surface followed by internalization, likely by a macropinocytotic mechanism [127-128]. This is unlikely to be the mode of uptake by CTP, as it is neither arginine-rich, nor is it cationic, with an isoelectric pH of 9.35 and hydrophilicity index of -0.4. Indeed our lab has started performing preliminary experiments to tease out the mechanism of transduction. In one set of preliminary experiments, H9C2 cells were incubated with 200uM of CTP-SA488 complex at 37C or 4°C for 30 mins. After equal number of washes, cells were fixed, counter-stained with DRAQ5 and confocal microscopy performed. The figure below (Figure 39) shows transduction occurring at 37°C with minimal to no transduction seen at 4°C, implying that transduction is an active, energy -dependent process, and not a simple diffusion of a peptide across the lipid cell membrane.

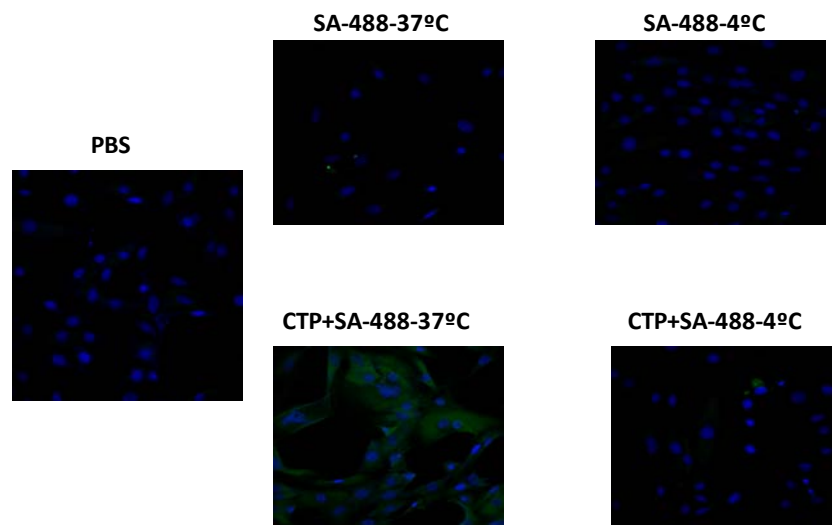


Figure 39. Temperature dependency of CTP's transduction ability.

Moreover viability studies were performed in H9C2 cells after incubating with increasing concentrations of CTP-NBD for 30 minutes at 37°C/5% CO₂. After the incubation period, cells were washed and viability assessed using a standard MTT assay. As shown in the graph below, no significant change in viability was noted with CTP-NBD, even at the highest end of the tested concentration. Therefore transduction is not likely simple uptake of CTP by compromised cells.

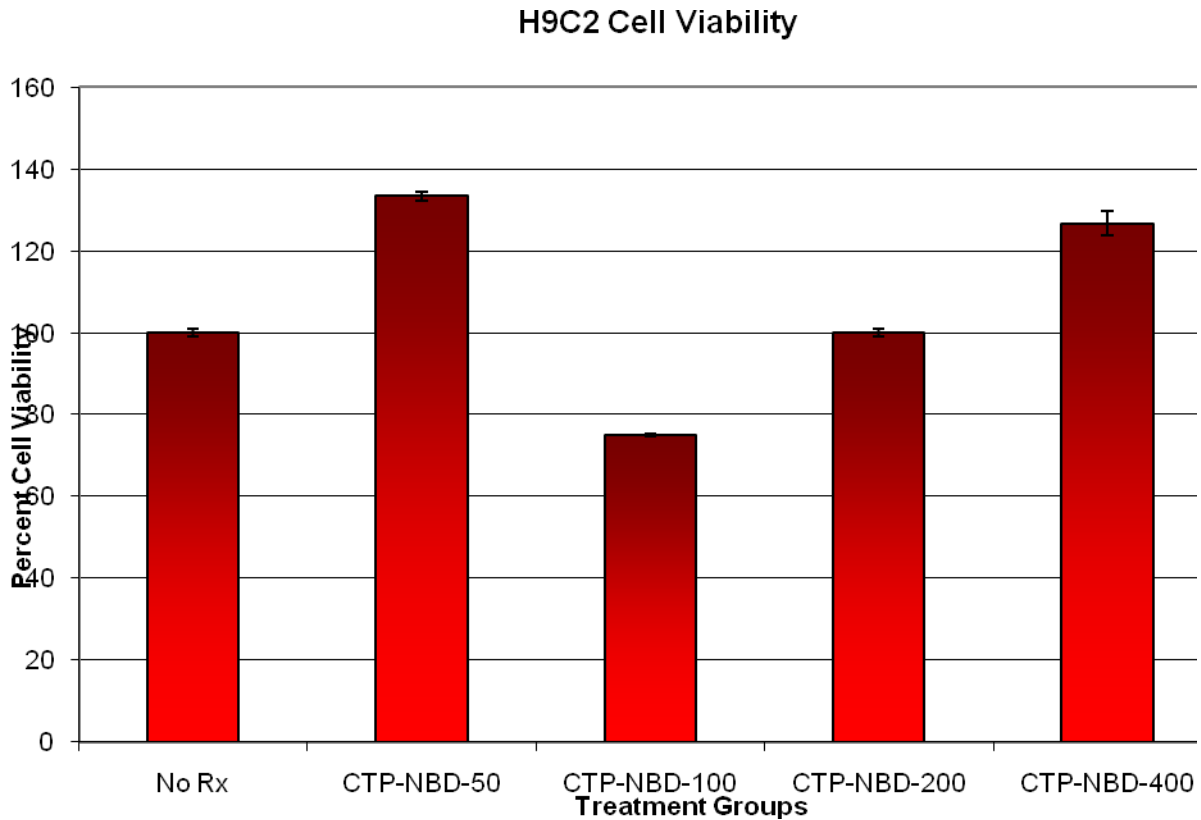


Figure 40. H9C2 cell viability after incubating with increasing concentrations of CTP-NBD.

Interestingly a group of investigators have identified the identical CTP sequence, via phage display, as binding preferentially to bone-like mineral and hydroxyapatite material [129-130]. Although this work involved *in vitro* phage display against immobilized hydroxyapatite discs, the fact that such a display led to the exact same sequence as CTP being identified suggests that this peptide may be able to bind to cardiac interstitium. However for this to happen, the heart endothelial barrier must be traversed first. Zhang and colleagues profiled heart vasculature endothelium using *in vivo* phage display as well as bacterial two-hybridization scheme, and identified a number of peptides able to bind anywhere from ~15 fold to 310 fold greater avidity to heart endothelial cells [39]. None of these identified peptides bear any

homology to the CTP sequence. Moreover, the high magnification confocal micrographs of H9C2 cells (Figure 11) showing punctate intracellular, cytoplasmic fluorescence, along with transduction experiments reported above, suggest that transduction with CTP is an energy dependent process involving binding of CTP to a ligand followed by endocytosis. The ligand CTP is targeting remains to be identified. The next step would then be to confirm the cytoplasmic substructure that CTP ends up in, using higher magnification confocal micrographs of H9C2 cells along with endocytic markers. The exact ligand CTP is targeting can be identified using a bacterial two-hybridization scheme similar to that reported by Zhang et. Al. [39]. Such mechanistic insights would be critical to assess CTP's ability to deliver cargoes, in addition to the size limitations, to the heart. It is likely that the size and/or nature of the cargo could very well diminish CTP's transduction ability.

I see the potential clinical utility of CTP as not only a therapeutic delivery vehicle, which of in itself would be of great benefit, but also as improving our diagnostic abilities. Recently attention has focused on patient exposure to medically necessary ionizing radiation [131] which can be considerable over time and have a cumulative effect. As was also pointed out in this study [131], a major portion of the ionizing radiation exposure is from nuclear studies of which cardiac nuclear studies constitute a significant percent. When injecting patients with radio-isotopes like Thallium or Technetium, the majority of the radiation is taken up by the liver and gut regions. Not only does that necessitate injecting a higher amount to target the heart, but also, not infrequently, degrades the cardiac image quality. The inferior wall of the left ventricle is particularly difficult to assess because of its proximity to the diaphragm as well as high background gut activity just underneath the diaphragm. Labeling CTP with a radioisotope, like technetium, has the potential to decrease total radiation exposure and actually increase image

quality by directing all of the radiation to the heart. The proof of principal and ability to label peptides with radio-isotopes and use for imaging has already been reported [132] and therefore is feasible.

Another interesting potential application of CTP would be to express it on coat-protein of adenoviral or adeno-associated virus to target viral particles to the heart. In this arena, we have started work with AAV viral vectors in collaboration with Dr. Nakai's lab. This lab has produced a gutted out version of the AAV9 vector, termed the AAV1.9-3 vector, which lack heparan binding sites. This viral vector has prolonged half-life in blood and limited transduction ability. This virus can be retargeted by placing an RGD motif back in its coat protein. Preliminary experiments assessing ability of AAV2, AAV1.9-3, AAV1.9-3RGD and AAV1.9-3-CTP (with CTP sequence placed at position 587 of the viral coat protein) to transduce H9C2 cells appear promising. The figure below demonstrates the ability to de-target and retarget AAV9 vector. Addition of CTP to the de-targeted virus appears to be cautiously promising, though much work remains to be done.

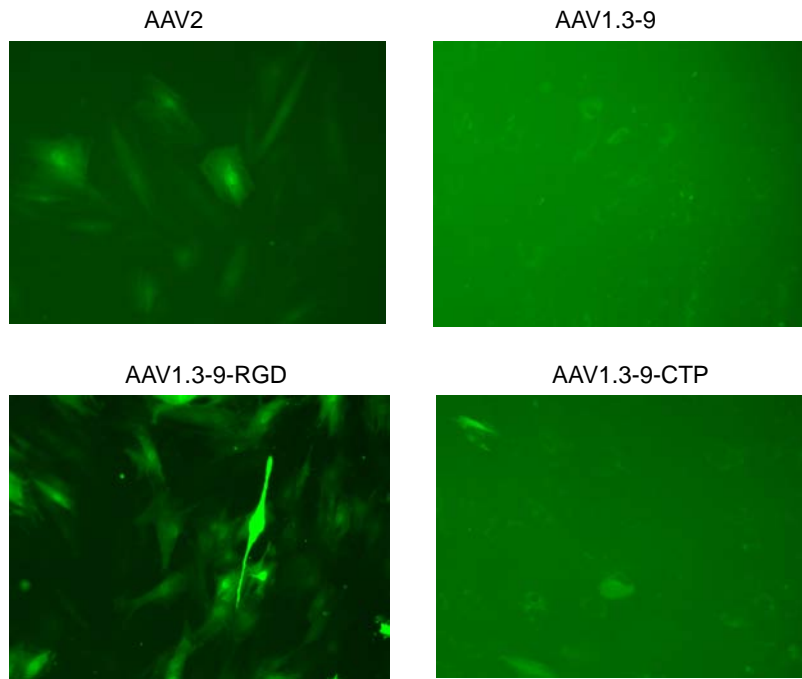


Figure 41. H9C2 cells transfected with different AAV viral vectors expressing EGFP.

Two major issues are the inability to package larger marker genes like LacZ into these modified viruses, and the sharp drop in titers that occurs with modification of the coat protein making large scale production difficult, if not impossible. These problems are in the process of being addressed and will hopefully help in making AAV vectors more cardiac specific.

5.0 METHODS

This chapter will outline in depth the step by step methods followed to do *in vitro* and *in vivo* phage display. It will be followed by details of the cell transfection protocols as well as the Luciferase read-out assay utilized to document TNF α mediated NF- κ B activation as well as inhibition of it by CTP-NBD fusion peptide. Later in the chapter, details will be provided of the mouse infarct model, euthanasia protocol as well as determination of infarct size on H&E histology slides.

5.1 PROTOCOL FOR PEPTIDE PHAGE DISPLAY

The protocol describes below the steps leading to a pre-screening cycle being performed *in vitro* on rat cardiomyoblast cell line, or H9C2 cells, utilizing a commercially available (New England Biolabs, cat#E8110S) M13, twelve amino acid peptide phage display library. After the first cycle *in vitro*, the subsequent three cycles were performed *in vivo*, as detailed below.

The protocol detailed below, utilizing peptide phage display to identify internalizing phage and the peptide sequence leading to internalization, is modified to target heart tissue *in vivo*. The process is complicated by the heterogeneity and complexity of the tissue being targeted, the sequestration of injected phage by organs of the reticuloendothelial system, largely the liver and spleen, and a large pool of contaminating, non-specific circulating phage. In

addition, the rigorous conditions that the phage displaying peptides are put through leads to loss of infective phage over subsequent cycles. Here we provide details of the protocol used to identify peptides transducing the heart with kidney being used as control tissue.

5.1.1 Materials

Cell Culture:

1. Dulbecco's Modified Eagle's Medium (DMEM; GIBCO/BRL)
2. Heat-inactivated fetal bovine serum (FBS; GIBCO/BRL)
3. Pen Strep stock solution (GIBCO; 15140)
4. Hepes buffer solution 1M (GIBCO; 15630)
5. Rat Cardiomyoblast Cell Line (H9C2 Cells) Media. Make the H9C2 cell media by adding 50ml of heat-inactivated FBS, 5ml of Hepes, and 5ml of Pen-Strep to 500ml of DMEM. Filter the mixture and store at 4°C.
6. Solution of trypsin (0.25%) and ethylenediamine tetraacetic acid (EDTA-1mM; GIBCO)

Phage Display

1. M13 12-mer peptide phage display library containing:
 - a. Phage display peptide library, 100ul, $\sim 1 \times 10^{13}$ pfu/ml, in TBS with 50% glycerol
 - b. -96 gIII sequencing primer 5' - HOCCC TCA TAG TTA GCG TAA CG -3', 100 pmol, 1 pmol/ μ l
 - c. -28 gIII sequencing primer 5' - HOGTA TGG GAT TTT GCT AAA CAA C -3', 100 pmol, 1 pmol/ μ l

- d. *E. coli* ER2738. Host strain supplied as 50% glycerol culture; not competent.
Store at -70°C .
2. LB Medium: 10 g Bacto-Tryptone, 5 g yeast extract, 5 g NaCl in 1 liter of H_2O .
Autoclave, store at 4°C .
 3. IPTG/Xgal Stock Solution: Mix 1.25 g IPTG (isopropyl- β -D-thiogalactoside) and 1 g Xgal (5-Bromo-4-chloro-3-indolyl- β -D-galactoside) in 25 ml DMF (dimethyl formamide). Solution should be stored at -20°C .
 4. LB/IPTG/Xgal Plates: 1 liter LB medium + 15 g/l agar. Autoclave, cool to $< 70^{\circ}\text{C}$, add 1 ml IPTG/Xgal Stock per liter and pour. Store plates at 4°C in the dark.
 5. Agar Top: 10g Bacto-Tryptone, 5g yeast extract, 5g NaCl, 7g Bacto-Agar in 1 liter of deionized H_2O . Autoclave, dispense into 50ml aliquots. Store at room temperature (will be solid).
 6. Tetracycline Stock Solution: 20mg/ml of tetracycline powder in a 1:1 Ethanol:Water.
Store at -20°C , light-protected. Vortex before use.
 7. LB+Tetracycline Media: To 1 liter of H_2O add 10 g Bacto-Tryptone, 5 g yeast extract, and 5 g NaCl. Autoclave, and allow to cool down to $< 70^{\circ}\text{C}$ or until lukewarm to touch.
Add 1ml of Tetracycline stock solution, mix and store at 4°C , light-protected, until ready for use. Do not use if color turns from yellow to brown or black.
 8. LB/Tetracycline Plates: Add 15g of Agar to a liter of LB medium. Autoclave and allow to cool to $< 70^{\circ}\text{C}$, add 1ml of tetracycline stock solution, pour into plates and allow to solidify. Store plates at 4°C , light-protected. Do not use plates if they turn brown or black.

9. TBS: 50 mM Tris-HCl (pH 7.5), 150 mM NaCl. Autoclave and store at room temperature.
10. PEG/NaCl: 20% (w/v) polyethylene glycol–8000, 2.5 M NaCl. Autoclave, mix well to combine separated layers while still warm. Store at room temperature.
11. Iodide Buffer: 10 mM Tris-HCl (pH 8.0), 1 mM EDTA, 4 M sodium iodide (NaI). Store at room temperature in the dark. Discard if color is evident.

Biopanning in mice

1. 8 to 12 week old albino, male or female mice (Balb/c or FVB; Jackson Labs)
2. 0.5ml Insulin syringes
3. Sterile phosphate buffered saline (PBS; GIBCO)
4. Avertin stock solution: Avertin (2, 2, 2-Tribromoethanol; Sigma-Aldrich) is mixed with 15. 5 ml *tert*-Amyl Alcohol (2-methyl-2-butanol; Fisher) for ~12 hours in a dark bottle at room temperature. Allow the mixture to go completely into solution, sterile filter and store at 4°C, light protected. On the day of use, mix 200ul of this stock solution with 10ml of PBS, sterile filter and wrap in foil before use. This will be the 2% Avertin working solution.
5. HBSS (Cellgro)
6. 10% Glucose. Dissolve 10gm of glucose in 100ml of deionized H₂O, sterile filter in a hood and store for later use
7. Heparin 1000U/ml (Lyphomed)
8. Collagenase II (50mg/ml; Worthington)
9. DNase I (20mg/ml; Roche)
10. Dulbecco's Modified Eagle's Medium 50:50/F12 (Cellgro)

11. Heat-inactivated fetal bovine serum (FBS; GIBCO/BRL)
12. Gentamycin 50mg/ml (1000x; GIBCO)
13. 75 μ M cell filters
2. Solution of trypsin (0.25%) and ethylenediamine tetraacetic acid (EDTA-1 mM; GIBCO)
15. HBSS-G: To 90 ml of HBSS, add 10 ml of 10% glucose solution.
16. HBSS-G-Heparin: To 50ml of HBSS-G, add 500ul of Heparin (1000U/ml stock solution). Make fresh on the day of use.
17. Digestion Enzyme: To 39ml of HBSS-G add 40ul of DNase I and 1.2 ml of Collagenase II. Make fresh on the day of use.
18. Plating medium: To 90 ml of DMEM 50:50/F12 add 10ml of the heat inactivated FBS and 100ul of Gentamycin stock solution.
19. 0.75% collagenase II: Add 75mg of collagenase II to 10ml of PBS. Make fresh on the day of use.
20. DMEM 50:50/F12/25% FBS: add 7.5ml DMEM/F12 to 2.5ml FBS. Will need 10 cc for each heart.

5.1.2 Methods

Peptide Phage Display

- a. Passage the rat cardiomyoblast cell line, H9C2 cells, for a minimum of 3 passages (after thawing from -180°C). Cells should be passaged once they are ~70% confluent. Do not allow to grow to complete confluency as they will begin to differentiate.
- b. After the third passage, trypsinized cells with Trypsin/EDTA and plate in a 6-well plate at a cell density of 2×10^5 cells/well. Twenty-four hours post-plating, aspirate and replace

with pre-warmed media, and add 10ul of the M13 peptide phage library ($\sim 10^{11}$ phage) to the media. Return cells to incubator for 6 hours.

- c. After the incubation period, wash cell extensively (at least 6x) with pre-warmed PBS, trypsinized cells, and centrifuge to collect cell pellet. Wash the cell pellet 1-2 times more with media. Aspirate the supernatant media above the cell pellet but not completely. Cell pellet may be stored at -80°C for later lysis and phage titration.
- d. Release internalized phage by subjecting the cell pellet to one freeze-thaw cycle by bringing the cell pellet from -80°C to either room temperature, or by placing in a 37°C water-bath. Pellet out the cell debris and use the supernatant for phage titration as detailed below.

Phage Titration

- a. Inoculate 100ml LB+tetracycline media in a round-bottomed flask with 10ul of E. coli, provided with the phage display library. Grow overnight at 37°C with gentle shaking (225 rpm). This will be the starter culture.
- b. Inoculate another 100ml of LB+tetracycline media with 1-2 drops of the starter culture. Incubate at 37°C for 1hr with gentle shaking.
- c. Melt agarose top in a microwave until liquid. Vortex to make sure it is homogenous. Dispense 3ml into 6 sterile culture tubes. Place the 6 culture tubes in a water-bath with temperature set to 45°C and maintain at this temperature until ready for use.
- d. To carry out infection, add 20 μl of cell extract (from Step 2.1d.) to 200ul of E. coli culture (from Step 2.2b.), vortex quickly, and incubate at room temperature for 1–5 minutes. This will be the 1×10^0 dilution. Take 20ul of this and add to another 200ul of

the starter culture (1×10^1) and so on until you have 1×10^6 dilutions. Use a new tip for each serial dilution.

- e. Transfer 200ul of each of these to the culture tubes containing 3ml of the melted agar top at 45°C , one infection at a time (from step 2.2d.), vortex briefly, and immediately pour culture onto a pre-warmed LB+Tetracycline plate or IPTG/X-gal plate (labeled 1×10^0 ----- 1×10^6). Pre-warm, for at least one hour, one LB/IPTG/Xgal plate per expected dilution at 37°C until ready for use. Gently tilt and rotate plate to spread top agar evenly.
- f. Allow the plates to cool for 5 minutes, invert, and incubate overnight at 37°C . Place in 37°C , light-protected (for either type of plates) for overnight growth.
- g. Next day count either the clear plaques in the case of LB+Tetracycline plates, or blue plaques in the case of Xgal plates. Some plates will have too numerous to count plaques and some might have too few. Count the ones with 10-200 plaques, multiply by the dilution factor and that will provide the number of phage per 20ul of the cell lysate. The total number of phage can be calculated by multiplying this number by the total lysate cell supernatant volume (in ul) divided by 20.

$$\text{Total No of Phage} = \text{Number of plaques in a plate} * \text{Dilution factor of the plate} * \text{total cell lysate volume}/20$$

Phage Amplification

- a. Inoculate 100ml LB+tetracycline media in a round-bottomed flask with 10ul of E. coli, provided with the phage display library. Grow overnight at 37°C with gentle shaking (225 rpm). This will be the starter culture.

- b. Inoculate another 100ml of LB+tetracycline media with 1-2 drops of the starter culture. Incubate at 37°C for 1hr with gentle shaking.
- c. Take 32ml of this culture and add 1-1.5ml of the cell lysate (from 2d. above) to it and grow for 4 hours at 37°C with gentle shaking (225 rpm).
- d. Spin down at 10,000rpms at 4°C for 20minutes.
- e. Discard the pellet. Take the 30ml of the supernatant and add 6ml of PEG/NaCl and keep at 4°C overnight.
- f. Next day spin the tube at 12,000rpm for 20minutes at 4°C.
- g. Discard the supernatant and dissolve the pellet in 1cc of TBS (in the hood). Transfer to eppendorf tube and add 200ul of PEG/NaCl (all in the hood). Place on ice for 1 hour.
- h. Spin the tube in cold room at 14,000rpm for 5 minutes.
- i. Discard the supernatant. Resuspend the pellet in 200ul of TBS. This is your amplified phage. Titer this amplified phage using the protocol detailed in Methods-2.3. This will be the amplified and titered phage used for next cycle of phage display, which will after this initial pre-screen, will be *in vivo*.

In vivo Peptide Phage Display

Weigh the mouse on a small animal scale and anesthetize using 12ul/gm of tissue weight of 2% Avertin solution administered intraperitoneally. Mouse will be anesthetized in 2-5 minutes. Inject 10ul of the peptide phage display library ($\sim 10^{11}$ pfu) intravenously, either retro-orbitally or through a tail vein injection. The M13 phage, after an intravenous injection, has a half-life of 4.5hrs, in the circulation. Allow the mouse to recover and circulate the phage for the desired number of half-lives ($\sim 3-6$ half-lives).

Isolating Cardiac Myocytes

- a. After the desired time of circulation, re-anesthetize the mouse using 2% Avertin, euthanize using either a CO₂ chamber or cervical dislocation, and open the chest cavity. Now place a nick in either the right atrium or right ventricle and using a small bore needle, inject the left ventricle with 3-5ml of HBSS-G-Heparin, so as to flush out all the red blood cells from the ventricular cavity and the coronary circulation.
- b. Dissect out the heart, trim the atria and great vessels, and weigh the resulting trimmed heart.
- c. Place a petri dish on ice, add 2-4ml of HBSS-G-Heparin, place heart pieces in it and chop as finely as possible.
- d. Transfer all of this to a round bottom 5cc tube and discard the supernatant.
- e. Add 2ml of Digestion Enzyme to the pieces, incubate (with rocking) at 37°C for 5 minutes.
- f. Collect the supernatant into DMEM 50:50/F12/25% FBS (10ml for each heart) media; keep at 37°C.
- g. Repeat the steps e-f above until all the tissue pieces are digested.
- h. Now place the accumulated tissue+DMEM+FBS through a 70µm filter.
- i. Centrifuge the filtered cells for 4 minutes at 1000rpm.
- b. Aspirate off the media, keep the pellet and resuspend the cells in 5-6ml of the plating medium.
- c. Now place in the cells and media in a 6" cell culture plate (to plate out the fibroblasts) and place in an incubator at 37°C for 2 hours (without disturbing).

- d. At the end of 2 hours, aspirate the top media, pellet the cells, resuspend in 1 ml of PBS, transfer to an eppendorf tube and place in -80°C to freeze.
- e. Put the cell pellet through one freeze-thaw cycle to lyse the cells and release the internalized phage. Pellet the cell debris by centrifuging at maximum speed for 60 sec in a table-top centrifuge. Use 20ul of this cell lysate/supernatant to titrate the released phage as detailed in the phage titration section above. This phage population is the population of interest that will be put through subsequent cycles of phage amplification (as detailed in the phage amplification section above) and re-injected into a mouse for a second cycle of peptide phage display. The number of phage recovered from the heart will be normalized to the weight of the heart (in grams).

Isolating Kidney Cells

- a. Inject phage library intravenously (reto-orbitally or via a tail vein injection) and allow to circulate for the decided number of hours.
- b. After the desired time of circulation, re-anesthetize the mouse using 2% Avertin, euthanize using either a CO_2 chamber or cervical dislocation, and open the chest cavity. Now place a nick in either the right atrium or right ventricle and using a small bore needle, inject the left ventricle with 3-5ml of HBSS-G-Heparin, so as to flush out all the red blood cells from the ventricular cavity and the coronary circulation.
- c. Dissect the kidney out and rinse in PBS.
- d. In a cell culture hood, cut the kidney into small pieces with autoclaved/sterile razor blade.
- e. Digest the minced tissue with 0.75% collagenase II at 37°C for 30 -45minutes.
- f. Pipette the digested tissue up and down.

- g. Filter the cells with 75 μ m filter.
- h. Trypsinize the cells for 10minutes at room temperature.
- i. Spin down the cells and wash with PBS twice.
- j. Resuspend in 1ml of PBS.
- k. Store in eppendorf tubes at -80°C.
- l. Put the cell pellet through one freeze-thaw cycle to lyse the cells and release the internalized phage. Pellet the cell debris by centrifuging at maximum speed for 60 sec in a table-top centrifuge. Use 20ul of this cell lysate/supernatant to titrate the released phage as detailed in phage titration section above. This phage population is the control phage and the released phage from heart, the target organ of interest, will be expressed as a ratio of the number of phage recovered from kidney. The number of phage recovered from the kidney will be normalized to the weight of the kidney (in grams).
- m. After 3 cycles of *in vivo* peptide phage display, 10 plaques were picked from phage recovered from the target organ, amplified and sequenced as detailed in Section “Phage Sequencing” below. A consensus sequence emerged after 4 cycles of phage display, which was termed “*Cardiac Targeting Peptide*” or *CTP*, and synthesized biotinylated, labeled with 6-carboxyfluorescein or as a fusion peptide with NBD or nemo-binding domain peptide..

Phage Sequencing

From the plate with <100 plaques, pick 10-20 for amplification and subsequent sequencing.

- a. Dilute an overnight culture of *E. coli* 1:100 in LB. Dispense 1 ml of diluted culture into culture tubes, one for each clone to be characterized.
- b. Use a sterile wooden stick or pipette tip to stab a plaque from a titering plate (important: plates should be <1–3 days old, stored at 4°C and have <100 plaques) and transfer to a tube containing the diluted culture. Pick well-separated plaques. This will ensure that each plaque contains a single DNA sequence.
- c. Incubate the tubes at 37°C with shaking for 4.5–5 hours (no longer).
- d. Transfer the cultures to microcentrifuge tubes, and centrifuge at 14,000 rpm for 30 seconds. Transfer the supernatant to a fresh tube and re-spin. Using a pipette, transfer the upper 80% of the supernatant to a fresh tube. This is the amplified phage stock and can be stored at 4°C for several weeks with little loss of titer. For long-term storage (up to several years), dilute 1:1 with sterile glycerol and store at –20°C.
- e. Transfer 500 µl of the amplified phage stock to a fresh microfuge tube. Add 200 µl of 20% PEG/2.5 M NaCl. Invert several times to mix, and let stand for 10–20 minutes at room temperature.
- f. Microfuge at 14,000 rpm for 10 minutes at 4°C and discard the supernatant. Phage pellet may not be visible. Re-spin briefly. Carefully pipet away and discard any remaining supernatant.
- g. Suspend the pellet thoroughly in 100 µl of Iodide Buffer by vigorously tapping the tube. Add 250 µl of ethanol and incubate 10–20 minutes at room temperature. Short incubation at room temperature will preferentially precipitate single-stranded phage DNA, leaving most phage protein in solution.

- h. Spin in a microfuge at 14,000 rpm for 10 minutes at 4°C, and discard the supernatant. Wash the pellet with 0.5 ml of 70% ethanol (stored at –20°C), re-spin, discard the supernatant, and briefly dry the pellet under vacuum or at room air.
- i. Resuspend the pellet in 30 µl of TE buffer. The template can be suspended in H₂O instead of TE if desired, but this is not recommended for long-term storage. In TE buffer, the phage DNA should be stable indefinitely at –20°C. Sequence this DNA using the sequencing primers provided with the peptide phage display library.

5.2 IN VITRO TRANSDUCTION EXPERIMENTS

5.2.1 Cell transduction experiments with CTP-6CF

In vitro cell transduction experiments were carried out using rat cardiomyoblasts (H9C2 cells), mouse fibroblast cell line (NIH/3T3), mouse fibrosarcoma cell line (MCA205), human epithelial cervical cancer cell line (HeLa cells) and human tubular kidney cell line (HK-2). Cells were passaged at least three times and either grown to confluence or 70% confluence (in the case of H9C2 cells) in the appropriate cell culture media. After at least 3 or more passages, cells were trypsinized, counted on a hemacytometer and plated onto collagen-coated cover-slips at a cell density of 2×10^5 cells/well in a 6-well tissue culture treated plate. Cells were left in the incubator, 37°C/5% CO₂ overnight. Next day media was aspirated, cells washed with pre-warmed 1ml of Optimem and left in 1ml of Optimem. To the cells CTP-6CF was added at a final concentration of 50, 100 or 200µM. A negative control group of incubating only with PBS was utilized. The stock solution of the peptide was made in PBS at a 1mM concentration. After addition of the

peptide, cells were returned to the incubator for 30 minutes. After the end of the incubation period, media was aspirated, cells washed with pre-warmed PBS 3 times. After the washes, 1ml of pre-warmed 2% paraformaldehyde was added and 1ul of DRAQ5 solution, a nuclear stain, was added to the paraformaldehyde. This was carried out at RT for 30 minutes, light-protected. After 30 minutes, paraformaldehyde was aspirated, cells washed with PBS once and cover-slips mounted onto glass-slides using permount. The slides were kept at 4°C, light -protected until next day when confocal microscopy was performed.

For confocal microscopy, laser intensities/gains were set using negative control (PBS injected) cells to minimize background fluorescence. Once the laser intensity for FITC was set, it was kept constant across all subsequent imaging. Also serial scanning was performed to prevent “bleed-through” from one laser wavelength to another.

As paraformaldehyde itself has auto-fluorescence, and boiling it can cause polymerization of the individual molecules forming large complexes that can precipitate at lower temperatures and cause fluorescence artifact, the protocol given below for making paraformaldehyde was followed. The 8% stock solution was stored at 4°C, light -protected, wrapped in foil, and diluted 4:1 in PBS down to 2% on the day of use.

5.2.2 8% Paraformaldehyde stock solution

1. For each 100mls of Paraformaldehyde, add 8 grams of paraformaldehyde resin to 70 ml of distilled water.
2. Heat to 70°C (it will not dissolve).
3. Add 1M NaOH drop by drop until the solution clears; usually requires a couple of drops.

4. Cool to room temperature.
5. Add 9mls of 1x PBS or 30 mls of 0.3M PBS
6. PH to 7.4
7. Filter and store at 4°C, light-protected, wrapped in foil.
8. On the day of use, dilute necessary amount of 8% paraformaldehyde down to 2% with a 4:1 dilution with PBS.

5.3 METHODOLOGY FOR TRANSFECTION OF CELLS AND INHIBITION OF NF-KB ACTIVATION

5.3.1 Materials

Materials specified are for 1 well of a 12-well plate. Scale up or down as necessary for the size of the well and multiply by the number of wells needed. For example, one well of a 96-well plate will need 6.25ul of Optimem. If the experiment is to be done in quadruplicate, would need 25ul for each group in the experiment.

50ul of Optimem/well

2ul of Lipofectamine/well

200ng of reporter plasmid DNA/well (plasmid expressing Luciferase under an NF-κB promoter site)

200ng of Renilla (control plasmid)/well

5.3.2 Methods

1. After 3-4 cell passages, split cells using Trypsin/EDTA, and plate onto a 96-well plate at a cell density of 2×10^4 /well. Return cells to the incubator.
2. Next day incubate relevant amount of Optimem and with Lipofectamine at RT for 5 mins (for every 50ul of Optimem use 2ul of Lipofectamine)..
3. Simultaneously incubate Optimem with the reporter plasmid DNA and the Renilla control plasmid, (ratio of 50ul of Optimem with 200ng of reporter plasmid DNA and 200ng of Renilla control plasmid), at RT for 5 mins.
4. Add 1 and 2 together in a 1:1 ratio and incubate at RT for 20 minutes.
5. While above incubation is going on, aspirate media from cells, wash 3x with pre-warmed antibiotic-free media and leave cells in 1ml of the antibiotic-free media (1ml for a 12-well plate; 125ul for a 96-well plate).
6. Add 12.5ul of the optimem+lipofectamine+DNA into each well of a 96-well plate (100ul per well of a 12-well plate) and leave in incubator o/n.
7. Next day, aspirate media, wash cells with pre-warmed Optimem once, and leave in 100ul of Optimem (for a 96-well plate). Add the peptides in the concentrations being tested and return cells to incubator for 30 minutes (or varying time-points as the experiment's hypothesis dictates).
8. Add murine (for H9C2 cells) or human TNF α (HeLa cells) at a concentration of 10ng/ml and return cells to incubator for 3 hours.

9. At the end of 3 hours, aspirate media, wash cells with pre-warmed PBS once, lyse cells with 100ul of cell lysis buffer for 5 minutes. Pipette up and down a few times to complete the lysis and add lysate to eppendorf tubes. Spin the debris down in a table-top centrifuge, at maximum speed (usually 14,000 rpm) for 5 minutes, and transfer 10ul each into two glass tubes for Luciferase and Renilla reading. The Luciferase and Renilla activity is read in a Luminometer using Luciferase and Renilla substrate.

5.4 MOUSE INFARCT MODEL

The following protocol for generating infarcts in mice was utilized and kept consistent from one set of experiments to another and between groups. Female, Balb/c, 10-20 week old mice were used. Female mice were chosen because of the ability to house 5/cage, as opposed to male mice (4/cage) and more importantly because female mice are able to tolerate cardiac insults better with lower post-operative mortality [125]. Mice were anesthetized with intraperitoneal (i.p.) injection of 2.5% Avertin (a mixture of 15.5 ml tert-amyl alcohol to 25 grams of 2-2-2 Tribromoethanol - stock solution diluted to 2.5% concentration with PBS) at a dose of 15ul/gm of body weight. Adequate anesthetic level was assessed by lack of response to toe-pinch and lack of a gag reflex. Mice were intubated, using direct visualization of the vocal chords, with a 22G cannula and placed on a Harvard rodent ventilator apparatus. Tube placement was confirmed by symmetric expansion of the thoracic cavity. Mice were ventilated with ~0.1cc/breath tidal volume at a rate of 110 breaths/minute.

Following successful intubation/ventilation, the chest cavity was opened using a left lateral thorotomy approach. Care was taken not to extend the surgical incision cephalad to the

level of the sternal head, as a large venous confluence is present in that region and cutting through them can lead to major, exsanguinating bleed. A self-retaining mouse retractor was placed inside the incision and the teeth opened to reveal the anterior surface of the heart. The pericardium was gently removed with blunt forceps. A suture, 6-0 prolene, blue, monofilament (Owens & Minor: #8714H) was placed along the lateral wall of the left ventricle (LV), ~2mm below the lowest dip of the left atrium and ligated with exactly 5 squarely-placed knots. Ischemia was confirmed by the resulting pallor of the myocardium and development of wall motion abnormality. The muscle layer and skin were closed in two layers with running sutures with 8-0 black, monofilament nylon suture (Owens& Minor: #2808G). The mice were extubated once spontaneous breathing was confirmed, and recovered on a heating pad. Post-operative pain was managed with subcutaneous injection of Ketoprofen, 5mg/Kg, on post-op day 0, 1 and 2 or with subcutaneous Buprenorphine, at a dose of 0.1mg/Kg body weight given once on the day of surgery and twice daily on post-op day 1 and 2. Mice also got one injection of subcutaneous Ampicillin, 100mg/Kg, after surgery for prophylaxis against post-surgical infection. Right after ligation and suture placement on the anterior surface of the heart to produce myocardial infarction, and before closing the chest wall, mice received i.p. peptides in different doses. The surgeon (myself) was always blinded to the treatment. Also surgeries were carried out in a rotational fashion so that any variation due to surgical technique was distributed equally over the treatment groups.

Mice were euthanized on post-operative day 7. On day of euthanasia, mice were anesthetized, chest cavity opened, and 1cc of 1M KCl injected via the right ventricle (RV) in order to arrest the heart in diastole to prevent contraction band necrosis. This was followed by injecting, through the right ventricle, 5cc of Glyo-fixx (formalin-substitute), heart dissected out

and placed in 15ml of Glyo-fixx, until tissue embedded for sectioning. After paraffin embedding, cross-sections of the heart were taken starting at the apex. The first section was taken once the LV cavity appeared, with second and third sections taken 10 microns apart and cephalad of the first section. The three sections were H&E stained, light microscopy photographs taken, and area of infarct in each section mapped out using computer software Metamorph and expressed as a percent of the whole heart. The infarct area from the three sections was averaged to give the final infarct size for each mouse.

BIBLIOGRAPHY

1. Wiviott, S.D., et al., *Performance of the thrombolysis in myocardial infarction risk index in the National Registry of Myocardial Infarction-3 and -4: a simple index that predicts mortality in ST-segment elevation myocardial infarction*. J Am Coll Cardiol, 2004. **44**(4): p. 783-9.
2. Rogers, W.J., et al., *Temporal trends in the treatment of over 1.5 million patients with myocardial infarction in the US from 1990 through 1999: the National Registry of Myocardial Infarction 1, 2 and 3*. J Am Coll Cardiol, 2000. **36**(7): p. 2056-63.
3. Kawano, S., et al., *Blockade of NF-kappaB improves cardiac function and survival after myocardial infarction*. Am J Physiol Heart Circ Physiol, 2006. **291**(3): p. H1337-44.
4. Pachori, A.S., et al., *Hypoxia-regulated therapeutic gene as a preemptive treatment strategy against ischemia/reperfusion tissue injury*. Proc Natl Acad Sci U S A, 2004. **101**(33): p. 12282-7.
5. Melo, L.G., et al., *Molecular and cell-based therapies for protection, rescue, and repair of ischemic myocardium: reasons for cautious optimism*. Circulation, 2004. **109**(20): p. 2386-93.
6. Frankel, A.D. and C.O. Pabo, *Cellular uptake of the tat protein from human immunodeficiency virus*. Cell, 1988. **55**(6): p. 1189-93.
7. Green, M. and P.M. Loewenstein, *Autonomous functional domains of chemically synthesized human immunodeficiency virus tat trans-activator protein*. Cell, 1988. **55**(6): p. 1179-88.
8. Joliot, A.H., et al., *alpha-2,8-Polysialic acid is the neuronal surface receptor of antennapedia homeobox peptide*. New Biol, 1991. **3**(11): p. 1121-34.
9. Fawell, S., et al., *Tat-mediated delivery of heterologous proteins into cells*. Proc Natl Acad Sci U S A, 1994. **91**(2): p. 664-8.
10. Allinquant, B., et al., *Downregulation of amyloid precursor protein inhibits neurite outgrowth in vitro*. J Cell Biol, 1995. **128**(5): p. 919-27.
11. Schwarze, S.R., et al., *In vivo protein transduction: delivery of a biologically active protein into the mouse*. Science, 1999. **285**(5433): p. 1569-72.
12. Derossi, D., et al., *The third helix of the Antennapedia homeodomain translocates through biological membranes*. J Biol Chem, 1994. **269**(14): p. 10444-50.
13. Pooga, M., et al., *Cell penetration by transportan*. FASEB J, 1998. **12**(1): p. 67-77.
14. Morris, M.C., et al., *A new peptide vector for efficient delivery of oligonucleotides into mammalian cells*. Nucleic Acids Res, 1997. **25**(14): p. 2730-6.
15. Futaki, S., et al., *Arginine-rich peptides. An abundant source of membrane-permeable peptides having potential as carriers for intracellular protein delivery*. J Biol Chem, 2001. **276**(8): p. 5836-40.

16. Mai, J.C., et al., *Efficiency of protein transduction is cell type-dependent and is enhanced by dextran sulfate*. J Biol Chem, 2002. **277**(33): p. 30208-18.
17. Choi, M., et al., *Inhibition of NF-kappaB by a TAT-NEMO-binding domain peptide accelerates constitutive apoptosis and abrogates LPS-delayed neutrophil apoptosis*. Blood, 2003. **102**(6): p. 2259-67.
18. Dave, S.H., et al., *Amelioration of chronic murine colitis by peptide-mediated transduction of the IkappaB kinase inhibitor NEMO binding domain peptide*. J Immunol, 2007. **179**(11): p. 7852-9.
19. Ribeiro, M.M., et al., *Heme oxygenase-1 fused to a TAT peptide transduces and protects pancreatic beta-cells*. Biochem Biophys Res Commun, 2003. **305**(4): p. 876-81.
20. Eguchi, A., et al., *Protein transduction domain of HIV-1 Tat protein promotes efficient delivery of DNA into mammalian cells*. J Biol Chem, 2001. **276**(28): p. 26204-10.
21. Josephson, L., et al., *High-efficiency intracellular magnetic labeling with novel superparamagnetic-Tat peptide conjugates*. Bioconjug Chem, 1999. **10**(2): p. 186-91.
22. Lewin, M., et al., *Tat peptide-derivatized magnetic nanoparticles allow in vivo tracking and recovery of progenitor cells*. Nat Biotechnol, 2000. **18**(4): p. 410-4.
23. Rothbard, J.B., et al., *Conjugation of arginine oligomers to cyclosporin A facilitates topical delivery and inhibition of inflammation*. Nat Med, 2000. **6**(11): p. 1253-7.
24. Torchilin, V.P., et al., *TAT peptide on the surface of liposomes affords their efficient intracellular delivery even at low temperature and in the presence of metabolic inhibitors*. Proc Natl Acad Sci U S A, 2001. **98**(15): p. 8786-91.
25. Chiu, Y.L., et al., *Visualizing a correlation between siRNA localization, cellular uptake, and RNAi in living cells*. Chem Biol, 2004. **11**(8): p. 1165-75.
26. Muratovska, A. and M.R. Eccles, *Conjugate for efficient delivery of short interfering RNA (siRNA) into mammalian cells*. FEBS Lett, 2004. **558**(1-3): p. 63-8.
27. Moschos, S.A., et al., *Lung delivery studies using siRNA conjugated to TAT(48-60) and penetratin reveal peptide induced reduction in gene expression and induction of innate immunity*. Bioconjug Chem, 2007. **18**(5): p. 1450-9.
28. Kumar, P., et al., *Transvascular delivery of small interfering RNA to the central nervous system*. Nature, 2007. **448**(7149): p. 39-43.
29. Endoh, T., M. Sisido, and T. Ohtsuki, *Cellular siRNA delivery mediated by a cell-permeant RNA-binding protein and photoinduced RNA interference*. Bioconjug Chem, 2008. **19**(5): p. 1017-24.
30. Lundberg, P., et al., *Delivery of short interfering RNA using endosomolytic cell-penetrating peptides*. FASEB J, 2007. **21**(11): p. 2664-71.
31. Sergeeva, A., et al., *Display technologies: application for the discovery of drug and gene delivery agents*. Adv Drug Deliv Rev, 2006. **58**(15): p. 1622-54.
32. Smith, G.P., *Filamentous fusion phage: novel expression vectors that display cloned antigens on the virion surface*. Science, 1985. **228**(4705): p. 1315-7.
33. Scott, J.K. and G.P. Smith, *Searching for peptide ligands with an epitope library*. Science, 1990. **249**(4967): p. 386-90.
34. Ackermann, H.W., *Frequency of morphological phage descriptions in 1995*. Arch Virol, 1996. **141**(2): p. 209-18.
35. Ackermann, H.W., *Frequency of morphological phage descriptions in the year 2000. Brief review*. Arch Virol, 2001. **146**(5): p. 843-57.

36. Ackermann, H.W., *5500 Phages examined in the electron microscope*. Arch Virol, 2007. **152**(2): p. 227-43.
37. Arap, W., R. Pasqualini, and E. Ruoslahti, *Cancer treatment by targeted drug delivery to tumor vasculature in a mouse model*. Science, 1998. **279**(5349): p. 377-80.
38. Kolonin, M.G., et al., *Reversal of obesity by targeted ablation of adipose tissue*. Nat Med, 2004. **10**(6): p. 625-32.
39. Zhang, L., J.A. Hoffman, and E. Ruoslahti, *Molecular profiling of heart endothelial cells*. Circulation, 2005. **112**(11): p. 1601-11.
40. Pasqualini, R., D.M. McDonald, and W. Arap, *Vascular targeting and antigen presentation*. Nat Immunol, 2001. **2**(7): p. 567-8.
41. Arap, W., et al., *Steps toward mapping the human vasculature by phage display*. Nat Med, 2002. **8**(2): p. 121-7.
42. Mi, Z., et al., *Identification of a synovial fibroblast-specific protein transduction domain for delivery of apoptotic agents to hyperplastic synovium*. Mol Ther, 2003. **8**(2): p. 295-305.
43. Rehman, K.K., et al., *Protection of islets by in situ peptide-mediated transduction of the Ikappa B kinase inhibitor Nemo-binding domain peptide*. J Biol Chem, 2003. **278**(11): p. 9862-8.
44. Sen, R. and D. Baltimore, *Inducibility of kappa immunoglobulin enhancer-binding protein Nf-kappa B by a posttranslational mechanism*. Cell, 1986. **47**(6): p. 921-8.
45. Sen, R. and D. Baltimore, *Multiple nuclear factors interact with the immunoglobulin enhancer sequences*. Cell, 1986. **46**(5): p. 705-16.
46. Makris, C., et al., *Female mice heterozygous for IKK gamma/NEMO deficiencies develop a dermatopathy similar to the human X-linked disorder incontinentia pigmenti*. Mol Cell, 2000. **5**(6): p. 969-79.
47. Rudolph, D., et al., *Severe liver degeneration and lack of NF-kappaB activation in NEMO/IKKgamma-deficient mice*. Genes Dev, 2000. **14**(7): p. 854-62.
48. Ting, A.T., F.X. Pimentel-Muinos, and B. Seed, *RIP mediates tumor necrosis factor receptor 1 activation of NF-kappaB but not Fas/APO-1-initiated apoptosis*. EMBO J, 1996. **15**(22): p. 6189-96.
49. Blonska, M., et al., *Restoration of NF-kappaB activation by tumor necrosis factor alpha receptor complex-targeted MEKK3 in receptor-interacting protein-deficient cells*. Mol Cell Biol, 2004. **24**(24): p. 10757-65.
50. Vallabhapurapu, S. and M. Karin, *Regulation and function of NF-kappaB transcription factors in the immune system*. Annu Rev Immunol, 2009. **27**: p. 693-733.
51. Malinin, N.L., et al., *MAP3K-related kinase involved in NF-kappaB induction by TNF, CD95 and IL-1*. Nature, 1997. **385**(6616): p. 540-4.
52. May, M.J., et al., *Selective inhibition of NF-kappaB activation by a peptide that blocks the interaction of NEMO with the IkappaB kinase complex*. Science, 2000. **289**(5484): p. 1550-4.
53. May, M.J., R.B. Marienfeld, and S. Ghosh, *Characterization of the Ikappa B-kinase NEMO binding domain*. J Biol Chem, 2002. **277**(48): p. 45992-6000.
54. Dai, S., et al., *The IkappaB kinase (IKK) inhibitor, NEMO-binding domain peptide, blocks osteoclastogenesis and bone erosion in inflammatory arthritis*. J Biol Chem, 2004. **279**(36): p. 37219-22.

55. di Meglio, P., A. Ianaro, and S. Ghosh, *Amelioration of acute inflammation by systemic administration of a cell-permeable peptide inhibitor of NF-kappaB activation*. *Arthritis Rheum*, 2005. **52**(3): p. 951-8.
56. Shibata, W., et al., *Cutting edge: The IkappaB kinase (IKK) inhibitor, NEMO-binding domain peptide, blocks inflammatory injury in murine colitis*. *J Immunol*, 2007. **179**(5): p. 2681-5.
57. De Plaen, I.G., et al., *Inhibition of nuclear factor-kappaB ameliorates bowel injury and prolongs survival in a neonatal rat model of necrotizing enterocolitis*. *Pediatr Res*, 2007. **61**(6): p. 716-21.
58. Long, Y.M., et al., *Cell-permeable Tat-NBD peptide attenuates rat pancreatitis and acinus cell inflammation response*. *World J Gastroenterol*, 2009. **15**(5): p. 561-9.
59. Ianaro, A., et al., *NEMO-binding domain peptide inhibits proliferation of human melanoma cells*. *Cancer Lett*, 2009. **274**(2): p. 331-6.
60. Tapia, M.A., et al., *Inhibition of the canonical IKK/NF kappa B pathway sensitizes human cancer cells to doxorubicin*. *Cell Cycle*, 2007. **6**(18): p. 2284-92.
61. Tas, S.W., et al., *Local treatment with the selective IkappaB kinase beta inhibitor NEMO-binding domain peptide ameliorates synovial inflammation*. *Arthritis Res Ther*, 2006. **8**(4): p. R86.
62. van den Tweel, E.R., et al., *Selective inhibition of nuclear factor-kappaB activation after hypoxia/ischemia in neonatal rats is not neuroprotective*. *Pediatr Res*, 2006. **59**(2): p. 232-6.
63. Biswas, D.K., et al., *NF-kappa B activation in human breast cancer specimens and its role in cell proliferation and apoptosis*. *Proc Natl Acad Sci U S A*, 2004. **101**(27): p. 10137-42.
64. Ashikawa, K., et al., *Evidence that activation of nuclear factor-kappaB is essential for the cytotoxic effects of doxorubicin and its analogues*. *Biochem Pharmacol*, 2004. **67**(2): p. 353-64.
65. Thomas, R.P., et al., *Selective targeting of the nuclear factor-kappaB pathway enhances tumor necrosis factor-related apoptosis-inducing ligand-mediated pancreatic cancer cell death*. *Surgery*, 2002. **132**(2): p. 127-34.
66. Craig, R., et al., *The cytoprotective effects of the glycoprotein 130 receptor-coupled cytokine, cardiotrophin-1, require activation of NF-kappa B*. *J Biol Chem*, 2001. **276**(40): p. 37621-9.
67. Hall, G., et al., *Inhibitor-kappaB kinase-beta regulates LPS-induced TNF-alpha production in cardiac myocytes through modulation of NF-kappaB p65 subunit phosphorylation*. *Am J Physiol Heart Circ Physiol*, 2005. **289**(5): p. H2103-11.
68. Wright, G., et al., *Endotoxin stress-response in cardiomyocytes: NF-kappaB activation and tumor necrosis factor-alpha expression*. *Am J Physiol Heart Circ Physiol*, 2002. **282**(3): p. H872-9.
69. Haudek, S.B., D.D. Bryant, and B.P. Giroir, *Differential regulation of myocardial NF kappa B following acute or chronic TNF-alpha exposure*. *J Mol Cell Cardiol*, 2001. **33**(6): p. 1263-71.
70. Norman, D.A., M.H. Yacoub, and P.J. Barton, *Nuclear factor NF-kappa B in myocardium: developmental expression of subunits and activation by interleukin-1 beta in cardiac myocytes in vitro*. *Cardiovasc Res*, 1998. **39**(2): p. 434-41.

71. Pelzer, T., et al., *Estrogen effects in the myocardium: inhibition of NF-kappaB DNA binding by estrogen receptor-alpha and -beta*. *Biochem Biophys Res Commun*, 2001. **286**(5): p. 1153-7.
72. Xuan, Y.T., et al., *Nuclear factor-kappaB plays an essential role in the late phase of ischemic preconditioning in conscious rabbits*. *Circ Res*, 1999. **84**(9): p. 1095-109.
73. N'Diaye, M., et al., *TNFalpha- and NF-kappaB-dependent induction of the chemokine CCL1 in human macrophages exposed to the atherogenic lipoprotein(a)*. *Life Sci*, 2009. **84**(13-14): p. 451-7.
74. Sanchez-Galan, E., et al., *Leukotriene B4 enhances the activity of nuclear factor-kappaB pathway through BLT1 and BLT2 receptors in atherosclerosis*. *Cardiovasc Res*, 2009. **81**(1): p. 216-25.
75. van Keulen, J.K., et al., *The Nuclear Factor-kappa B p50 subunit is involved in flow-induced outward arterial remodeling*. *Atherosclerosis*, 2009. **202**(2): p. 424-30.
76. Gareus, R., et al., *Endothelial cell-specific NF-kappaB inhibition protects mice from atherosclerosis*. *Cell Metab*, 2008. **8**(5): p. 372-83.
77. Crosara-Alberto, D.P., R.Y. Inoue, and C.R. Costa, *FAK signalling mediates NF-kappaB activation by mechanical stress in cardiac myocytes*. *Clin Chim Acta*, 2009. **403**(1-2): p. 81-6.
78. Liang, Y.J., et al., *Mechanical stress enhances serotonin 2B receptor modulating brain natriuretic peptide through nuclear factor-kappaB in cardiomyocytes*. *Cardiovasc Res*, 2006. **72**(2): p. 303-12.
79. Li, T., et al., *MyD88-dependent nuclear factor-kappaB activation is involved in fibrinogen-induced hypertrophic response of cardiomyocytes*. *J Hypertens*, 2009. **27**(5): p. 1084-93.
80. Freund, C., et al., *Requirement of nuclear factor-kappaB in angiotensin II- and isoproterenol-induced cardiac hypertrophy in vivo*. *Circulation*, 2005. **111**(18): p. 2319-25.
81. Young, D., et al., *Blockade of NF-kappaB using IkappaB alpha dominant-negative mice ameliorates cardiac hypertrophy in myotrophin-overexpressed transgenic mice*. *J Mol Biol*, 2008. **381**(3): p. 559-68.
82. Gupta, S., et al., *Prevention of cardiac hypertrophy and heart failure by silencing of NF-kappaB*. *J Mol Biol*, 2008. **375**(3): p. 637-49.
83. Ha, T., et al., *Attenuation of cardiac hypertrophy by inhibiting both mTOR and NFkappaB activation in vivo*. *Free Radic Biol Med*, 2005. **39**(12): p. 1570-80.
84. Gupta, S., D. Young, and S. Sen, *Inhibition of NF-kappaB induces regression of cardiac hypertrophy, independent of blood pressure control, in spontaneously hypertensive rats*. *Am J Physiol Heart Circ Physiol*, 2005. **289**(1): p. H20-9.
85. Tillmanns, J., et al., *Caught in the act: in vivo molecular imaging of the transcription factor NF-kappaB after myocardial infarction*. *Biochem Biophys Res Commun*, 2006. **342**(3): p. 773-4.
86. Maulik, N., et al., *An essential role of NFkappaB in tyrosine kinase signaling of p38 MAP kinase regulation of myocardial adaptation to ischemia*. *FEBS Lett*, 1998. **429**(3): p. 365-9.
87. Meldrum, D.R., *Mechanisms of cardiac preconditioning: ten years after the discovery of ischemic preconditioning*. *J Surg Res*, 1997. **73**(1): p. 1-13.

88. Morgan, E.N., et al., *An essential role for NF-kappaB in the cardioadaptive response to ischemia*. *Ann Thorac Surg*, 1999. **68**(2): p. 377-82.
89. Frantz, S., et al., *Tissue-specific effects of the nuclear factor kappaB subunit p50 on myocardial ischemia-reperfusion injury*. *Am J Pathol*, 2007. **171**(2): p. 507-12.
90. Li, H.L., et al., *Targeted cardiac overexpression of A20 improves left ventricular performance and reduces compensatory hypertrophy after myocardial infarction*. *Circulation*, 2007. **115**(14): p. 1885-94.
91. Trescher, K., et al., *Inflammation and postinfarct remodeling: overexpression of IkappaB prevents ventricular dilation via increasing TIMP levels*. *Cardiovasc Res*, 2006. **69**(3): p. 746-54.
92. Trescher, K., et al., *Adenovirus-mediated overexpression of inhibitor kappa B-alpha attenuates postinfarct remodeling in the rat heart*. *Eur J Cardiothorac Surg*, 2004. **26**(5): p. 960-7.
93. Hua, F., et al., *Blocking the MyD88-dependent pathway protects the myocardium from ischemia/reperfusion injury in rat hearts*. *Biochem Biophys Res Commun*, 2005. **338**(2): p. 1118-25.
94. Sakaguchi, T., et al., *A novel strategy of decoy transfection against nuclear factor-kappaB in myocardial preservation*. *Ann Thorac Surg*, 2001. **71**(2): p. 624-9; discussion 629-30.
95. Morishita, R., et al., *In vivo transfection of cis element "decoy" against nuclear factor-kappaB binding site prevents myocardial infarction*. *Nat Med*, 1997. **3**(8): p. 894-9.
96. Misra, A., et al., *Nuclear factor-kappaB protects the adult cardiac myocyte against ischemia-induced apoptosis in a murine model of acute myocardial infarction*. *Circulation*, 2003. **108**(25): p. 3075-8.
97. Meili-Butz, S., et al., *Dimethyl fumarate, a small molecule drug for psoriasis, inhibits Nuclear Factor-kappaB and reduces myocardial infarct size in rats*. *Eur J Pharmacol*, 2008. **586**(1-3): p. 251-8.
98. Moss, N.C., et al., *IKKbeta inhibition attenuates myocardial injury and dysfunction following acute ischemia-reperfusion injury*. *Am J Physiol Heart Circ Physiol*, 2007. **293**(4): p. H2248-53.
99. Onai, Y., et al., *Inhibition of IkappaB phosphorylation in cardiomyocytes attenuates myocardial ischemia/reperfusion injury*. *Cardiovasc Res*, 2004. **63**(1): p. 51-9.
100. Pye, J., et al., *Proteasome inhibition ablates activation of NF-kappa B in myocardial reperfusion and reduces reperfusion injury*. *Am J Physiol Heart Circ Physiol*, 2003. **284**(3): p. H919-26.
101. Altavilla, D., et al., *IRFI 042, a novel dual vitamin E-like antioxidant, inhibits activation of nuclear factor-kappaB and reduces the inflammatory response in myocardial ischemia-reperfusion injury*. *Cardiovasc Res*, 2000. **47**(3): p. 515-28.
102. Yeh, C.H., et al., *Inhibition of NFkappaB activation with curcumin attenuates plasma inflammatory cytokines surge and cardiomyocytic apoptosis following cardiac ischemia/reperfusion*. *J Surg Res*, 2005. **125**(1): p. 109-16.
103. Yeh, C.H., et al., *Inhibition of NF-kappa B activation can attenuate ischemia/reperfusion-induced contractility impairment via decreasing cardiomyocytic proinflammatory gene up-regulation and matrix metalloproteinase expression*. *J Cardiovasc Pharmacol*, 2005. **45**(4): p. 301-9.

104. Timmers, L., et al., *Targeted deletion of nuclear factor kappaB p50 enhances cardiac remodeling and dysfunction following myocardial infarction*. *Circ Res*, 2009. **104**(5): p. 699-706.
105. Wakatsuki, S., et al., *A novel IKK inhibitor suppresses heart failure and chronic remodeling after myocardial ischemia via MMP alteration*. *Expert Opin Ther Targets*, 2008. **12**(12): p. 1469-76.
106. Frantz, S., et al., *Absence of NF-kappaB subunit p50 improves heart failure after myocardial infarction*. *FASEB J*, 2006. **20**(11): p. 1918-20.
107. Squadrito, F., et al., *Gene transfer of IkappaBalpha limits infarct size in a mouse model of myocardial ischemia-reperfusion injury*. *Lab Invest*, 2003. **83**(8): p. 1097-104.
108. Kupatt, C., et al., *Retroinfusion of NFkappaB decoy oligonucleotide extends cardioprotection achieved by CD18 inhibition in a preclinical study of myocardial ischemia and retroinfusion in pigs*. *Gene Ther*, 2002. **9**(8): p. 518-26.
109. Hescheler, J., et al., *Morphological, biochemical, and electrophysiological characterization of a clonal cell (H9c2) line from rat heart*. *Circ Res*, 1991. **69**(6): p. 1476-86.
110. Stathopoulou, K., I. Beis, and C. Gaitanaki, *MAPK signaling pathways are needed for survival of H9c2 cardiac myoblasts under extracellular alkalosis*. *Am J Physiol Heart Circ Physiol*, 2008. **295**(3): p. H1319-H1329.
111. Saeedi, R., et al., *Metabolic actions of metformin in the heart can occur by AMPK-independent mechanisms*. *Am J Physiol Heart Circ Physiol*, 2008. **294**(6): p. H2497-506.
112. Saeedi, R., et al., *AMP-activated protein kinase influences metabolic remodeling in H9c2 cells hypertrophied by arginine vasopressin*. *Am J Physiol Heart Circ Physiol*, 2009. **296**(6): p. H1822-32.
113. Venkatakrishnan, C.D., et al., *HSP27 regulates p53 transcriptional activity in doxorubicin-treated fibroblasts and cardiac H9c2 cells: p21 upregulation and G2/M phase cell cycle arrest*. *Am J Physiol Heart Circ Physiol*, 2008. **294**(4): p. H1736-44.
114. Turakhia, S., et al., *Doxorubicin-induced cardiotoxicity: direct correlation of cardiac fibroblast and H9c2 cell survival and aconitase activity with heat shock protein 27*. *Am J Physiol Heart Circ Physiol*, 2007. **293**(5): p. H3111-21.
115. Molenaar, T.J., et al., *Uptake and processing of modified bacteriophage M13 in mice: implications for phage display*. *Virology*, 2002. **293**(1): p. 182-91.
116. Ivanenkov, V., F. Felici, and A.G. Menon, *Uptake and intracellular fate of phage display vectors in mammalian cells*. *Biochim Biophys Acta*, 1999. **1448**(3): p. 450-62.
117. Lundberg, M. and M. Johansson, *Positively charged DNA-binding proteins cause apparent cell membrane translocation*. *Biochem Biophys Res Commun*, 2002. **291**(2): p. 367-71.
118. Lundberg, M., S. Wikstrom, and M. Johansson, *Cell surface adherence and endocytosis of protein transduction domains*. *Mol Ther*, 2003. **8**(1): p. 143-50.
119. Gump, J.M. and S.F. Dowdy, *TAT transduction: the molecular mechanism and therapeutic prospects*. *Trends Mol Med*, 2007. **13**(10): p. 443-8.
120. Madge, L.A. and M.J. May, *Inhibiting proinflammatory NF-kappaB signaling using cell-penetrating NEMO binding domain peptides*. *Methods Mol Biol*, 2009. **512**: p. 209-32.
121. Bergmann, M.W., et al., *Effect of NF-kappa B Inhibition on TNF-alpha-induced apoptosis and downstream pathways in cardiomyocytes*. *J Mol Cell Cardiol*, 2001. **33**(6): p. 1223-32.

122. del Valle, J., et al., *A new method for determining blood-brain barrier integrity based on intracardiac perfusion of an Evans Blue-Hoechst cocktail*. J Neurosci Methods, 2008. **174**(1): p. 42-9.
123. Rakos, G., et al., *Evans Blue fluorescence permits the rapid visualization of non-intact cells in the perilesional rim of cold-injured rat brain*. Acta Neurobiol Exp (Wars), 2007. **67**(2): p. 149-54.
124. Kin, H., et al., *Neutrophil depletion reduces myocardial apoptosis and attenuates NFkappaB activation/TNFalpha release after ischemia and reperfusion*. J Surg Res, 2006. **135**(1): p. 170-8.
125. Cavasin, M.A., et al., *Gender differences in cardiac function during early remodeling after acute myocardial infarction in mice*. Life Sci, 2004. **75**(18): p. 2181-92.
126. Kelly, K.A., et al., *In vivo phage display selection yields atherosclerotic plaque targeted peptides for imaging*. Mol Imaging Biol, 2006. **8**(4): p. 201-7.
127. Wadia, J.S., R.V. Stan, and S.F. Dowdy, *Transducible TAT-HA fusogenic peptide enhances escape of TAT-fusion proteins after lipid raft macropinocytosis*. Nat Med, 2004. **10**(3): p. 310-5.
128. Kaplan, I.M., J.S. Wadia, and S.F. Dowdy, *Cationic TAT peptide transduction domain enters cells by macropinocytosis*. J Control Release, 2005. **102**(1): p. 247-53.
129. Segvich, S., et al., *Identification of peptides with targeted adhesion to bone-like mineral via phage display and computational modeling*. Cells Tissues Organs, 2009. **189**(1-4): p. 245-51.
130. Segvich, S.J., H.C. Smith, and D.H. Kohn, *The adsorption of preferential binding peptides to apatite-based materials*. Biomaterials, 2009. **30**(7): p. 1287-98.
131. Fazel, R., et al., *Exposure to low-dose ionizing radiation from medical imaging procedures*. N Engl J Med, 2009. **361**(9): p. 849-57.
132. van den Borne, S.W., et al., *Molecular imaging of interstitial alterations in remodeling myocardium after myocardial infarction*. J Am Coll Cardiol, 2008. **52**(24): p. 2017-28.